HIGH ACCURACY AB INITIO QUANTUM CHEMISTRY IN COMBUSTION STUDIES

by

ANDREW C. SIMMONETT

(Under the Direction of Henry F. Schaefer III)

ABSTRACT

The thermochemistry and spectral properties of intermediates and transition structures, found in combustion environments, are computed using rigorous computational techniques. The highly accurate coupled cluster family of methods, extending all the way up to the quasiperturbative treatment of quadruple excitations [CCSDT(Q)] are utilized to obtain accurate energetics within the focal point approach. Anharmonic vibrational frequencies are extracted from accurate quartic force fields using vibrational perturbation theory. The unimolecular dissociation of ortho-benzyne is characterized as a retro-Diels-Alder process with a barrier height of 88.0 ± 0.5 kcal mol^{-1} and an enthalpy of 52.4 ± 0.5 kcal mol^{-1}. Related to this work, the enthalpy of formation for Diacetylene $\Delta_f H_0^o$ = 109.4 ± 0.3 kcal mol^{-1} is computed from the corresponding quantity for acetylene and high level computational methods, explicitly accounting for vibrational anharmonicity. The characteristic vibrational frequencies of the NCCO radical are computed to facilitate its monitoring in kinetics studies. Our computations yield (ν_1, ν_2) = (2171, 1898) cm^{-1}, in contrast to the experimentally derived values (2093, 1774) cm^{-1}, at which no absorption could be observed in subsequent experiments.

INDEX WORDS: coupled cluster theory, vibrational perturbation theory, basis set extrapolation, focal point analysis, computational thermochemistry

HIGH ACCURACY AB INITIO QUANTUM CHEMISTRY IN COMBUSTION STUDIES

by

ANDREW C. SIMMONETT

MSci (Hons.) Computational Chemistry, University of Nottingham, England, 2004

A Dissertation Submitted to the Graduate Faculty of The University of Georgia in Partial Fulfillment of the Requirements for the Degree

DOCTOR OF PHILOSOPHY

ATHENS, GEORGIA

2008

HIGH ACCURACY AB INITIO QUANTUM CHEMISTRY IN COMBUSTION STUDIES

by

ANDREW C. SIMMONETT

Major Professor: Henry F. Schaefer III

Committee: Geoffrey D. Smith
Nigel G. Adams

Electronic Version Approved:

Maureen Grasso
Dean of the Graduate School
The University of Georgia
May 2008

DEDICATION

For my parents, whose constant support means so much. Even from 4067 miles away.

ACKNOWLEDGEMENTS

After four fun, fruitful and fast-moving years I have many people to thank, and will probably forget some important names; please don't be offended if you're one of them. First and foremost, I have to thank Kim who has tolerated me on a daily basis throughout this rollercoaster ride and made these last few years so enjoyable. Many other people have had to put up with me but none more so than Kim who has dealt with my forgetfulness, complaints and general absent-mindedness admirably. I'm thankful for her reminders that the world is not entirely composed of greek letters, 1s and 0s. The Schurmeiers have all been very kind to me and I'm extremely grateful for all the warm hospitality I receive every holiday in P'Town. Meeting up with Melissa and Eli has always been a highlight of that rare event known as "spare time", so I can't forget them either. People always extol the virtues of Southern Hospitality but, great as it is, it doesn't compare to the warmness of Midwesterners.

That's not to ignore the many great people back in Blighty. I dedicated this work to my parents because it's them that got me to this point. Growing up I was always encouraged to find independence and to work hard. I don't think I ever learned any science from either of my parents, but these principles instilled from a young age have served me better than any more scientific lesson ever could. My fond memories of time with my siblings and many friends ensure that England will always be "home" even if I am across the pond.

On a more scientific note, I have to give credit to Peter Gill for being such a great scientific leader, lecturer, mentor and all round great bloke. I had the pleasure of working with him and Andrew Gilbert during my more formative years and it was that experience that

persuaded me to embark on this crazy adventure. On that note, I have to credit Andrew with teaching me the power of programming and scripting the 'proper' way.

If they were the people that persuaded me to continue my studies, it was a great stay here in the summer of 2003 that persuaded me to come to Athens. Michael Schuurman and Betsy Burtner were very generous hosts for that summer and introduced me to the many great things that Athens has to offer. Credit is also due to Steven Wheeler who has been my mentor and landlord at various points in my CCQC life. His seemingly casual, but amazingly rigorous approach has really influenced me, and his ability to hack things together to make them work sometimes borders on miraculous. Talking of hacking things together, I must thank Jet, our resident computer guru, for all of his hard work and helpful advice throughout my time here. Francesco has been a great friend, collaborator and office mate for a long time and long may it continue. Working with him, and the rest of the PSI3 community, has been a real inspiration over the last few years and has motivated me to continually strive to be a better programmer.

Finally I am extremely indebted to Dr. Schaefer and the other faculty members who have been so helpful to me. I really appreciate the freedom that Dr. Schaefer has given me, not to mention the many opportunities to travel. Dr. Allen's relentless pursuit of the right answer for the right reason has shaped my scientific ideals greatly, and I'm thankful for his many words of sage advice in the face of some tough projects. Dr. Yamaguchi has also provided some very helpful words, particularly when it comes to programming the various theories we commonly use. Finally my committee has had to endure many boring talks that do not directly pertain to their fields, but have still offered me great advice and guidance over the years. I chose them because they had the most overlap with my studies at the time and I don't regret making that choice. Even if they do. Before this sounds more like a bad Oscars speech, let's talk science…

TABLE OF CONTENTS

Page

CHAPTER 1

INTRODUCTION AND BACKGROUND

1.1 Introduction

The modeling of combustion chemistry is an overwhelmingly complex task, requiring simultaneous solution of coupled differential equations to model the time evolution of the myriad constituent elementary reactions. The success of such approaches hinges on the accurate knowledge of the kinetics and thermochemistry of the molecules produced and consumed. The direct measurement of such quantities is often precluded by the fleeting existence of intermediates and transition states, which are commonly encountered during combustion processes where excess amounts of energy are present.

Quantum chemistry has enjoyed a meteoric rise in applicability since its inception in the last century, due to the combination of improved methodology and faster computers. Through judicious application of wavefunction theory, we can compute thermochemistry well within "chemical accuracy" (*ca.* 1 kcal mol^{-1}) and fundamental vibrational frequencies within 10 cm^{-1} of those observed experimentally for many of the species pertinent to combustion chemistry. Obtaining these parameters, however, is not trivial and well-calibrated approximations must be made along the way. The aim of this dissertation is to demonstrate that a fruitful synergy between experimental and theoretical chemistry can be established in order to advance our understanding of combustion chemistry and, hence, develop cleaner, more efficient fuels.

1.2 Theoretical Methods

The problem facing quantum chemists is twofold. Practically, an analytic solution to the exact non-relativistic Schrödinger is not possible, so solutions are sought within a certain basis. Often the term "basis set" is used to describe the one-particle basis employed in such computations. These functions are commonly atom-centered Gaussian functions that resemble

the "atomic orbitals" frequently encountered in chemistry. Including an infinite number of these functions would provide all of the freedom needed and would, therefore, not be an approximation. However, this is not possible, so working within a finite basis set introduces an error, hereafter denoted "basis set error" and is the first major hurdle for computational chemists.

The second problem is that having chosen a one-particle basis set, we must correctly describe electron correlation *i.e.* the phenomenon of electrons of opposite spin correlating their motions to avoid each other. This is commonly achieved by expanding the wavefunction in a basis of Slater determinants *i.e.* by explicitly including different occupations of the molecular orbitals in the wavefunction. It is the type of orbital occupations considered and their weighting factor that distinguishes the many post Hartree-Fock methods. It is widely accepted that, of these costly methods, the coupled cluster ansatz, first introduced to electronic structure by Čížek and Paldus,[1,2] is the most efficient.

In coupled cluster, the wavefunction is parameterized by an exponential excitation operator

$$\left|\Psi\right\rangle = e^{T}\left|\Phi\right\rangle, \tag{1.1}$$

where T is an excitation operator and the reference function $\left|\Phi\right\rangle$ is commonly a solution to the Hartree-Fock equations. A rigorous and clear overview of coupled cluster methods can be found in the excellent review by Crawford and Schaefer.[3] Having defined the functional form of the wavefunction, we need to specify T. In coupled cluster with single and double excitations (CCSD), we define

$$T = T_1 + T_2, \tag{1.2}$$

and all single excitations are effected by T_1, with double excitations introduced through the T_2 operator. The commutative nature of the excitation operator allows us to employ the power

series expansion of the exponential operator. Combining equations (1.1) and (1.2) and performing a power series expansion, we can rewrite the CCSD wavefunction:

$$e^{T_1+T_2}\left|\Phi\right\rangle = \left(1 + T_1 + T_2 + \frac{(T_1+T_2)^2}{2!} + \frac{(T_1+T_2)^3}{3!} + \cdots\right)\left|\Phi\right\rangle. \tag{1.3}$$

The important point here is that in equation (1.3) we see that, ignoring numerical denominators, terms such as T_1^3 and T_2T_1 arise, which are triple excitations; likewise, the T_2^2, T_1^4 and $T_2T_1^2$ entities are quadruple excitation operators, so there are product terms in the wavefunction that introduce higher-order excitation character. The appearance of these higher-level operators is the main reason for the efficiency of the coupled cluster approach. The coupled nature of the equations makes them amenable only to iterative solution.

The main drawback to such an approach is the exorbitant computational time required for large systems. There is a term in the CCSD equations that scales as $O(o^2v^4)$, where v is the number of unoccupied orbitals in the wavefunction (and hence increases with one-particle basis set augmentation) and o is the number of occupied orbitals (which increases with the number of electrons in the system). Choosing the cluster operator T such that

$$T = T_1 + T_2 + T_3, \tag{1.4}$$

defines the coupled cluster with single, double and triple excitations (CCSDT). This is analogous to CCSD, but has even more unfavorable scaling, $O(o^3v^5)$, and is still an iterative approach. However, by performing a CCSD computation and applying perturbation theory to the resulting wavefunction, the popular CCSD(T) model is obtained.[4] This powerful method is commonly referred to as the "gold standard" of quantum chemistry due to its efficiency and high accuracy. The (T) correction is a single non-iterative correction to the CCSD wavefunction, that scales as $O(o^3v^4)$, but is easily parallelizable. A single CCSD(T) computation with a reasonable basis set will usually deliver 1-2 kcal mol^{-1} accuracy for relative energies. In order to obtain

more accuracy, higher-order corrections are needed, such as the CCSDT(Q) approach,[5] which applies a non-iterative quadruple excitation term to the aforementioned CCSDT wavefunction in an analogous manner to the (T) correction to CCSD.

The application of these methods, however, requires careful thought. The complete basis set limit of a Hartree-Fock calculation, which neglects electron correlation, is not likely to be very accurate, just as a highly correlated wavefunction computed with a small basis set will be unreliable. In order to compute energies to high precision, we have to combine these two extremes, which we effect through focal point analyses; this concept will be further expounded, but first we will investigate the computation of energies in the limit of an infinite one-particle basis set.

1.3 Basis Set Extrapolation

The necessity to construct wavefunctions in a one-particle basis set introduces basis set truncation error. In Hartree-Fock theory, the wavefunction is written as an antisymmetrized product of one-electron functions and the electrons all move in the average field produced by all of the electrons (which is the origin of its alternative name, self consistent field theory or SCF). The one-particle nature of this wavefunction is highly suitable to description with a one-particle basis set, thus Hartree-Fock is relatively insensitive to the choice of basis set.

Feller demonstrated[6] that the Hartree-Fock energy exhibits an exponential dependence on the maximum angular momentum in the basis set, as long as the basis set is correctly balanced. Dunning has constructed a family of such bases that are now ubiquitous in quantum chemistry, denoted cc-pV*X*Z, where *X* is the "cardinal number" of the basis set, *i.e.* the number of functions used to describe the valence electrons of each atom. The genius of their

construction is that in incrementing the number of functions to describe valence electrons (*e.g. p* orbitals for carbon), extra higher and lower angular momentum functions are introduced; this leads to consistent behavior of the energy upon incrementation of the cardinal number, which is imperative for extrapolation. For the Hartree-Fock energy, the energy for a given cardinal number, *E(X)*, can be expressed as

$$E(X) = A + Be^{-CX}, \tag{1.5}$$

where *A*, *B* and *C* are parameters to be determined by fitting to three computations with different basis sets. The asymptote of this expression yields the complete basis set (CBS) limit, *viz*:

$$E(\infty) = \lim_{X \to \infty} A + Be^{-CX} = A. \tag{1.6}$$

Correlated computations pose a larger problem, however. Here we are trying to model electrons avoiding each other, which is necessarily a two-body phenomenon. There is a rapid decay in the wavefunction, known as the Coulomb hole, as two electrons approach each other, forming a cusp at the coalescence point of the two electrons. This feature of correlated wavefunctions is incredibly difficult to model with a one-particle basis set, hence correlated wavefunctions exhibit significantly more basis set dependence than those devoid of this many-body effect. Using the same Dunning basis sets, Helgaker and co-workers have shown[7] that extrapolation can be performed upon correlation energies, which follow the form

$$E(X) = A + BX^{-3}, \tag{1.7}$$

leading to the simple expression for the CBS correlation energy:

$$E(\infty) = \lim_{X \to \infty} A + BX^{-3} = A. \tag{1.8}$$

A more rigorous and efficient route to removing the basis set error from correlated wavefunctions is through explicitly correlated methods. These methods are similar to conventional coupled cluster and perturbation theories, but have two-electron terms appended to

the conventional products of one-electron functions. These additional terms were originally chosen to be geminals over the interelectronic distance operator r_{12} and are therefore commonly called R12 methods. These additional terms can explicitly model the problematic electron-electron cusp and the Coulomb hole, delivering rapid convergence to the complete basis set limit. Their computational cost is not much greater than their conventional predecessors and it is not inconceivable that these methods will supplant extrapolation techniques within the next few years.

1.4 The Focal Point Approach

Combining the concepts of the preceding sections, the focal point analysis of Allen and co-workers aims to eliminate errors arising from both inexact correlation treatment and basis set truncation. Focal point analyses yield accurate relative energies, however key assumptions must be introduced to make the approach tractable; these will be analyzed here.

First, the geometries of the individual species are optimized at a high level of theory. Around the equilibrium geometry on the "exact" potential energy surface, the energy is approximately quadratic with respect to small displacements. Small errors in the equilibrium geometry will lead to small errors in the absolute energies, which in turn will be largely canceled when calculating relative energies. For this reason, no re-optimization of the geometry is performed as part of the focal point analysis.

Having chosen the reference geometries, a hierarchical series of single point energies are computed, increasing the basis set and the correlation treatment as far as the system size permits. Coupled cluster theory with x-fold excitations included is exact for an x electron system, within a given one-electron basis. This crucial property combined with the advantages discussed above

makes it the method of choice to define the correlation hierarchy in the focal point regime. The resulting energies are extrapolated to compute the CBS limit for those excitation levels where, at least, the basis sets cc-pVTZ and cc-pVQZ can be used. For CCSDT and higher theories, it is often the case that calculations with the cc-pVTZ and cc-pVQZ basis sets are prohibitively expensive, and here a different approximation is introduced.

For each theory that is too expensive to be evaluated with a large basis set, the difference in the energy computed by that theory and the energy emanating from highest level for which extrapolation is performed is assumed to be independent of basis set. This defines the additivity approximation, whereby the difference between two correlation treatments is computed in a small basis and appended to the energy difference computed at the lower level in the complete basis set limit. As a concrete example, consider the case where CCSD(T) energies can be computed using large basis sets and extrapolated, but only cc-pVDZ computations are tractable for CCSDT. Here the complete basis set limit CCSDT energy for CCSDT would be approximated in the focal point regime as

$$E_{\mathrm{CCSDT}}^{\infty} \approx E_{\mathrm{CCSD(T)}}^{\infty} + E_{\mathrm{CCSDT}}^{\mathrm{cc-pVDZ}} - E_{\mathrm{CCSD(T)}}^{\mathrm{cc-pVDZ}} \tag{1.9}$$

Besides the convenience of this additivity assumption, there is a good physical justification for making the approximation. The Coulomb hole that introduces the strong basis set sensitivity to the energy is primarily a two-body effect. The wavefunction is non-zero at the coalescence point of two electrons with opposite spin since the Pauli Exclusion Principle is not violated. Therefore, it is important to model the two-body terms accurately to describe the Coulomb hole, since there is a non-zero contribution to the energy in vicinity of the electron-electron coalescence point. Furthermore, the energy contribution is quite significant in these regions, as the denominator in the Coulomb term of the Hamiltonian is small. Now, considering

the difference between CCSDT and CCSD(T), the two-body terms are cancelled by the subtraction, as both CCSDT and CCSD(T) contain them. There are some remaining three-body terms, but these pose less of a problem. Firstly, the energetic contribution from these terms is small to begin with, so the basis set dependence is also small. Moreover, at the coalescence point of three electrons the wavefunction must be zero as two of the electrons must have the same spin, violating the Pauli Principle; energetically, there is no contribution from regions of configuration space with a zero wavefunction. Given the absence of a significant cusp to model, we can expect the three body and higher terms to be easily modeled in a small basis, thus justifying the assumption of additivity.

We have already noted that an equation analogous to (1.9) defines the final focal point energy but, despite this simple form, a large table showing all of the energies computed at lower levels of theory is usually reported. For example, the CCSD cc-pVTZ energy will be tabulated, but will have no bearing on the final focal point energy; these intermediate results are useful for monitoring convergence with respect to level of theory and thus afford an estimate of the error bars. This feature sets the focal point analysis apart from related high accuracy extrapolation procedures, such as HEAT[8,9] and the W*n* family of methods from the group of Jan Martin.[10,11] The behavior of the energies with respect to basis set size must be monotonic for extrapolation to succeed and this is clearly visualized in a focal point table. Inspecting the difference in relative energies predicted by the highest levels of theory is a good indicator of how close to the exact non-relativistic Born-Oppenheimer energy the final result is.

We conclude this discussion by noting that a number of the energies that enter into a focal point table are computed automatically with the higher-level computations. For example, to obtain a CCSD(T) energy, we first run Hartree-Fock to obtain orbitals, perturbation theory

provides an initial guess for the iterative CCSD procedure, which in turn is necessary for the target CCSD(T) energy. Thus, a single calclulation yields Hartree-Fock, second order Møller-Plesset perturbation theory (MP2), CCSD and CCSD(T) energies. Notwithstanding the sound physical principles set out above, we must concede that the absolute energies from a focal point analysis may not be reliable; however, the relative energies are, as they benefit from a large degree of error cancellation.

1.5 Auxiliary Corrections

So far we have focused on obtaining an exact result within the Born-Oppenheimer approximation neglecting relativity. The Born-Oppenheimer approximation, an adiabatic approximation whereby the timescale of electronic motion is assumed to be much shorter than that of the nuclei, is often justified by considering the large ratio of the nuclear mass to the electronic mass. In this spirit, we recognize that the approximation, although a very strong one, may be less valid in the presence of hydrogen atoms. Commonly, the diagonal Born-Oppenheimer correction (DBOC)[12,13] is computed; this is a first order term that can be essential in the pursuit of "subchemical accuracy" (*ca.* 0.1 kcal mol^{-1}). The DBOC retains the concept of the potential energy surface – something that is missing in the absence of the adiabatic approximation – however a mass-dependence is introduced meaning that isotopically substituted molecules have distinct potential energy surfaces.

The molecules investigated herein comprise only first-row elements and hydrogen. The relatively light nuclei in these molecules do not have sufficient charge to induce significant relativistic behavior in the core electrons, which is observed in heavier elements. For this reason, a first order perturbative treatment[14] is enough to account for relativistic effects in first-row

elements. This correction is composed of mass-velocity and Darwin terms, leading to the acronym MVD.

1.6 Anharmonic Vibrational Frequencies

As part of this study, we will compute fundamental vibrational frequencies; in one instance our motive will be to provide values for spectroscopic characterization and another study will require accurate zero point vibrational energies. We begin by ascribing some coordinate system to the molecule, with indices *i, j, k, l*..., that forms a complete, non-redundant set. We can expand the potential energy using a power series expansion in these coordinates:

$$V(\mathbf{x}) = V_0 + \frac{1}{2}\sum_{ij} \mathrm{H}_{ij}\mathrm{x}_i\mathrm{x}_j + \frac{1}{6}\sum_{ijk} \mathrm{H}_{ijk}\mathrm{x}_i\mathrm{x}_j\mathrm{x}_k + \frac{1}{24}\sum_{ijkl} \mathrm{H}_{ijkl}\mathrm{x}_i\mathrm{x}_j\mathrm{x}_k\mathrm{x}_l + \cdots, \tag{1.10}$$

which lacks a gradient term because we assume that the expansion is centered at a stationary point on the potential energy surface, and the numerical prefactors account for the unrestricted nature of the summations. The tensors, **H**, are the force constants and the vector **x** describes a displacement from equilibrium. The most common method for computing characteristic frequencies is to invoke the harmonic oscillator approximation, under which the potential energy surface is quadratic around the equilibrium (stationary) point, *i.e.* only the first two terms in equation (1.10) are retained. The advantage of doing so is that only second derivatives of the energy with respect to nuclear displacements are required; analytic formulae for the solution of these exist for all common levels of theory, although they are seldom implemented for coupled cluster theory due to the high complexity of the equations. The harmonic potential typically overestimates the curvature, resulting in frequencies that are consistently too high. Realizing this, Scott and Radom[15] performed a systematic study of harmonic frequencies and compared them to experimental values, resulting in some recommended scale factors for various levels of

theory that will give good approximations to fundamental frequencies from harmonic frequencies. This is a pragmatic route to reasonably accurate frequencies for large systems, but in smaller molecules, more rigorous methodology exists.

As in many facets of quantum chemistry, perturbation theory offers a viable route to fundamental frequencies. All perturbation theories stem from the concept of partitioning the exact Hamiltonian operator into two parts: a zeroth-order term that is close to the full Hamiltonian whose exact solution is known, and a small perturbation that delivers the terms missing from the zeroth-order Hamiltonian. In vibrational perturbation theory, the zeroth-order Hamiltonian is the chosen to be the harmonic oscillator Hamiltonian. Second order vibrational perturbation theory (VPT2) then introduces the anharmonic (cubic and quartic) potential terms (*cf.* equation (1.10), terms 3 and 4), as well as anharmonic kinetic energy terms, including Coriolis effects and centrifugal distortion, as a perturbation. The important point to note here is the implicit assumption that the harmonic oscillator provides a faithful representation; if this is not true, such as in many weakly-bound systems, perturbation theory breaks down.

Another potential pitfall occurs when Fermi resonance occurs. This happens when a combination or overtone band has nearly the same frequency as a fundamental, subject to symmetry restrictions. To see the how this may influence the structure of the perturbation theory, we will show some of the equations that define the anharmonicity constants, the rest of which have been detailed elsewhere.[16] The diagonal constants are given by

$$x_{\mathrm{rr}} = \frac{1}{16}\phi_{\mathrm{rrrr}} - \sum_{\mathrm{s}} \frac{\phi_{\mathrm{rrs}}^2(8\omega_{\mathrm{r}}^2 - 3\omega_{\mathrm{s}}^2)}{16\omega_{\mathrm{s}}(4\omega_{\mathrm{r}}^2 - \omega_{\mathrm{s}}^2)}, \tag{1.11}$$

where the tensors $\boldsymbol{\phi}$ are the force constants expressed in dimensionless normal coordinates. Careful consideration of equation (1.11) reveals the diagonal anharmonicity constant will be close to $-\infty$ when $2\omega_{\mathrm{r}} \approx \omega_{\mathrm{s}}$ and the cubic force constant in the numerator, ϕ_{rrs}, is non-zero; this

situation results in a catastrophic breakdown of VPT2 and we must proceed with caution. The problematic term in this equation can be factored as follows:

$$\frac{\phi_{\mathrm{rrs}}^2(8\omega_{\mathrm{r}}^2 - 3\omega_{\mathrm{s}}^2)}{16\omega_{\mathrm{s}}(4\omega_{\mathrm{r}}^2 - \omega_{\mathrm{s}}^2)} = \frac{\phi_{\mathrm{rrs}}^2}{32}\left[\frac{1}{2\omega_{\mathrm{r}} + \omega_{\mathrm{s}}} - \frac{1}{2\omega_{\mathrm{r}} - \omega_{\mathrm{s}}} + \frac{4}{\omega_{\mathrm{s}}}\right], \tag{1.12}$$

and in the presence of an overtone-type Fermi resonance, we can make the replacement

$$\frac{\phi_{\mathrm{rrs}}^2}{32}\left[\frac{1}{2\omega_{\mathrm{r}} + \omega_{\mathrm{s}}} - \frac{1}{2\omega_{\mathrm{r}} - \omega_{\mathrm{s}}} + \frac{4}{\omega_{\mathrm{s}}}\right] \rightarrow \frac{\phi_{\mathrm{rrs}}^2}{32}\left[\frac{1}{2\omega_{\mathrm{r}} + \omega_{\mathrm{s}}} + \frac{4}{\omega_{\mathrm{s}}}\right], \tag{1.13}$$

which circumvents the instability induced in the equations. The excluded term is then introduced by explicit diagonalization of a small Hamiltonian matrix that couples the interacting mode; this procedure is detailed in Chapter 2. An analogous situation exists for the off-diagonal anharmonicity constants, involving the resonance $\omega_{\mathrm{r}} \approx \omega_{\mathrm{s}} + \omega_{\mathrm{t}}$, and is treated analogously. Full details are omitted here, as they have been provided in the literature.[16]

One interesting point to notice is that the reduced normal coordinate system employed here has a mass-dependence. To compute fundamental vibrational frequencies, we need at most the semi-diagonal quartic force constants, ϕ_{iijj}, which is fortuitous as the partial quartic force field is easier to compute than the full force field. However, in our analysis, we commonly want to compute isotopic shifts, so we compute the full set of quartic force constants, ϕ_{ijkl}, which permits transformation to any quartic representation of the potential energy.

Having derived the anharmonicity constants, the vibrational energy levels of an asymmetric top molecule are given by

$$G(\mathbf{v}) = \sum_{\mathrm{r}} \omega_{\mathrm{r}}(\mathrm{v}_{\mathrm{r}} + \frac{1}{2}) + \sum_{\mathrm{r} \geq \mathrm{s}} x_{\mathrm{rs}}(\mathrm{v}_{\mathrm{r}} + \frac{1}{2})(\mathrm{v}_{\mathrm{s}} + \frac{1}{2}) + \cdots, \tag{1.14}$$

from which we neglect the higher terms within the VPT2 framework. The zero point vibrational energy (ZPVE) is then given by

$$G(0) = \sum_{r} \frac{\omega_r}{2} + \sum_{r \geq s} \frac{x_{rs}}{4}, \tag{1.15}$$

with some additional kinetic energy contributions. Furthermore, the fundamental vibrational frequency ν_r is defined using equation (1.14) as $G(v_r=1) - G(v_r=0)$, leading to the simple form

$$\nu_r = \omega_r + 2x_{rr} + \sum_{s \neq r} \frac{x_{rs}}{2}. \tag{1.16}$$

1.7 Kinetics and Thermodynamics in Combustion

We have already alluded to the complexity of modeling combustion reactions. The first step in constructing a quantitative model is the determination of the elementary reactions that have a significant contribution to the global process. This is commonly achieved by performing a cursory search of the potential energy surface for a given set of atoms with a low level of theory, such as density functional theory (DFT). Significant errors could result if these relative energies and barrier heights were naïvely used to model the chemistry, as DFT typically underestimates barrier heights, and can fail seriously when multi-reference character is present (*i.e.* the wavefunction is not qualitatively well described by a single electronic configuration). For this reason, the important pathways are refined using theory and/or experiments. In an excellent review article,[17] Jim Miller – a major player in the field of combustion modeling – has demonstrated the importance of accurate kinetics and thermochemistry for elementary reaction steps and underlined the difficulty in obtaining such data.

Reaction rates can be computed theoretically using theories such as transition state theory (TST)[18] or the more elaborate Rice-Ramsperger-Kassel-Marcus (RRKM) theory.[19] Alternatively, the familiar Arrhenius form of the rate expression, or modifications thereof can be derived from experiments, typically using laser induced fluorescence (LIF) and diode laser

absorption detection.[20] Relative energies are usually obtained via enthalpies of formation,[†] due to the transferability of this quantity amongst reactions. Therefore accurate enthalpies of formation are required and theory can aid in the computation of these, as we will demonstrate in this dissertation.

There are two routes to the computation of enthalpies of formation: direct and indirect. The direct route would be to follow the definition of the enthalpy of formation and compute the enthalpy change in proceeding from the constituent elements in their natural state. Given that all molecules of interest here contain carbon, we would need to be able to compute the energy of a carbon atom in graphite, which is not feasible. The indirect approach invokes Hess' law to compute the enthalpy change in going from some reference compound(s), whose enthalpy of formation is known, to the target compound. In this framework, the atomization (dissociation of the molecule to gaseous atoms) route is one possibility since the enthalpy of formation of gaseous atoms is well-determined for most elements and the reactions are simply defined. The drawback, however is that the enthalpy change must be computed to unreasonable precision.

If we consider a collection of gaseous atoms combining to form a molecule, there is a ZPVE present in the molecule that is absent in the collection of atoms. Therefore, the vibrational levels must be known to very high precision, as there is no possibility of error cancellation. Also, if the molecule is a closed shell species, there will be no spin-orbit coupling to compute, which is present in the atoms with high-spin ground states; this will also lead to a situation devoid of any error cancellation.

To remedy this situation, we employ reactions that use reference compounds with a similar structure to the target compound, thus maximizing error cancellation.[21] Such reaction

[†] The term "heat of formation" is commonly used instead of "enthalpy of formation", however the latter is preferred, as heat is not a state function.

schemes can be categorized as follows. Isogyric reactions are simply chosen to conserve spin on both sides of the equation, this precludes almost all atomization approaches, which commonly dissociate low-spin molecules to high-spin atoms. Isodesmic reactions[22] stipulate that the same connectivity is present on each side of the equation, while homodesmotic reactions[23] impose the additional constraint that the sum of hybridization types at each carbon center be preserved. These reactions were originally conceived to maximize error cancellation at a time when computational power was not conducive to high-level computations. Even though more accurate computations are not affordable, it still makes sense to take advantage of as much error cancellation as possible.

1.8 Prospectus

We begin by computing the fundamental frequencies of a transient radical, NCCO, in Chapter 2. The purpose of this work is to provide accurate fundamental frequencies onto which a diode laser can be tuned in order to perform experimental kinetics studies. Such experiments have previously been attempted, but to no avail due to an apparent misassignment of the vibrational frequencies of NCCO. Simultaneously we refine the enthalpy of formation for this radical. In Chapter 3, we revisit the enthalpy of formation for the important diacetylene molecule, which is a remarkably stable intermediate in combustion, utilizing the methodology described above and considering the effects of vibrational anharmonicity. In Appendix A, which is not included as a chapter due to its collaborative nature, we investigate the unimolecular decomposition of ortho-benzyne into acetylene and the aforementioned diacetylene molecule, providing accurate energetics for the lowest energy retro-Diels-Alder pathway.

REFERENCES

[1] J. Čížek, Adv. Chem. Phys. **14**, 35 (1969).

[2] J. Čížek and J. Paldus, Int. J. Quantum Chem **5**, 359 (1971).

[3] T. D. Crawford and H. F. Schaefer, Rev. Comput. Chem. **14**, 33 (2000).

[4] K. Raghavachari, G. W. Trucks, J. A. Pople, and M. Head-Gordon, Chem. Phys. Lett. **157**, 479 (1989).

[5] Y. J. Bomble, J. F. Stanton, M. Kallay, and J. Gauss, J. Chem. Phys. **123**, 054101 (2005).

[6] D. Feller, J. Chem. Phys. **98**, 7059 (1993).

[7] T. Helgaker, W. Klopper, H. Koch, and J. Noga, J. Chem. Phys. **106**, 9639 (1997).

[8] Y. J. Bomble, J. Vázquez, M. Kállay, C. Michauk, P. G. Szalay, A. G. Császár, J. Gauss, and J. F. Stanton, J. Chem. Phys. **125**, 064108 (2006).

[9] A. Tajti, P. G. Szalay, A. G. Császár, M. Kállay, J. Gauss, E. F. Valeev, B. A. Flowers, J. Vázquez, and J. F. Stanton, J. Chem. Phys. **121**, 11599 (2004).

[10] J. M. L. Martin and G. De Oliviera, J. Chem. Phys. **111**, 1843 (1999).

[11] A. D. Boese, M. Oren, O. Atasoylu, J. M. L. Martin, M. Kállay, and J. Gauss, J. Chem. Phys. **120**, 4129 (2004).

[12] H. Sellers and P. Pulay, Chem. Phys. Lett. **103**, 463 (1984).

[13] N. C. Handy, Y. Yamaguchi, and H. F. Schaefer, J. Chem. Phys. **84**, 4481 (1986).

[14] R. D. Cowan and D. C. Griffin, J. Opt. Soc. Am. **66**, 1010 (1976).

[15] A. P. Scott and L. Radom, J. Phys. Chem. **100**, 16502 (1996).

[16] D. A. Clabo, W. D. Allen, R. B. Remington, Y. Yamaguchi, and H. F. Schaefer, Chem. Phys. **123**, 187 (1988).

[17] J. A. Miller, M. J. Pilling, and J. Troe, Proc. Comb. Inst. **30**, 43 (2005).

[18] L. B. Harding, S. J. Klippenstein, and J. A. Miller, J. Phys. Chem. A **112**, 522 (2008).

[19] R. A. Marcus, J. Chem. Phys. **20**, 359 (1952).

[20] W. Feng, J. P. Meyer, and J. F. Hershberger, J. Phys. Chem. A **110**, 4458 (2006).

[21] S. E. Wheeler, PhD. Thesis, University of Georgia, 2006.

[22] W. J. Hehre, R. Ditchfield, L. Radom, and J. A. Pople, J. Am. Chem. Soc. **92**, 4796 (1970).

[23] P. George, M. Trachtman, C. W. Bock, and A. M. Brett, Theor. Chem. Acc. **38**, 121 (1975).

CHAPTER 2

IN SEARCH OF DEFINITIVE SIGNATURES OF THE ELUSIVE NCCO RADICAL[†]

[†] A. C. Simmonett, F. A. Evangelista, W. D. Allen, and H. F. Schaefer, J. Chem. Phys. **127** 014306 (2007). Reprinted here with permission of the American Institute of Physics.

2.1 ABSTRACT

Previous experimental assignments of the fundamental vibrational frequencies of NCCO have been brought into question by subsequent unsuccessful attempts to observe IR signatures of this radical at these frequencies. Here we compute the fundamental vibrational frequencies by applying second-order vibrational perturbation theory (VPT2) to the complete quartic force field computed at the all-electron (AE) coupled cluster singles, doubles, and perturbative triples level [CCSD(T)] with the correlation-consistent, polarized core-valence quadruple-zeta (cc-pCVQZ) basis set, which has tight functions to correctly describe core correlation. The AE-CCSD(T)/cc-pCVQZ geometric parameters are r_e(N-C) = 1.1623 Å, r_e(C-C) = 1.4370 Å, r_e(C-O) = 1.1758 Å, θ_e(N-C-C) = 168.55°, and θ_e(C-C-O) = 132.22°. Our CCSD(T)/cc-pCVQZ values of the characteristic stretching frequencies ν_1 and ν_2 are 2171 cm^{-1} and 1898 cm^{-1}, respectively, in stark contrast to the experimentally-derived values of 2093 cm^{-1} and 1774 cm^{-1}. Finally, focal-point extrapolations using correlation-consistent basis sets cc-pVXZ (X = D,T,Q,5,6) and electron correlation treatments as extensive as full coupled cluster singles, doubles, and triples (CCSDT) with perturbative accounting of quadruple excitations [CCSDT(Q)] determine the vibrationless barrier to linearity of NCCO and the dissociation energy (D_0) of NCCO → NC + CO to be 8.4 kcal mol^{-1} and 26.5 kcal mol^{-1}, respectively. Using our precisely determined dissociation energy, we recommend a new 0 K enthalpy of formation for NCCO of 50.9 ± 0.3 kcal mol^{-1}.

2.2 INTRODUCTION

The NCCO radical is thought to be an important intermediate in combustion chemistry, but no gas-phase IR signatures of this species have ever been detected unambiguously. This absence of information is not through a lack of attention, as a number of experimental[1-5] and theoretical[6-9] studies concerning NCCO have been published in the literature. The isoelectronic HCCCO radical has also been investigated as an intermediate in combustion chemistry.[10,11]

Generation of NCCO from many precursors has been well documented,[12-16] reinforcing the viability of this radical in combustion processes. Such parent compounds include carbonyl cyanide[2,12] [$CO(CN)_2$], pivaloyl cyanide[2] [$NCC(O)C(CH_3)_3$], methyl cyanoformate[2] [$NCC(O)OCH_3$], and acetyl cyanide[14] [$CH_3C(O)CN$]. The photofragment translational energy spectroscopy study of Furlan, Scheld, and Huber[13] measured the product kinetic energy distributions and determined the preferred dissociation channels from all of these potential precursors. They identified NCCO as the major product of photolysis of methyl cyanoformate, carbonyl cyanide and pivaloyl cyanide at 193 nm, but showed that acetyl cyanide generates the CN radical as the major product at the same wavelength. McNavage, Dailey, and Dai[2] were thus motivated to photodissociate the first three compounds in order to perform the first vibrational characterization of the NCCO radical. The photolysis species were probed by means of time-resolved Fourier transform infra-red emission spectroscopy (TR-FTIRES). The spectra emanating from the different precursors were disentangled by means of two-dimensional cross-spectra correlation analysis,[1] devised to elucidate the features due to NCCO; this analysis yielded (ν_1, ν_2) values of (2093, 1774) cm^{-1}.

Inspired by this research, Hershberger and co-workers[17] intended to use these characteristic frequencies to monitor the NCCO radical via infrared diode laser absorption

spectroscopy in order to study the kinetics of its reactions with NO_x species. Despite using methyl cyanoformate and acetyl cyanide precursors, which have proved to be reliable sources of NCCO, no signals were observed that could be definitively ascribed to the ν_1 mode of the NCCO radical. Instead, both CN radicals and hot bands of vibrationally excited CO were found in this region. The stability of NCCO has been demonstrated by neutralization-recombination mass spectrometry (NRMS),[4] which also confirmed the stability of its cation and the bonding connectivity. This bodes well for future spectroscopic studies; however, the absorption frequencies must be definitively determined to facilitate the detection and monitoring of this important species.

Despite a number of studies in the literature, there is a dearth of highly accurate vibrational information from theory. The highest-level theoretical vibrational frequencies reported thus far are due to Francisco and Liu.[7] They applied the [UQCISD, UQCISD(T)] methods, in conjunction with the modest 6-31G(d) basis set, which yielded ν_1 = (2293, 2304) cm^{-1} and ν_2 = (1939, 1936) cm^{-1}, within the harmonic approximation. The UQCISD values were then scaled by a factor of 0.9537 in accord with the accepted recommendations of Scott and Radom[18] to account for anharmonicity. Their study indicated that ν_1 is the most intense mode, an order of magnitude stronger than ν_2. All other modes were found to be an order of magnitude weaker than the ν_2 mode, which places strong emphasis on the critical ν_1 (CN stretching) and ν_2 (CO stretching) modes from a spectroscopic viewpoint.

The principal aim of this study is to pinpoint the fundamental vibrational frequencies of NCCO using state-of-the-art computational methods, paying particular attention to the highest intensity (ν_1 and ν_2) modes to facilitate the detection of this species in combustion environments. In order to examine the fate of NCCO produced with excess energy, we ascertain the dissociation

energy with respect to CN and CO. This information will also permit the accurate determination of the enthalpy of formation for NCCO. Finally, the converged barrier to linearity is computed to assess whether large-amplitude bending should complicate the rovibrational structure of NCCO.

2.3 Theoretical Methods

Optimized equilibrium geometries and full quartic force fields of all species were computed at the highly accurate all-electron coupled cluster singles, doubles, and perturbative triples [CCSD(T)] level. The large correlation consistent, core-valence polarized, quadruple zeta (cc-pCVQZ) basis set of Woon and Dunning was used.[19] For the N, C, and O atoms, the cc-pCVQZ basis is a [15*s*9*p*5*d*3*f*1*g* / 8*s*7*p*5*d*3*f*1*g*] set, and for NCCO it comprises 322 contracted Gaussian functions. All electrons were correlated to obtain near spectroscopic accuracy for the quartic force field; the prefix AE will be adopted to denote all-electron computations to avoid confusion with the valence computations employed in the energy refinements. This combination of correlation treatment and basis set has been validated in an extensive study of 19 molecules,[20] which showed the mean absolute deviation in bond lengths to be 0.0009 Å for direct minimization of the energy at the aforementioned level of theory, relative to highly precise, empirically-determined structures. The corresponding error in the bond angles was 0.52°. These mean absolute errors were reduced to an impressive 0.0006 Å and 0.21° with the exclusion of the H_2O_2 molecule from the test set, prompting the authors to call for an experimental reinvestigation of this molecule.

To circumvent potential problems with spin contamination, all open-shell computations were based upon a single-determinant, restricted open-shell Hartree-Fock (ROHF) reference

function, unless otherwise stated. The coupled cluster energy was computed using the generalized approach of Watts, Gauss, and Bartlett.[21] This use of restricted orbitals with no restrictions placed on the amplitudes is most appropriately termed ROHF-UCCSD(T), but for brevity we refer to this method as ROCCSD(T) hereafter. In the closed-shell case (the CO molecule), the reference function was a restricted Hartree-Fock (RHF) determinant and the CCSD(T) energy could be computed within a fully restricted formalism.[22] In order to compute the perturbative triples contribution efficiently in the open-shell case, the orbitals are rotated to the semicanonical basis,[21,23,24] which can lift the degeneracy of the α and β orbitals and, hence, introduce some spin contamination. This is readily quantified by computing the spin contamination[25] $\left\langle \hat{S}^2 - \hat{S}_z^2 - \hat{S}_z \right\rangle$ for the CCSD wavefunction, which is an important diagnostic to assess the quality of the final result. For all of the displaced geometries required in the quartic force field computation, this spin contamination in the wavefunction was found to lie between 0.0030 and 0.0034, with a mean of 0.0032, indicating the presence of a negligible and consistent amount across the geometric configuration space sampled.

In order to quantify the anharmonicity contributions to the fundamental frequencies, the third and fourth derivatives of the molecular energy, with respect to nuclear coordinates, were computed. This was effected by numerical differentiation of tightly converged energies at displaced geometries, again using the AE-ROCCSD(T)/cc-pCVQZ level of theory. The internal coordinates were chosen as

$$
\begin{aligned}
S_1 &= r(\mathrm{N-C}) \\
S_2 &= r(\mathrm{C-C}) \\
S_3 &= r(\mathrm{C-O}) \\
S_4 &= \alpha_x(\mathrm{N-C-C\text{-}O}) = \sin(\rho)\cos(\tau) \\
S_5 &= \theta(\mathrm{C-C-O}) \\
S_6 &= \alpha_y(\mathrm{N-C-C\text{-}O}) = \sin(\rho)\sin(\tau) \\
\rho &\equiv \theta(\mathrm{N-C-C})
\end{aligned}
\tag{2.1}
$$

where r represents a bond length between two connected atoms, θ is a valence bond angle, and τ is the N-C-C-O torsional angle. The linear bending coordinates α_x and α_y change sign as the N-C-C angle progresses through linearity, thus averting singularities; for this reason, their use was advocated in a study of the geometrically similar HNCO molecule.[26] The full quartic force field in internal coordinates is provided as Supplementary Material.[27]

Computation of the quartic force field required 263 energies at displaced geometries, which were converged to 10^{-11} E_h in order to maintain sufficient numerical precision. Vibrational anharmonicities were computed by application of second-order perturbation theory[26,28-34] (VPT2) to the quartic force field represented in reduced normal coordinates. The *Mathematica*[35] program INTDIF2005[36,37] was used to compute the force constants in internal coordinates; INTDER2005[38,39] was used to execute the nonlinear transformation to the Cartesian space,[40,41] whereupon the ANHARM[39,42] program was run for the VPT2 analysis.

For the determination of the barrier to linearity and dissociation energy, the valence focal point analysis scheme of Allen and co-workers[43-46] was invoked in order to refine the coupled cluster energetics. This method involves systematically increasing both the correlation treatment and the basis set used, allowing extrapolation[47,48] to the complete basis set (CBS) limit, while monitoring convergence towards the full configuration interaction (FCI) limit. The frozen core approximation was initially employed, and the cc-pV*X*Z (*X* = D, T, Q, 5, 6) basis sets of

Dunning and co-workers[49,50] were used, due to their high suitability for such extrapolations. Finally, the core correlation contribution was computed as

$$\Delta E_{core} = E^{cc-pCVQZ}_{CCSD(T)(AE)} - E^{cc-pCVQZ}_{CCSD(T)(fc)} \tag{2.2}$$

where AE (first term) denotes all electrons correlated and fc (second term) signifies only valence electrons correlated. This core correction was applied to the valence-only results to correct for the assumption of a frozen core in performing the focal point analysis.

Many flavors of open-shell perturbation theory exist when using a restricted reference function, due to the inherent ambiguity in choice of zeroth-order Hamiltonian.[51] We chose to employ the ZAPT2 method of Lee and Jayatilaka,[52] due to its computational efficiency and lack of spin contamination at second order. However, it should be noted that these values serve only as a convergence monitor, because the ROCCSD(T) energies were obtained with basis sets ranging all the way up to those used for the ZAPT2 computations; the main correlation sequence in the focal point analysis is the increase in completeness of coupled cluster model. To account for the effects of connected quadruple excitations in coupled cluster theory, we also explicitly computed energies at the newly developed CCSDT(Q) level.[53,54] The treatment of connected quadruple excitations in this highly accurate method stems from a non-hermitian perturbation theory, in the same vain as the triples correction in the now commonplace CCSD(T) model. The CCSDT(Q) method has been shown[53] to deliver results very close to the full quadruples coupled cluster model (CCSDTQ) for a test set of 24 small molecules of varying multiplicity, composed of first-row main group elements. The perturbative quadruple excitation methods are currently only implemented for UHF and RHF reference functions; however, the explicit inclusion of triple excitations is sufficient to overcome the major effects of the spin contamination (which is

severe for the CN radical) encountered in the unrestricted Hartree-Fock solution, so UCCSDT(Q) can be expected to perform as well as ROCCSDT(Q).[55]

To improve upon the Born-Oppenheimer approximation, whereby the electronic energy is evaluated under the assumption of stationary nuclei, the Diagonal Born-Oppenheimer correction[56,57] (DBOC) was appended to the final result. The DBOC does not diminish the concept of a potential energy surface; however it does introduce a mass dependence. Following the highly accurate HEAT protocol,[58] the DBOC was computed at the restricted Hartree-Fock level with the aug-cc-pVTZ basis set.[59]

Further refinements came from consideration of scalar relativistic effects at first-order, by including the effect of one-electron Darwin terms and mass-velocity contributions. This treatment, which was performed at the all-electron CCSD(T)/aug-cc-pCVTZ level, has been advocated for first row atoms,[60,61] where additional second-order Douglas-Kroll corrections are negligible.

All electronic structure computations were carried out using the MOLPRO 2002.6 suite of programs,[62] ACESII,[63,64] MPQC,[65] and the string-based MRCC code[54] of Kállay and co-workers.

2.4 Results And Discussion

The optimized geometries for all species are shown in Figure 2.1. The C_s symmetry structure obtained for the $^2A'$ ground state of NCCO is qualitatively consistent with those determined in previous studies. Our AE-CCSD(T)/cc-pCVQZ geometry has bond lengths that are more contracted than the AE-CCSD(T)/cc-pCVTZ structure reported by Sumiyoshi, Takada, and Endo.[3] Comparison with experimental r_e geometries[66,67] for the diatomic species inspires

confidence in the AE-CCSD(T)/cc-pCVQZ method, with deviations of only 0.0001 Å and 0.0007 Å for CN and CO, respectively.

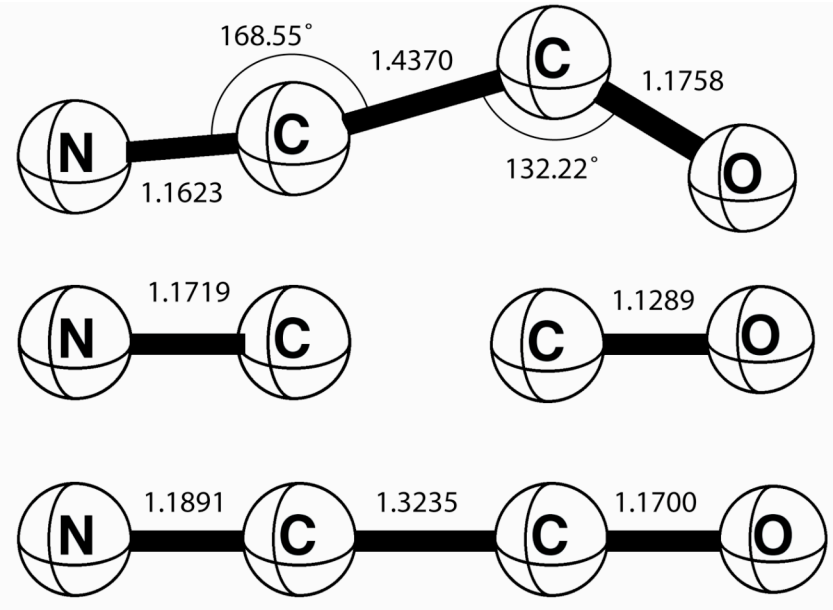

Figure 2.1. The AE–CCSD(T)/cc–pCVQZ equilibrium geometries (Å and deg) of NCCO ($\widetilde{X}\ ^2A'$), CN ($X\ ^2\Sigma^+$), CO($X\ ^1\Sigma^+$), and the NCCO ($^2\Pi$) stationary point. For CN, high–resolution diode laser spectroscopy[67] gives r_e = 1.1718 Å, while for CO, a fit to many high–resolution spectroscopic measurements[66] yields r_e =1.1283 Å.

Table 2.1. Rotational constants (MHz) of $\widetilde{X}\ ^2A'$ NCCO.

Method	Reference	Rigid Rotor Assumed?	A	B	C	(B+C)/2
QCISD/6-31G(d)	7	yes	162068	4756	4621	4689
QCISD(T)/6-31G(d)	7	yes	164315	4730	4598	4664
AE-ROCCSD(T)/cc-pCVTZ	3	yes	178470	4789	4664	4727
AE-ROCCSD(T)/cc-pCVQZ	This work	yes	180728	4813	4688	4750
AE-ROCCSD(T)/cc-pCVQZ	This work	no[a]	191651	4795	4670	4732
Experiment	3	no[b]				4736

[a] Anharmonicity introduced through explicit consideration of vibration-rotation interaction constants and centrifugal distortion constants within a vibrational perturbation theory framework.[30]

[b] Single rotational constant obtained from fitting experimental rotational transitions to a linear $^2\Sigma$ Hamiltonian.

Table 2.1 shows the rotational constants of the NCCO molecule, from various theoretical and experimental studies. Although no experimental geometry has been reported for NCCO *per se*, Sumiyoshi *et al.*[3] provided an experimental rotational constant, which was obtained by fitting their observed rotational transition frequencies using a standard $^2\Sigma$ Hamiltonian involving a single, averaged rotational constant. Our post-rigid-rotor rotational constants were obtained by explicit consideration of the vibration-rotation interaction constants as well as the centrifugal distortion constants. These vibration-rotation interaction constants (α_i) appear in Table 2.2. Assuming prolate near-symmetric top behavior, the average of our $\widetilde{B}$ and $\widetilde{C}$ rotational constants may be compared with Sumiyoshi's single averaged constant, and indeed the two do agree remarkably well, to within 0.01% (Table 2.1). Without such anharmonicity corrections, the AE-ROCCSD(T)/cc-pCVQZ averaged rotational constant shows an error of 0.3% with respect to the experimentally determined value.

Table 2.2. Vibration-rotation interaction constants (10^{-3} cm^{-1}) for the NCCO molecule, derived from the AE-ROCCSD(T)/cc-pCVQZ anharmonic force field.

	NCCO	^{15}NCCO	N^{13}CCO	NC^{13}CO	NCC^{18}O
α_1^A	–177.8	–173.0	–171.3	–169.7	–174.7
α_2^A	193.2	189.6	191.3	175.8	192.8
α_3^A	–206.0	–212.1	–212.3	–162.0	–219.1
α_4^A	–406.5	–400.4	–399.5	–390.0	–381.4
α_5^A	–1224.9	–1218.7	–1453.6	–1039.5	–1025.1
α_6^A	1093.3	1086.1	1325.4	918.0	898.1
α_1^B	1.107	1.077	1.052	1.100	1.057
α_2^B	0.211	0.205	0.214	0.202	0.198
α_3^B	1.100	1.048	1.115	1.045	1.057
α_4^B	–0.014	–0.008	–0.030	–0.008	–0.006
α_5^B	–0.351	–0.347	–0.323	–0.360	–0.324
α_6^B	–0.831	–0.803	–0.810	–0.814	–0.789
α_1^C	0.928	0.910	0.881	0.912	0.888
α_2^C	0.322	0.307	0.322	0.313	0.304
α_3^C	0.985	0.941	0.995	0.937	0.945
α_4^C	0.035	0.035	0.027	0.039	0.034
α_5^C	–0.577	–0.561	–0.552	–0.583	–0.531
α_6^C	–0.475	–0.465	–0.457	–0.456	–0.461

In their theoretical study of NCCO, Francisco and Liu concluded[7] that "the linear structure is on the seam of crossing between the ground and the $\tilde{A}\ ^2A''$ state potential energy surfaces" which, in other words, indicates that NCCO in its linear $^2\Pi$ state is a Renner-Teller molecule. We also found this to be the case, with optimization of the $\tilde{A}\ ^2A''$ state, starting from the $\tilde{X}\ ^2A'$ geometry, leading to the $^2\Pi$ linear structure (Figure 2.1). Furthermore, we computed harmonic vibrational frequencies of the linear $^2\Pi$ state (Table 2.3), revealing three positive force constants and one negative force constant for the bending modes, as opposed to the two doubly-degenerate modes with positive curvature expected for a closed-shell, linear tetra–atomic

molecule at its equilibrium geometry. The negative curvature occurs along the bending mode leading to the $^2A'$ ground state, while bending in the perpendicular plane, to a $^2A''$ state, has positive curvature, which casts this molecule as a case (C) Renner-Teller system.[68] These results are confirmed by the vibrationless barrier to linearity and the $^2A'' \leftarrow \widetilde{X}\ ^2A'$ vertical excitation energy, which are 8.4 kcal mol^{-1} and 38.4 kcal mol^{-1}, respectively, at the AE-ROCCSD(T)/cc-pCVQZ level of theory.

Table 2.3. Harmonic vibrational frequencies (cm^{-1}), computed at the AE-ROCCSD(T)/cc-pCVQZ level of theory.

Mode[a]	IR Intensity[b]	$\widetilde{X}\ ^2A'$ NCCO	$^2\Pi$ NCCO	$X\,^1\Sigma^+$ CO + $X\,^2\Sigma^+$ CN
ω_1 (a')	26.2	2214	2261	2076 (CN)
ω_2 (a')	152.6	1919	1890	2174 (CO)
ω_3 (a')	13.9	818	906	
ω_4 (a')	14.2	588	593	
ω_5 (a')	10.0	222	234	
ω_6 (a'')	8.0	269	303	
			421i	

[a] The normal mode designation corresponds to the $^2A'$ structure.

[b] The infrared intensity (km mol^{-1}) from a frozen-core computation at the ROCCSD/cc-pVTZ level, within the harmonic approximation.

The IR intensities for NCCO computed at the valence ROCCSD(T)/cc-pVTZ level, within the double harmonic approximation are shown in Table 2.3, along with the AE-ROCCSD(T)/cc-pCVQZ harmonic vibrational frequencies of all species involved in this study. Our IR intensities reveal that the ω_2 mode (CO stretch) is actually the most intense (153 km mol^{-1}), with the ω_1 (CN stretch) giving the next strongest signal (26 km mol^{-1}). Given that the lowest IR intensity is 8 km mol^{-1}, we find a much smaller range of intensities than Francisco and Liu did[7] from their UQCISD(T)/6-31G(d) computations; their values ranged from 1333 km mol^{-1} (ω_1) down to 2 km mol^{-1} (ω_4). Furthermore, their relatively low ω_2 intensity of 135 km

mol^{-1} places far more emphasis on the CN stretching mode that those set forth in the current work.

Table 2.4. Vibrational frequencies (cm^{-1}) of various isotopologues of $\tilde{X}\ ^2A'$ NCCO at the AE-ROCCSD(T)/cc-pCVQZ level of theory, from second-order vibrational perturbation theory (VPT2).[a]

Mode	Description	ω	Δ[b]	Δ_{res}[c]	ν	TED[d]
NCCO						
$\nu_1(a')$	C-N stretch	2213.6	–42.6	0.0	2171	$S_1(91) - S_2(8)$
$\nu_2(a')$	C-O stretch	1918.5	–20.5	0.0	1898	$S_3(96)$
$\nu_3(a')$	C-C stretch	817.9	–22.9	2.0	797	$S_2(87) + S_1(6)$
$\nu_4(a')$	sym. in-plane bend	588.1	–10.7	0.0	577	$S_5(59) + S_4(34)$
$\nu_5(a')$	asym. in-plane bend	222.2	–0.4	0.0	222	$S_4(63) - S_5(37)$
$\nu_6(a'')$	N-C-C out-of-plane bend	268.9	0.7	0.0	270	$S_6(100)$
^{15}NCCO						
$\nu_1(a')$	C-N stretch	2184.8	–41.3	0.0	2144	$S_1(91) - S_2(9)$
$\nu_2(a')$	C-O stretch	1918.1	–20.8	0.0	1897	$S_3(96)$
$\nu_3(a')$	C-C stretch	811.6	–22.5	2.0	791	$S_2(86) + S_1(6)$
$\nu_4(a')$	sym. in-plane bend	585.2	–10.6	0.0	575	$S_5(59) + S_4(34)$
$\nu_5(a')$	asym. in-plane bend	220.3	–0.4	0.0	220	$S_4(63) - S_5(37)$
$\nu_6(a'')$	N-C-C out-of-plane bend	266.9	0.8	0.0	268	$S_6(100)$
N^{13}CCO						
$\nu_1(a')$	C-N stretch	2162.1	–38.9	0.0	2123	$S_1(92) - S_2(8)$
$\nu_2(a')$	C-O stretch	1918.3	–20.7	0.0	1898	$S_3(96)$
$\nu_3(a')$	C-C stretch	812.4	–23.3	1.6	791	$S_2(88) + S_1(5)$
$\nu_4(a')$	sym. in-plane bend	578.7	–10.3	0.0	568	$S_5(61) + S_4(33)$
$\nu_5(a')$	asym. in-plane bend	219.4	-0.2	0.0	219	$S_4(64) - S_5(36)$
$\nu_6(a'')$	N-C-C out-of-plane bend	261.3	1.0	0.0	262	$S_6(100)$

[a] Most abundant isotopic species assumed, unless otherwise stated.

[b] Second-order vibrational anharmonicity from VPT2 theory.

[c] Additional contribution to the anharmonicity from the (ν_3, $\nu_4+\nu_5$) resonance.

[d] Total energy distribution.[74,75] The percentage p contribution to the total energy (kinetic and potential) to each normal mode from the internal coordinate x is denoted $S_x(p)$. The internal coordinates are defined in the text. The sign of each term represents the relative phase of each internal coordinate in the normal mode eigenvector.

Table 2.4 (continued). Vibrational frequencies (cm^{-1}) of various isotopologues of $\tilde{X}\ ^2A'$ NCCO at the AE-ROCCSD(T)/cc-pCVQZ level of theory, from second-order vibrational perturbation theory (VPT2).[a]

Mode	Description	ω	Δ^b	Δ_{res}^c	ν	TED[d]
$NC^{13}CO$						
$\nu_1(a')$	C-N stretch	2212.8	–42.8	0.0	2170	$S_1(92) - S_2(8)$
$\nu_2(a')$	C-O stretch	1874.2	–19.7	0.0	1855	$S_3(97)$
$\nu_3(a')$	C-C stretch	801.3	–21.1	-3.0	777	$S_2(89) + S_1(6)$
$\nu_4(a')$	sym. in-plane bend	583.4	–10.7	0.0	573	$S_5(60) + S_4(35)$
$\nu_5(a')$	asym. in-plane bend	220.7	-0.6	0.0	220	$S_4(62) - S_5(38)$
$\nu_6(a'')$	N-C-C out-of-plane bend	268.5	0.5	0.0	269	$S_6(100)$
$NCC^{18}O$						
$\nu_1(a')$	C-N stretch	2213.6	–43.1	0.0	2170	$S_1(91) - S_2(8)$
$\nu_2(a')$	C-O stretch	1875.4	–18.4	0.0	1857	$S_3(96)$
$\nu_3(a')$	C-C stretch	813.6	–23.0	1.0	792	$S_2(86) + S_1(6)$
$\nu_4(a')$	sym. in-plane bend	579.5	–10.1	0.0	569	$S_5(58) + S_4(35)$
$\nu_5(a')$	asym. in-plane bend	268.7	0.5	0.0	269	$S_4(62) - S_5(38)$
$\nu_6(a'')$	N-C-C out-of-plane bend	219.1	–0.5	0.0	219	$S_6(100)$

[a] Most abundant isotopic species assumed, unless otherwise stated.

[b] Second-order vibrational anharmonicity from VPT2 theory.

[c] Additional contribution to the anharmonicity from the (ν_3, $\nu_4+\nu_5$) resonance.

[d] Total energy distribution.[74,75] The percentage p contribution to the total energy (kinetic and potential) to each normal mode from the internal coordinate x is denoted $S_x(p)$. The internal coordinates are defined in the text. The sign of each term represents the relative phase of each internal coordinate in the normal mode eigenvector.

Table 2.4 shows the AE ROCCSD(T)/cc-pCVQZ harmonic and fundamental vibrational frequencies for all monosubstituted isotopologues of NCCO, whereas Table 2.5 gives the underlying anharmonicity constants χ_{ij}. As a point of calibration, the harmonic frequency and anharmonicity (ω_e, $\omega_e x_e$) values that we obtain for CO are (2173.6, 13.1) cm^{-1}, comparing very favorably with the experimental values[69] of (2169.8, 13.3) cm^{-1}. Likewise, for the CN radical we obtained parameters of (2076.1, 12.9) cm^{-1} in accord with the experimentally well-determined values[70] of (2068.6, 13.1) cm^{-1}.

Table 2.5. Anharmonicity constants χ_{ij} (cm^{-1}) for various isotopologues of $\tilde{X}\ ^2A'$ NCCO, computed at the AE-ROCCSD(T)/cc-pCVQZ level using vibrational perturbation theory.[a]

	NCCO	^{15}NCCO	N^{13}CCO	NC^{13}CO	NCC^{18}O
χ_{11}	–14.689	–14.241	–13.967	–14.750	–14.706
χ_{12}	–1.241	–1.002	0.054	–1.210	–1.565
χ_{22}	–12.798	–12.710	–12.728	–12.280	–12.298
χ_{31}	–6.491	–6.503	–5.960	–6.092	–7.025
χ_{32}	15.169	14.467	14.620	13.909	17.464
χ_{33}	–12.421	–12.190	–12.267	–11.540	–13.027
χ_{41}	–7.381	–7.304	–6.850	–7.593	–7.164
χ_{42}	–3.043	–3.100	–3.038	–2.722	–3.075
χ_{43}	–6.848	–6.461	–7.769	–15.223	–7.896
χ^*_{43}	–9.438	–9.180	–9.550	–9.135	–8.943
χ_{44}	–0.698	–0.715	–0.618	–0.749	–0.664
χ_{51}	–2.640	–2.030	–1.127	–3.005	–2.848
χ_{52}	–1.278	–1.832	–2.645	–0.878	–0.985
χ_{53}	2.189	2.316	1.336	–6.320	0.500
χ^*_{53}	–0.400	–0.403	–0.445	–0.232	–0.547
χ_{54}	–3.486	–3.435	–2.692	4.944	–1.726
χ^*_{54}	–0.897	–0.716	–0.911	–1.145	–0.679
χ_{55}	–0.470	–0.488	–0.432	–0.451	–0.474
χ_{61}	–8.718	–8.703	–8.106	– 8.651	–8.744
χ_{62}	0.624	0.624	0.598	0.611	0.601
χ_{63}	4.998	5.341	3.725	5.514	5.115
χ_{64}	2.187	2.022	2.221	2.151	2.262
χ_{65}	6.268	6.215	6.478	5.885	5.916
χ_{66}	–0.976	–0.986	–0.749	–1.119	–1.020

[a] Anharmonicity constants computed with the (ν_3, $\nu_4+\nu_5$) interaction included. Asterisks denote the same quantity with this resonance excluded.

The computation of fundamental vibrational frequencies for NCCO is complicated by the potential resonance (ν_3, $\nu_4+\nu_5$), which involves the C-C stretch, the C-C-O in-plane bend and the N-C-C in-plane bend. In order to circumvent small (ν_3, $\nu_4+\nu_5$) resonance denominators, this interaction was excluded from the VPT2 summations and instead was treated in first order. A resonance cutoff of 16 cm^{-1} is sufficient to ensure that only this term is excluded from the summations for all five isotopologues examined herein. The (ν_3, $\nu_4+\nu_5$) interaction was treated in first order by diagonalization of the 2×2 matrix

$$\begin{bmatrix} \omega_3 & \phi_{345}/\sqrt{8} \\ \phi_{345}/\sqrt{8} & \omega_4+\omega_5 \end{bmatrix}, \tag{2.3}$$

whose off-diagonal element involving the cubic force constant ϕ_{345} in the reduced normal coordinate space is the matrix element of the cubic anharmonic potential across the zeroth-order states ω_3 and $\omega_4+\omega_5$. It should be noted that the full application of VPT2 with no resonances excluded yielded vibrational frequencies within 0.7 cm^{-1} of those obtained by singling out the (ν_3, $\nu_4+\nu_5$) resonance, with the exception of the $NC^{13}CO$ isotopologue, where the ν_3 values differed by 3 cm^{-1}. The effect of excluding the resonating term from the analysis can be seen in Table 2.5, which contains the anharmonicity constants χ_{ij} both with the neglect of, and the inclusion of the resonance triad in the summations.

Focusing on the important (ν_1, ν_2) stretching modes, we predict these bands to lie at very different wavelengths than those proposed by McNavage *et al.*,[2] (2093, 1774) cm^{-1}, who based their assignment on IR emission signals. Our ν_1 value of 2171 cm^{-1} is in a region of the experimentally-derived spectrum where a signal is observed, but was ascribed to byproducts. We see no signal in the observed spectrum that corresponds to our ν_2 value of 1898 cm^{-1}.

Moreover, the fundamental vibrational frequencies from the NIST-JANAF tables, compiled by Dorofeeva and co-workers[9] (2249, 1703) cm^{-1} show significant deviation from those set forth in this work. Dorofeeva *et al.* used experimentally-derived force constants from the carbonyl cyanide [$CO(CN)_2$] precursor molecule, with scaling by comparison to the bending force constants in COX_2 and XCO (X = F, Cl, Br), to assign their values by normal coordinate analysis. Our CO stretch of 1898 cm^{-1} is unusual when compared to a typical carbonyl stretching frequency of around 1715 cm^{-1}, indicative of a very strong CO bond. This observation is in accord with the unusually short CO bond length of 1.176 Å in Fig. 1 (*cf.* 1.203 Å in formaldehyde[71]).

Table 2.6. Fundamental vibrational frequencies (cm^{-1}) of $\tilde{X}\ ^2A'$ NCCO.

Method	ν_1	ν_2	ν_3	ν_4	ν_5	ν_6
UQCISD/6–31G(d) unscaled [a]	2293	1939	795	562	205	271
UQCISD/6–31G(d) scaled [b]	2187	1849	758	536	195	258
UQCISD/6–31G(d) rescaled [c]	2087	1764	723	511	187	245
AE–ROCCSD(T)/cc–pCVQZ[d]	**2171**	**1898**	**797**	**577**	**222**	**270**

[a] Harmonic frequencies from Francisco and Liu[7] without any scaling.

[b] Harmonic frequencies from Francisco and Liu[7] scaled by 0.9538, as recommended by Scott and Radom.[18]

[c] Harmonic frequencies, scaled by 0.91, as performed by McNavage *et al.*[2] to match their observed frequencies.

[d] This research, fundamental frequencies from second–order vibrational perturbation theory.

McNavage *et al.*[2] showed that by scaling Francisco and Liu's QCISD/6-31G(d) harmonic frequencies[7] by 0.91, very good agreement can be reached with their experimentally inferred ν_1 and ν_2. This scale factor is significantly lower than that of 0.9538 suggested by Scott and Radom,[18] who arrived at their value through careful calibration. Indeed, the smaller value is more typical of the scale factor necessary for a calculation completely devoid of electron correlation. For clarity, Table 2.6 shows a listing of the vibrational frequencies resulting from

our VPT2 analysis, juxtaposed with Francisco and Liu's harmonic frequencies, scaled by these two different scale factors. Our current values are definitive, and thus are listed in boldface.

No experimental data exist for vibrational modes ν_3 through ν_6, although their IR intensities are all within a factor of about 3 of the IR intensity we computed for ν_1, which suggests that they should be detectable. The anharmonicity correction for ν_5 and ν_6 is remarkably small and contributes less than 1 cm^{-1} in all of the isotopologues considered here, bolstering the validity of VPT2 theory. Accordingly, we find no evidence of large-amplitude bending motion or quasilinearity in this system.

Table 2.7. Valence focal point analysis of the barrier to linearity (kcal mol^{-1}) for $\tilde{X}\ ^2A'$ NCCO.[a]

Basis Set	ΔE_e RHF	$+\delta$ ZAPT2	$+\delta$ CCSD	$+\delta$ CCSD(T)	$+\delta$ CCSDT	$+\delta$ CCSDT(Q)	ΔE_e CCSDT(Q)
cc–pVDZ	+15.31	– 7.18	+3.01	– 1.19	+0.12	– 0.16	+9.90
cc–pVTZ	+15.24	– 8.39	+3.18	– 1.27	+0.12	[– 0.16]	[+8.72]
cc–pVQZ	+15.32	– 8.63	+3.22	– 1.29	[+0.12]	[– 0.16]	[+8.59]
cc–pV5Z	+15.25	– 8.63	+3.25	– 1.29	[+0.12]	[– 0.16]	[+8.56]
cc–pV6Z	+15.24	– 8.65	+3.28	– 1.29	[+0.12]	[– 0.16]	[+8.55]
CBS limit	[+15.24]	[– 8.67]	[+3.31]	[– 1.29]	[+0.12]	[– 0.16]	**[+8.55]**

$\Delta E_{b,0}$ (final) = ΔE_e[CBS CCSDT(Q)] + Δ_{core}[CCSD(T)/cc–pCVQZ] + $\Delta_{relativistic}$[CCSD(T)/cc–pCVTZ] + Δ_{DBOC}[HF/aug–cc–pVTZ]

= 8.55 – 0.23 + 0.05 + 0.01 = **8.37 kcal mol^{-1}**

Fit	$a + bc^{-cX}$	$a + bX^{-3}$	$a + bX^{-3}$	$a + bX^{-3}$	additive	additive
Points (X)	4,5,6	5,6	5,6	5,6		

[a] For correlated methods the symbol δ denotes the increment in the relative energy (ΔE_e) with respect to the preceding level of theory in the hierarchy ROHF→ZAPT2→ROCCSD→ROCCSD(T) →ROCCSDT→UCCSDT(Q). Square brackets signify results obtained from basis set extrapolations detailed in the last rows of the table; all other entries are from explicit electronic structure computations. Final predictions are boldfaced.

The classical barrier to linearity of NCCO and its constituent terms are shown in Table 2.7. Our final value of 8.4 kcal mol^{-1} is large enough to justify the treatment of the ground state molecule as a semi-rigid body, which is implicit to the VPT2 analysis. Sumiyoshi and co-workers[3] report the CCSD(T)/cc-pCVTZ classical barrier to linearity to be 8.9 kcal mol^{-1} which is consistent with our findings. Yu *et al.* showed[8] that B3LYP/6-311G(d) gives a classical barrier of 4.2 kcal mol^{-1}, which rises to 10.0 kcal mol^{-1} with a CCSD(T)/6-311G(2d) single-point calculation at the B3LYP geometry; this highlights the importance of rigorous correlation treatment. Our focal point treatment exhibits excellent convergence with respect to basis set, as can be seen in the CCSD(T) column of energy differences, where the difference between the complete basis set limit and highest explicitly computed agree to within 0.01 kcal mol^{-1}. The correlation treatment represents a tougher problem, although the difference between the CCSDT(Q)/cc-pVDZ and CCSDT/cc-pVDZ values is only –0.16 kcal mol^{-1}, which indicates good convergence towards the full CI limit. The DBOC and relativistic contributions to this quantity are very small, with values of 0.01 kcal mol^{-1} and 0.05 kcal mol^{-1}, respectively. However, the core correlation correction, which accounts for the valence-only treatment employed in the focal point analysis, contributes a significant –0.23 kcal mol^{-1}. Given the good convergence exhibited by the focal point analysis, we assign an uncertainty of ± 0.2 kcal mol^{-1} to our barrier to linearity.

Table 2.8. Valence focal point analysis of the fragmentation energy (kcal mol^{-1}) of $\widetilde{X}\ ^2A'$ NCCO, to $^2\Sigma^+$ CN + CO.[a]

Basis Set	ΔE_e RHF	$+\delta$ ZAPT2	$+\delta$ CCSD	$+\delta$ CCSD(T)	$+\delta$ CCSDT	$+\delta$ CCSDT(Q)	ΔE_e CCSDT(Q)
cc–pVDZ	+20.31	+10.04	– 7.93	+0.49	– 0.49	– 0.01	+22.41
cc–pVTZ	+20.87	+13.34	– 7.55	+0.74	– 0.50	[– 0.01]	[+26.89]
cc–pVQZ	+20.62	+14.31	– 7.44	+0.84	[– 0.50]	[– 0.01]	[+27.81]
cc–pV5Z	+20.71	+14.51	– 7.41	+0.88	[– 0.50]	[– 0.01]	[+28.18]
cc–pV6Z	+20.71	+14.59	– 7.38	+0.89	[– 0.50]	[– 0.01]	[+28.29]
CBS limit	+20.71	+14.69	[– 7.35]	[+0.90]	[– 0.50]	[– 0.01]	**[+28.44]**

ΔE_0 (final) = ΔE_e[CBS CCSDT(Q)] + Δ_{ZPVE}[CCSD(T)/cc–pCVQZ] + Δ_{core}[CCSD(T)/cc–pCVQZ] + $\Delta_{relativistic}$[CCSD(T)/cc–pCVTZ] + Δ_{DBOC}[HF/aug–cc–pVTZ]

= 28.44 – 2.50 + 0.75 – 0.19 + 0.03 = **26.53 kcal mol^{-1}**

Fit	$a + bc^{-cX}$	$a + bX^{-3}$	$a + bX^{-3}$	$a + bX^{-3}$	additive	additive
Points (X)	4,5,6	5,6	5,6	5,6		

[a] See footnote a of Table 2.7 for notation.

Table 2.8 details our determination of the dissociation energy of NCCO, with respect to CN and CO. The final answer is unusually small at 26.5 kcal mol^{-1}, which is undoubtedly due to the great stability of the diatomic dissociation products, CN and CO. We find excellent convergence with respect to both basis set and correlation treatment; the CCSDT(Q)/cc-pVDZ and CCSDT/cc-pVDZ energies are separated by only 0.01 kcal mol^{-1}, as are the CCSD(T)/cc-pV6Z and CCSD(T)/cc-pV5Z values. As before, a small correction results from consideration of the DBOC, although relativity provides −0.19 kcal mol^{-1} of the energy difference. Again, we see a large core correction, which is 0.75 kcal mol^{-1} in this instance. The zero point vibrational energy (ZPVE) corrections were computed from the cubic (ϕ_{ijk}) and quartic (ϕ_{iijj}) force constants, in reduced normal coordinates, via the following expression:[72]

$$ZPVE = \frac{1}{2}\sum_{i}\omega_i - \frac{1}{32}\sum_{ijk}\frac{\phi_{iik}\phi_{kjj}}{\omega_k} - \frac{1}{48}\sum_{ijk}\frac{\phi_{ijk}^2}{\omega_i+\omega_j+\omega_k} + \frac{1}{32}\sum_{ij}\phi_{iijj} + Z_{kinetic} \quad (2.4)$$

Subsumed within this expression is the contribution from the commonly overlooked G_0 term, which contributes just 0.03 kcal mol^{-1} to the NCCO dissociation energy. The final term in the ZPVE expression arises from vibrational angular momentum and its leading contributions are

$$Z_{kinetic} = -\frac{1}{4}\sum_{\alpha=(a,b,c)} B_e^{\alpha}\left\{1 - \sum_{i>j}(\zeta_{ij}^{\alpha})^2\frac{(\omega_i-\omega_j)^2}{\omega_i\omega_j}\right\}, \quad (2.5)$$

where B_e^{α} and ζ_{ij}^{α} are the equilibrium rotational constants and Coriolis constants, respectively. This analysis yielded a sizable ZPVE contribution of −2.50 kcal mol^{-1} to the fragmentation energy. As with the barrier to linearity, we observe sufficient convergence with respect to correlation treatment and basis set augmentation to assign an uncertainty of ± 0.2 kcal mol^{-1} to our dissociation energy.

The NIST-JANAF tables[9] quote the 0 K enthalpy of formation ($\Delta_f H_0°$) for NCCO as 49.5 ± 2.4 kcal mol^{-1}, based on the isodesmic reaction:

$$NCCO + HCN \rightarrow C_2N_2 + HCO \quad (2.6)$$

Their value is derived from the data provided by Francisco and Liu,[7] who used experimental enthalpies of formation for HCN, C_2N_2 and HCO, coupled with the aforementioned reaction's enthalpy at the QCISD(T) level of theory, with a range of modest basis sets. Yu and co-workers[8] examined the same reaction scheme, also using experimental enthalpies of formation, but their reaction enthalpy came from G3//B3LYP theory;[73] this resulted in a larger $\Delta_f H_0°$ for NCCO of 51.3 kcal mol^{-1}.

The enthalpy of formation of CO from the active thermochemical tables (ATcT) of Ruscic[58] is $\Delta_f H_0° = -27.20 \pm 0.04$ kcal mol^{-1}. The best available $\Delta_f H_0°$ value for CN is

apparently 104.63 ± 0.1 kcal mol^{-1}, from the elemental reaction approach of the highly accurate HEAT protocol.[58] Combining these enthalpies of formation of CO and CN with our accurate NC-CO dissociation energy, we arrive at $\Delta_f H_0°$(NCCO) = 50.9 ± 0.3 kcal mol^{-1}. This new value is consistent with previous determinations, but has much less uncertainty associated with it.

2.5 Conclusions

Through explicit consideration of anharmonicity, we have examined the vibrational frequencies of the NCCO molecule within a high-level *ab initio* [AE-ROCCSD(T)/cc-pCVQZ] framework. Our final fundamental frequencies (ν_1 = 2171, ν_2 = 1898, ν_3 = 797, ν_4 = 577, ν_5 = 222, ν_6 = 270 cm^{-1}) differ significantly from those inferred from experimental studies. In light of failed attempts to detect NCCO in kinetic studies using these experimental frequencies, we suggest that the present theoretical values be adopted for future attempts. Our highly accurate theoretical fundamental frequencies should greatly aid spectroscopic efforts to definitively characterize this important radical.

We have provided precise values for the classical barrier to linearity of NCCO (8.4 kcal mol^{-1}) and its dissociation energy with respect to CN and CO (D_0 = 26.5 kcal mol^{-1}). Because the dissociation energy is unusually small, the NCCO radical should be produced with small amounts of excess energy in order to avoid decomposition. Our recommended 0 K enthalpy of formation of NCCO, $\Delta_f H_0°$ = 50.9 ± 0.3 kcal mol^{-1}, is based on our highly converged dissociation energy and accurate enthalpies of formation for CN and CO from the literature. It has an uncertainty almost an order of magnitude smaller than previous values, warranting its adoption in thermochemical databases.

2.6 ACKNOWLEDGMENTS

A.C.S. would like to acknowledge Drs. Justin Turney and Yukio Yamaguchi for valuable input. This work was supported by the U. S. Department of Energy (DOE), Basic Energy Sciences grant number DE-FG02-97ER14748. The DOE computing resources of the NERSC facility of the Lawrence Berkeley National Laboratory were essential to this research.

REFERENCES

[1] W. McNavage and H. L. Dai, J. Chem. Phys. **123,** 184104 (2005).

[2] W. McNavage, W. Dailey, and H. L. Dai, Can. J. Chem. **82,** 925 (2004).

[3] Y. Sumiyoshi, H. Takada, and Y. Endo, Chem. Phys. Lett. **387,** 116 (2004).

[4] G. A. McGibbon, C. A. Kingsmill, J. K. Terlouw, and P. C. Burgers, Int. J. Mass Spectrom. Ion Proc. **121,** R11 (1992).

[5] J. F. Hershberger, Proceedings of the 26th Annual Combustion Research Conference, Warrenton, Virginia, May 31 - June 3, 2005.

[6] W. J. Ding, W. H. Fang, and R. Z. Liu, Chem. Phys. Lett. **351,** 9 (2002).

[7] J. S. Francisco and R. F. Liu, J. Chem. Phys. **107,** 3840 (1997).

[8] G. T. Yu, Y. H. Ding, X. R. Huang, H. T. Bai, and C. C. Sun, J. Phys. Chem. A **109,** 2364 (2005).

[9] O. Dorofeeva, V. P. Novikov, and D. B. Neumann, J. Phys. Chem. Ref. Data **30,** 475 (2001).

[10] T. Imamura and N. Washida, Int. J. Chem. Kinet. **33,** 440 (2001).

[11] D. R. Lander, K. G. Unfried, G. P. Glass, and R. F. Curl, J. Phys. Chem. **94,** 7759 (1990).

[12] A. Furlan, H. A. Scheld, and J. R. Huber, Chem. Phys. Lett. **282,** 1 (1998).

[13] A. Furlan, H. A. Scheld, and J. R. Huber, J. Phys. Chem. A **104,** 1920 (2000).

[14] R. J. Horwitz, J. S. Francisco, and J. A. Guest, J. Phys. Chem. A **101,** 1231 (1997).

[15] H. Y. Lee, A. M. Mebel, and S. H. Lin, Int. J. Quant. Chem. **90,** 566 (2002).

[16] H. A. Scheld, A. Furlan, and J. R. Huber, J. Chem. Phys. **111,** 923 (1999).

[17] J. F. Herschberger, Proceedings of the 26th Annual Combustion Research Conference, Warrenton, Virginia, May 31 - June 3, 2005.

[18] A. P. Scott and L. Radom, J. Phys. Chem. **100,** 16502 (1996).

[19] D. E. Woon and T. H. Dunning, J. Chem. Phys. **103,** 4572 (1995).

[20] K. L. Bak, J. Gauss, P. Jorgensen, J. Olsen, T. Helgaker, and J. F. Stanton, J. Chem. Phys. **114,** 6548 (2001).

[21] J. D. Watts, J. Gauss, and R. J. Bartlett, J. Chem. Phys. **98,** 8718 (1993).

[22] K. Raghavachari, G. W. Trucks, J. A. Pople, and M. Head-Gordon, Chem. Phys. Lett. **157,** 479 (1989).

[23] W. J. Lauderdale, J. F. Stanton, J. Gauss, J. D. Watts, and R. J. Bartlett, Chem. Phys. Lett. **187,** 21 (1991).

[24] P. J. Knowles, J. S. Andrews, R. D. Amos, N. C. Handy, and J. A. Pople, Chem. Phys. Lett. **186,** 130 (1991).

[25] J. F. Stanton, J. Chem. Phys. **101,** 371 (1994).

[26] A. L. L. East, C. S. Johnson, and W. D. Allen, J. Chem. Phys. **98,** 1299 (1993).

[27] See EPAPS Document number ??? for a pdf file containing the full quadratic, cubic, and quartic force constants in internal coordinates. This document can be reached via a direct link in the online article's HTML reference section or via the EPAPS homepage http://www.aip.org/pubservs/epaps.html.

[28] H. H. Nielsen, Rev. Mod. Phys. **23,** 90 (1951).

[29] J. K. G. Watson, in *Vibrational Spectra and Structure*, edited by J. R. Durig (Elsevier, Amsterdam, 1977), Vol. 6, pp. 1.

[30] D. A. Clabo, W. D. Allen, R. B. Remington, Y. Yamaguchi, and H. F. Schaefer, Chem. Phys. **123,** 187 (1988).

[31] W. D. Allen, Y. Yamaguchi, A. G. Császár, D. A. Clabo, R. B. Remington, and H. F. Schaefer, Chem. Phys. **145,** 427 (1990).

[32] I. M. Mills, in *Molecular Spectroscopy: Modern Research*, edited by K. N. Rao and C. W. Mathews (Academic Press, New York, 1972), pp. 115.

[33] D. Papousek and M. R. Aliev, *Molecular Vibrational-Rotational Spectra*. (Elsevier, Amsterdam, 1982).

[34] K. Aarset, A. G. Császár, E. L. Sibert, III, W. D. Allen, H. F. Schaefer, III, W. Klopper, and J. Noga, J. Chem. Phys. **112,** 4053 (2000).

[35] *Mathematica*, Wolfram Research, Inc., Champaign, IL (2003).

[36] INTDIF2005 is an abstract program written by Wesley D. Allen for *Mathematica* to perform general numerical differentiations to high orders of electronic structure data.

[37] R. L. DeKock, M. J. McGuire, P. Piecuch, W. D. Allen, H. F. Schaefer, K. Kowalski, S. A. Kucharski, M. Musial, A. R. Bonner, S. A. Spronk, D. B. Lawson, and S. L. Laursen, J. Phys. Chem. A **108,** 2893 (2004).

[38] INTDER2005 is a general program written by Wesley D. Allen, which performs sundry vibrational analyses and higher order nonlinear transformations among force field representations.

[39] See program descriptions in K. Sarka and J. Demaison, in *Computational Molecular Spectroscopy*, edited by P. Jensen and P. R. Bunker (Wiley, Chichester, 2000), pp. 255.

[40] W. D. Allen and A. G. Császár, J. Chem. Phys. **98,** 2983 (1993).

[41] W. D. Allen, A. G. Császár, V. Szalay, and I. M. Mills, Mol. Phys. **89,** 1213 (1996).

[42] ANHARM is a FORTRAN program written for VPT2 analysis written by Yukio Yamaguchi and Henry F. Schaefer (Center for Computational Chemistry, University of Georgia, Athens, GA, 30602, USA).

[43] A. L. L. East and W. D. Allen, J. Chem. Phys. **99,** 4638 (1993).

[44] M. S. Schuurman, S. R. Muir, W. D. Allen, and H. F. Schaefer, J. Chem. Phys. **120,** 11586 (2004).

[45] J. M. Gonzales, C. Pak, R. S. Cox, W. D. Allen, H. F. Schaefer, A. G. Császár, and G. Tarczay, Chem. Eur. J. **9,** 2173 (2003).

[46] A. G. Császár, W. D. Allen, and H. F. Schaefer, J. Chem. Phys. **108,** 9751 (1998).

[47] T. Helgaker, W. Klopper, H. Koch, and J. Noga, J. Chem. Phys. **106,** 9639 (1997).

[48] D. Feller, J. Chem. Phys. **98,** 7059 (1993).

[49] T. Van Mourik and T. H. Dunning, Int. J. Quant. Chem. **76,** 205 (2000).

[50] T. H. Dunning, J. Chem. Phys. **90,** 1007 (1989).

[51] T. D. Crawford, H. F. Schaefer, and T. J. Lee, J. Chem. Phys. **105,** 1060 (1996).

[52] T. J. Lee and D. Jayatilaka, Chem. Phys. Lett. **201,** 1 (1993).

[53] Y. J. Bomble, J. F. Stanton, M. Kallay, and J. Gauss, J. Chem. Phys. **123,** 054101 (2005).

[54] M. Kállay and J. Gauss, J. Chem. Phys. **123,** 214105 (2005).

[55] The (ROCCSDT,UCCSDT) barriers to linearity, with a cc-pVDZ basis at the AE-CCSD(T)/cc-pCVQZ geometry, are (10.06, 9.96) kcal mol^{-1} and the corresponding

dissociation energies are (22.42, 22.44) kcal mol^{-1}. These small differences will diminish further with the perturbative inclusion of the effects of connected quadruple excitations.

[56] N. C. Handy, Y. Yamaguchi, and H. F. Schaefer, J. Chem. Phys. **84,** 4481 (1986).

[57] H. Sellers and P. Pulay, Chem. Phys. Lett. **103,** 463 (1984).

[58] A. Tajti, P. G. Szalay, A. G. Császár, M. Kállay, J. Gauss, E. F. Valeev, B. A. Flowers, J. Vázquez, and J. F. Stanton, J. Chem. Phys. **121,** 11599 (2004).

[59] R. A. Kendall, T. H. Dunning, and R. J. Harrison, J. Chem. Phys. **96,** 6796 (1992).

[60] E. R. Davidson, Y. Ishikawa, and G. L. Malli, Chem. Phys. Lett. **84,** 226 (1981).

[61] C. W. Bauschlicher, J. M. L. Martin, and P. R. Taylor, J. Phys. Chem. A **103,** 7715 (1999).

[62] MOLPRO is a package of ab initio programs written by H.-J. Werner, P. J. Knowles, R. Lindh, F. R. Manby, M. Schütz, P. Celani, T. Korona, G. Rauhut, R. D. Amos, A. Bernhardsson, A. Berning, D. L. Cooper, M. J. O. Deegan, A. J. Dobbyn, F. Eckert, C. Hampel, G. Hetzer, A. W. Lloyd, S. J. McNicholas, W. Meyer, M. E. Mura, A. Nicklaß, P. Palmieri, R. Pitzer, U. Schumann, H. Stoll, A. J. Stone, R. Tarroni, and T. Thorsteinsson.

[63] J. F. Stanton, J. Gauss, J. D. Watts, W. J. Lauderdale, and R. J. Bartlett, Int. J. Quant. Chem. **44 (S26),** 879 (1992).

[64] J.F. Stanton, J. Gauss, J.D. Watts, P.G. Szalay, R.J. Bartlett with contributions from A.A. Auer, D.B. Bernholdt, O. Christiansen, M.E. Harding, M. Heckert, O. Heun, C. Huber, D. Jonsson, J. Jusélius, W.J. Lauderdale, T. Metzroth, C. Michauk, D.R. Price, K. Ruud, F. Schiffmann, A. Tajti, M.E. Varner, J. Vázquez and the integral packages: MOLECULE

(J. Almlöf and P.R. Taylor), PROPS (P.R. Taylor), and ABACUS (T. Helgaker, H.J. Aa. Jensen, P. Jørgensen, and J. Olsen). Current version see http://www.aces2.de. .

[65] The Massively Parallel Quantum Chemistry Program (MPQC), Version 2.3.1, Curtis L. Janssen, Ida B. Nielsen, Matthew L. Leininger, Edward F. Valeev, Edward T. Seidl, Sandia National Laboratories, Livermore, CA, USA, 2004.

[66] J. A. Coxon and P. G. Hajigeorgiou, J. Chem. Phys. **121,** 2992 (2004).

[67] M. Hübner, M. Castillo, P. B. Davis, and J. Röpcke, Spect. Act. A **61,** 57 (2005).

[68] T. J. Lee, D. J. Fox, H. F. Schaefer, and R. M. Pitzer, J. Chem. Phys. **81,** 356 (1984).

[69] A. Lefloch, Mol. Phys. **72,** 133 (1991).

[70] C. V. V. Prasad, P. F. Bernath, C. Frum, and R. Engleman, J. Mol. Spectrosc. **151,** 459 (1992).

[71] S. Carter and N. C. Handy, J. Mol. Spectrosc. **179,** 65 (1996).

[72] M. S. Schuurman, W. D. Allen, and H. F. Schaefer, J. Comput. Chem. **26,** 1106 (2005).

[73] A. G. Baboul, L. A. Curtiss, P. C. Redfern, and K. Raghavachari, J. Chem. Phys. **110,** 7650 (1999).

[74] W. D. Allen, A. G. Császár, and D. A. Horner, J. Am. Chem. Soc. **114,** 6834 (1992).

[75] P. Pulay and F. Török, Acta Chim. Hung. **44,** 287 (1965).

CHAPTER 3

THE ENTHALPY OF FORMATION AND ANHARMONIC FORCE FIELD OF DIACETYLENE[†]

[†] A. C. Simmonett, H. F. Schaefer, and W. D. Allen, submitted to the Journal of Physical Chemistry A.

3.1 ABSTRACT

The enthalpy of formation for the diacetylene molecule (C_4H_2) is pinpointed using state-of-the-art computational methodology, accounting for high-order correlation effects, relativity, non-Born Oppenheimer effects and anharmonic vibrational frequencies. Molecular energies are determined by consideration of coupled cluster with singles and doubles (CCSD), quasiperturbative triples [CCSD(T)], full triple excitations (CCSDT) and perturbative quadruples [CCSDT(Q)] in concert with Dunning's correlation consistent family of basis sets (cc-pV*X*Z, *X*=D,T,Q,5,6). Our fundamental vibrational frequencies are derived from an all electron CCSD(T) quartic force field, computed using Dunning's quadruple-ζ cc-pCVQZ basis, which includes tight functions to provide a satisfacory description of core correlation. For diacetylene, our computed fundamental frequencies reproduce the full experimental vibrational spectrum within 6.9 cm^{-1}. No empirical scale factors are employed throughout. Using this *ab initio* methodology, we compute the enthalpy for the isodesmic reaction 2 H–C≡C–H → H–C≡C–C≡C–H + H_2 to be (0.03, 0.81) kcal mol^{-1} at (0, 298.15) K which, combined with acetylene's enthalpy of formation from the literature yields $\Delta_f H_0^\circ$(diacetylene) = 109.4 ± 0.3 kcal mol^{-1} and $\Delta_f H_{298}^\circ$(diacetylene) = 109.7 ± 0.3 kcal mol^{-1}. Existing estimates of the diacetylene heat for formation range from 102 to 113 kcal mol^{-1}.

3.2 INTRODUCTION

The diacetylene molecule is prevalent in hydrocarbon combustion and flame models[1-5] and is of great significance in interplanetary atmospheric chemistry due to its propensity to absorb ultraviolet radiation.[6,7] The structure, spectroscopy and reactivity of this molecule has

received great attention from the theoretical[1,8-10] and experimental[7,9,11-19] communities over the years; however its heat of formation is not precisely known.

Diacetylene has two long long-lived triplet excited states that are just 60 and 72 kcal mol^{-1} above the ground state[20] unlike acetylene, where the excitation energy is significantly higher.[21] Recognizing the chemical importance of the chemical reactivity of these excited states, Zwier has performed a systematic survey of the reactions of triplet diacetylene with a number of small hydrocarbons.[7,20,22-25]

Ellison and co-workers observed both acetylene and diacetylene as the exclusive products in the pyrolysis of *ortho*-benzyne at temperatures below 1500 K, which was attributed to a retro-Diels-Alder fragmentation process.[26] The *ortho*-benzyne diradical is a product of hydrogen abstraction from the phenyl radical, which is an endoergic process that costs about 78 kcal mol^{-1}. Likewise, the phenyl radical is a product of hydrogen abstraction from benzene; this is consistent with Kiefer's observation that pyrolysis of benzene itself predominantly yields acetylene and diacetylene in equal measures.[27] Fuels containing aromatic compounds will thus generate significant quantities of diacetylene during the combustion process. The group of Leone recently investigated the formation of diacetylene and larger polyynes from reactions of the ethynyl radical, C_2H using time-resolved mass spectrometry.[28] They concluded that the reaction of C_2H with propyne yields diacetylene with a yield between 50% and 70%, in contrast to the reaction with allene, which favors C_4H_5 isomers, producing diacetylene with a yield of less than 30%.

In the 1980s, it was proposed[29,30] that the "even carbon" reaction

$$n\text{-}C_4H_3 + C_2H_2 \rightarrow C_6H_5\cdot \qquad (3.1)$$

might generate the critical first aromatic ring in soot formation processes; one possible source for the requisite C_4H_3 is hydrogen addition to diacetylene.[31,32] This ring formation concept is not

restricted to acetylene reacting with a radical, and diacetylene has been proposed to react in an analogous way with phenyl radical to form an equilibrium with the napthyl radical (Scheme 3.1).[33] While reaction (3.1) has been studied extensively, Miller and Melius[5] have played down its importance due to the relatively low concentration of *n*-C_4H_3 present, brought about by isomerization to the lower energy *i*-C_4H_3 isomer. The "odd carbon" pathway involving the recombination of two propargyl radicals is generally considered the dominant mechanism leading to the formation of the first aromatic ring en route to soot particles. Interestingly, Kaiser and co-workers have shown that the propargyl radical can react with carbon atoms to form diacetylene in its ground electronic state, expelling a hydrogen atom in the process.[34]

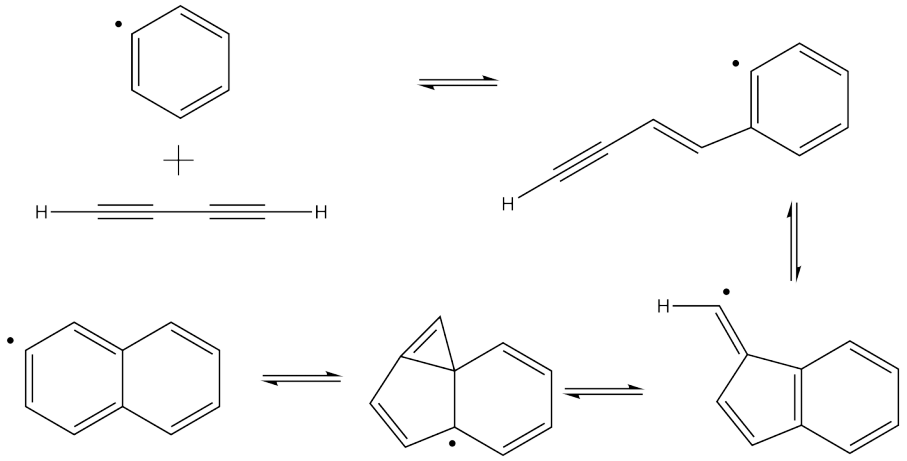

Scheme 3.1. The equilibration of diacetylene and phenyl radical with napthyl radical, as proposed by Hausmann and Homann.[33]

With diacetylene enjoying such a rich participation in combustion and pyrolysis processes, it is important to fully understand the thermodynamics of this fully unsaturated C_4 moiety, in order to correctly model reactions. A 1962 study[35] of carbon- and hydrogen-containing molecules quotes the standard enthalpy of formation for diacetylene as 111.3 kcal mol^{-1}. The application of MNDO semi-empirical theory[36] yields 102.2 kcal mol^{-1} with the

slightly more elaborate AM1 model[37] predicts 106.1 kcal mol^{-1}. These studies both quote an experimental enthalpy of formation of 113.0 kcal mol^{-1} for diacetylene although it is not clear whether this is correct; this value is quoted in their source[38] with the disclaimer "…reported the enthalpy of dissociation (presumably to elements at 298°K) of biacetylene as –113 kcal/mole". More recently, based on group additivity arguments, Stein and Fahr[39] predicted a value of 105 kcal mol^{-1}. After surveying a number of different group increments in the literature, Kiefer and Von Drasek[40] reassessed this to be 111 kcal mol^{-1} in 1990; the higher value was subsequently concluded to be more consistent with observations from a time of flight mass spectrometry study of acetylene pyrolysis, performed by Kiefer and co-workers.[41] Diacetylene is not included in the data tables reported by JANAF or those of Gurvich. In this Article, we use state-of-the-art computational methods to determine the enthalpy of formation of diacetylene to unprecedented accuracy.

3.3 METHODS

We focus our attention on accurately pinpointing the enthalpy change for the isogyric reaction:

$$2\ \mathrm{H–C{\equiv}C–H} \rightarrow \mathrm{H–C{\equiv}C–C{\equiv}C–H} + \mathrm{H_2} \qquad (3.2)$$

Given that the enthalpy of formation of acetylene is readily available in the literature,[42-45] and that of H_2 is zero by definition, the enthalpy of reaction (3.2) is sufficient to determine the enthalpy of formation for diacetylene. The active thermochemical tables of Ruscic[45] deliver $\Delta_f H_0^\circ$(acetylene) = 54.69±0.07 kcal mol^{-1}, which compares well with high level *ab initio* studies and is consequently adopted in this study.[43,45]

Our reference geometries are those given by the popular coupled cluster theory with singles, doubles and perturbative triple excitations [CCSD(T)] method,[46,47] in conjunction with the large core-valence correlation consistent quadruple-ζ basis set, cc-pCVQZ, of Woon and Dunning.[48] All electrons are correlated in these computations and this cc-pCVQZ basis comprises 396 contracted Gaussian functions for the diacetylene molecule. This level of theory has been shown to be highly reliable for computing the equilibrium geometry of single-reference molecules, including multiply bonded hydrocarbons.[26,49]

The relative energies were then refined through use of the valence focal point analysis[50-53] at these geometries. In the focal point analysis, the basis set is systematically increased and extrapolation is performed[54,55] to remove the basis set error. Simultaneously, the complexity of the correlation treatment is increased in order to monitor the convergence towards the full configuration interaction limit. The highest level used here is the recently developed CCSDT(Q) method,[56] which includes a contribution from quadruple excitations in a fashion analogous to the triples in the popular CCSD(T) theory. The cc-pV*X*Z family of basis sets[57,58] (*X*=D, T, Q, 5, 6) were used for this study and the *1s* orbitals on carbon were constrained to be doubly occupied. To correct for the frozen core approximation in the focal point analysis, the following correction was appended

$$\Delta E_{\text{core}} = E^{\text{cc-pCVQZ}}_{\text{CCSD(T)(AE)}} - E^{\text{cc-pCVQZ}}_{\text{CCSD(T)(fc)}}, \tag{3.3}$$

where AE denotes an all-electron computation and fc a frozen core computation. The largest CCSD(T) energy computation for diacetylene involved 742 basis functions.

The presence of hydrogen atoms raises concerns about the error introduced by the Born Oppenheimer approximation, which underlies the electronic structure calculations. To quantify this, we computed the diagonal Born Oppenheimer correction[59,60] (DBOC) at the Hartree-Fock

level, using the aug-cc-pVQZ basis set. Although relativistic effects are typically small for molecules comprising only first row atoms, their presence was accounted for by appending the mass-velocity and Darwin one-electron terms,[61] computed at the CCSD(T)/cc-pCVQZ level, to the total energies.

The symmetrized internal coordinates used to obtain vibrational frequencies in this study are listed in Table 3.1. The *x* and *y* components of the bending coordinates are related by cylindrical symmetry, as documented by Strey and Mills.[62] The quartic force field was computed using a reduced set of coordinates, which involved only the bending modes in the *xy* plane, totaling (5,9) coordinates for (acetylene, diacetylene), and invoking these symmetry relations to complete the force constant list. Further computational savings were made through the consideration of Abelian point group symmetry, and realizing that a positive displacement along an antisymmetric coordinate is tantamount to a negative displacement. After considering these symmetries, only 98 energy computations are required to obtain the full quartic force field for acetylene and 502 for that of diacetylene. The quartic force fields in internal coordinates were transformed to reduced normal coordinates, thus making them suitable for the application of second-order vibrational perturbation theory (VPT2)[63-70] to obtain vibrational anharmonicities.

Table 3.1. Definition of internal coordinates used in this study.[a] The atom numbering is depicted in Figure 3.1.

Coordinate	Diacetylene	Acetylene
S_1	$\frac{1}{\sqrt{2}}(r_{35}+r_{46})$	$\frac{1}{\sqrt{2}}(r_{13}+r_{24})$
S_2	$\frac{1}{\sqrt{2}}(r_{13}+r_{24})$	r_{12}
S_3	r_{12}	$\frac{1}{\sqrt{2}}(r_{13}-r_{24})$
S_4	$\frac{1}{\sqrt{2}}(r_{35}-r_{46})$	$\frac{1}{\sqrt{2}}(\theta^x_{213}-\theta^x_{124})$
S_5	$\frac{1}{\sqrt{2}}(r_{13}-r_{24})$	$\frac{1}{\sqrt{2}}(\theta^y_{213}-\theta^y_{124})$
S_6	$\frac{1}{\sqrt{2}}(\theta^x_{135}-\theta^x_{246})$	$\frac{1}{\sqrt{2}}(\theta^x_{213}+\theta^x_{124})$
S_7	$\frac{1}{\sqrt{2}}(\theta^y_{135}-\theta^y_{246})$	$\frac{1}{\sqrt{2}}(\theta^y_{213}+\theta^y_{124})$
S_8	$\frac{1}{\sqrt{2}}(\theta^x_{213}-\theta^x_{124})$	
S_9	$\frac{1}{\sqrt{2}}(\theta^y_{213}-\theta^y_{124})$	
S_{10}	$\frac{1}{\sqrt{2}}(\theta^x_{135}+\theta^x_{246})$	
S_{11}	$\frac{1}{\sqrt{2}}(\theta^y_{135}+\theta^y_{246})$	
S_{12}	$\frac{1}{\sqrt{2}}(\theta^x_{213}+\theta^x_{124})$	
S_{13}	$\frac{1}{\sqrt{2}}(\theta^y_{213}+\theta^y_{124})$	

[a] In these definitions, r represents a bond length and θ^{α}_{abc} defines a linear bend between atoms a, b and c in the αz plane (assuming orientation along the z axis), defined as $\theta^{\alpha}_{abc} = \sin^{-1}[\mathbf{e}_d \cdot (\mathbf{e}_{bc} \times \mathbf{e}_{ba})]$, where $\mathbf{e}_d$ is a fixed direction vector perpendicular to the αz plane**.**

The out-of-plane *gerade* bending modes in conjugated molecules have been shown to be highly susceptible to intramolecular basis set superposition error by Lee, Martin and Taylor.[71,72] The consequence of this is an underestimation of the harmonic vibrational frequency; indeed it has been shown that an inappropriate choice of basis set can lead to imaginary frequencies for these vibrational modes in arenes.[73] The use of atomic natural orbital (ANO) basis sets[74]

alleviates this somewhat, due to the high degree of flexibility afforded by the large primitive sets of Gaussian functions used to construct them. However, such bases are currently only available without tightly contracted functions to correctly describe core correlation. Freezing the 1*s* electrons can have a significant effect on the geometries and predicted vibrational frequencies of a system, particularly when multiple bonds are present.[49,75]

For this reason, we used the aforementioned cc-pCVQZ basis set with the accurate CCSD(T) method to compute the fundamental vibrational frequencies, correlating all electrons throughout. We further motivate this choice by considering that there are two π_g vibrational modes in the two acetylene molecules on the left of equation (3.2), just as there are in the diacetylene molecule on the right hand side; the intramolecular basis set superposition error results in a systematic underestimation of the harmonic vibrational frequencies of these modes, so we can expect to see a high degree of cancellation of the errors introduced.

All molecular energies were computed using the ACESII[76,77] and Molpro[78] suites of electronic structure codes, while the DBOC correction was evaluated using PSI3.[79] The force fields were generated using the MATHEMATICA[80] program INTDIF2005,[81] the nonlinear transformation to Cartesian coordinates was performed with INTDER2005,[82,83] and the ANHARM[83,84] program provided the VPT2 analysis.

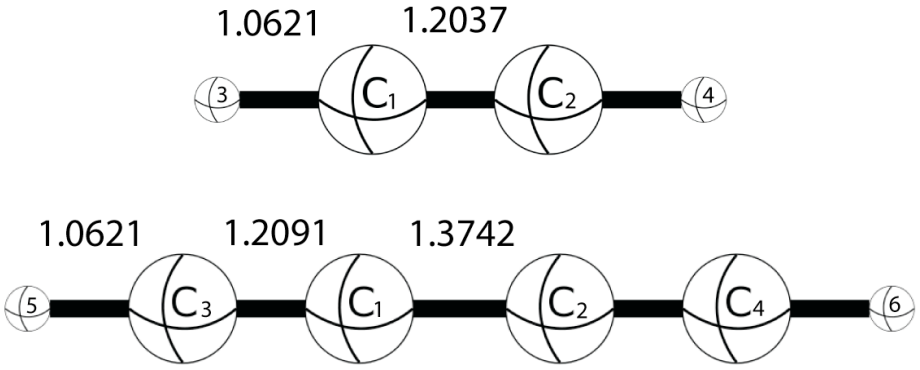

Figure 3.1. The all electron CCSD(T) cc-pCVQZ geometries (Å) of acetylene and diacetylene. For acetylene, the empirically corrected experimental bond lengths[85] are 1.0617±0.0005 and 1.2036±0.0006 Å for the C-H and C≡C bonds, respectively. The subscript atom labels depict the ordering used in the internal coordinate definition (Table 3.1).

3.4 Results and Discussion

The equilibrium geometries of the species considered here are shown in Figure 3.1. The bond length of H_2 from our cc-pVQZ CCSD calculation is 0.7419 Å, which agrees well with the experimental[86] value of 0.7414 Å; this is not surprising since CCSD corresponds to the configuration interaction limit for a two-electron system. A more meaningful calibration is afforded by scrutinizing the bond lengths in acetylene. Such a comparison reveals that the CCSD(T) cc-pCVQZ geometries are in very good agreement with the empirically corrected experimental bond lengths[85] reported by Pawłowski *et al.*, exhibiting errors of just 0.0004 and 0.0001 Å. By appending the equilibrium rotational constant with the vibration-rotation interaction constants, which are shown in Table 3.2, we can directly compare to those measured directly in high resolution vibrational spectroscopy. The latter experiments have been performed by Kabbadj and co-workers,[87] yielding B_0 = 1.1766 cm^{-1}, which compares well to our computed

value of 1.1753 cm^{-1}; just a 0.11% error. Similarly, the computed B_0 for diacetylene is 0.14620 cm^{-1}, which is just 0.14% lower than the experimental value[14] of 0.14641 cm^{-1}.

Table 3.2. Vibration-rotation interaction constants (10^{-3} cm^{-1}) at the all electron CCSD(T) cc-pCVQZ level of theory for acetylene and diacetylene.

Acetylene					
α_1^A	6.876	α_2^A	6.041	α_3^A	5.845
α_4^A	–1.459	α_5^A	–2.216		
Diacetylene					
α_1^A	0.2167	α_2^A	0.6552	α_3^A	0.3135
α_4^A	0.2170	α_5^A	0.3911	α_6^A	–0.0825
α_7^A	–0.2786	α_8^A	–0.0714	α_9^A	–0.4194

Table 3.3 shows the valence focal point analysis of the reaction indicated in equation (3.2), for which we seek accurate thermochemistry. It is apparent that the reaction is remarkably insensitive to the basis set used, which lends credence to the assumption that the difference between the CCSDT(Q) and CCSDT energies is constant for all basis sets larger than cc-pVTZ. The effect of introducing these perturbative quadruple excitations lowers the computed reaction energy by only 0.34 kcal mol^{-1}, which is indicative that the final focal point result is well converged towards the full configuration interaction limit. Clearly, large amounts of dynamical correlation are imperative for the precise computation of this reaction energy, as 0.34 kcal mol^{-1} is not a negligible contribution.

Table 3.3. Valence focal point analysis of the reaction 2 H–C≡C–H → H–C≡C–C≡C–H + H_2 (kcal mol^{-1}).[a]

Basis Set	ΔE_e RHF	$+\delta$ MP2	$+\delta$ CCSD	$+\delta$ CCSD(T)	$+\delta$ CCSDT	$+\delta$ CCSDT(Q)	ΔE_e CCSDT(Q)
cc–pVDZ	+8.91	–8.13	+4.81	–1.73	+0.28	–0.34	[+3.80]
cc–pVTZ	+9.34	–8.31	+4.87	–1.79	+0.34	–0.41	[+4.04]
cc–pVQZ	+9.45	–8.37	+4.88	–1.82	+0.35	[–0.41]	[+4.09]
cc–pV5Z	+9.50	–8.29	+4.84	–1.83	[+0.35]	[–0.41]	[+4.17]
cc–pV6Z	+9.51	–8.28	+4.82	–1.83	[+0.35]	[–0.41]	[+4.15]
CBS limit	[+9.51]	[–8.27]	[+4.79]	[–1.84]	[+0.35]	[–0.41]	**[+4.13]**

$\Delta E_{r,0}$ (final) = ΔE_e[CBS CCSDT(Q)] + Δ_{core}[CCSD(T)/cc–pCVQZ] + $\Delta_{relativistic}$[CCSD(T)/cc–pCVQZ] + Δ_{DBOC}[HF/aug–cc–pVQZ] + Δ_{ZPVE}[VPT2/CCSD(T)/cc-pCVQZ]

= 4.13 – 0.11 + 0.03 + 0.01 – 4.03 = **0.03 kcal mol^{-1}**

Fit	$a + be^{-cX}$	$a + bX^{-3}$	$a + bX^{-3}$	$a + bX^{-3}$	additive	additive
Points (X)	4,5,6	5,6	5,6	5,6		

[a] For correlated methods the symbol δ denotes the increment in the relative energy (ΔE_e) with respect to the preceding level of theory in the hierarchy RHF→MP2→CCSD→CCSD(T) →CCSDT→CCSDT(Q). Square brackets signify results obtained from basis set extrapolations or the assumption of additivity. Final predictions are boldfaced.

The auxiliary corrections considered here all have a minor effect on the final computed reaction energy. The core correction is the most significant and contributes just –0.11 kcal mol^{-1}. The DBOC and relativistic corrections are an order of magnitude smaller still, and contribute just 0.01 and 0.03 kcal mol^{-1}, respectively.

Table 3.4. Fundamental and harmonic frequencies (cm^{-1}) for H_2, acetylene, and diacetylene.[a]

	VPT2 CCSD(T) cc-pCVQZ			Experiment			
	ω	Δ	ν	ω		ν	
H_2							
ν_1 (σ_g)	4403.5	–122.7	4158.0	4403		4160.3	
Acetylene							
ν_1 (σ_g)	3508.4	–134.6	3373.8	3496.9	(3501.5)	3372.9	(3371.7)
ν_2 (σ_g)	2013.4	–35.7	1977.7	2010.7	(2013.3)	1974.4	(1974.8)
ν_3 (σ_u)	3416.1	–126.4	3289.7	3415.4	(3417.6)	3288.6	(3288.8)
ν_4 (π_g)	606.3	45.7	652.0	624.0	(621.5)	612.9	(612.6)
ν_5 (π_u)	747.6	–14.6	733.1	746.7	(746.8)	730.3	(730.4)
Diacetylene							
ν_1 (σ_g)	3463.3	–129.6	3333.7	3489 ± 35		3332.2	
ν_2 (σ_g)	2243.0	–47.2	2195.8	2222 ± 22		2188.9	
ν_3 (σ_g)	894.4	–27.5	867.0	885 ± 9		872.0	
ν_4 (σ_u)	3464.5	–130.7	3333.8	3490 ± 35		3333.7	
ν_5 (σ_u)	2064.0	–38.3	2025.8	2050 ± 21		2022.2	
ν_6 (π_g)	636.3	–7.6	628.7	638 ± 6		625.6	
ν_7 (π_g)	484.5	2.3	486.9	490 ± 5		482.7	
ν_8 (π_u)	639.6	–10.8	628.8	641 ± 6		628.0	
ν_9 (π_u)	221.4	–3.6	217.8	223 ± 2		220.1	

[a] Experimental values for H_2 taken from Herzberg[88] and Huber and Herzberg.[86] The experimental values for acetylene are those quoted in Table 2 of Martin, Lee and Taylor,[71] except those in parentheses, which come from Temsamani and Herman.[89] For diacetylene, the experimental harmonic frequencies are those of Williams and Macdonald,[9] which were derived from empirically corrected gas phase fundamental frequencies. The corresponding observed fundamentals are from McNaughton and Bruget.[19]

The vibrational frequencies of H_2, acetylene, and diacetylene are shown in Table 3.4. The agreement with experiment is very good in general, particularly for the harmonic components; however the aforementioned intramolecular basis set superposition error is evident for the centrosymmetric π bending modes of acetylene and, to a lesser degree, diacetylene. Consequently, the harmonic frequencies are underestimated and the anharmonic corrections are overestimated. The magnitude of this error appears to be much greater for acetylene than for diacetylene, implying that the presence of the extra carbon atoms increases the basis set completeness significantly, reducing the extent to which neighbors' basis functions impinge

upon distortion from linearity. A further test of the force field for diacetylene is detailed in Table 3.5, where the harmonic and fundamental frequencies of mono- and di-deuterated diacetylene are tabulated. The anharmonicity constants and *l*-type doubling constants for acetylene and diacetylene are tabulated in Table 3.6 and Table 3.7, respectively.

Table 3.5. Fundamental and harmonic frequencies (cm^{-1}) for mono- and di-deuteroacetylene from theory (CCSD(T) cc-pCVQZ, this work) and experiment.[a]

	H–C≡C–C≡C–D				D–C≡C–C≡C–D			
	ω Theory	ω Exp.	ν Theory	ν Exp.	ω Theory	ω Exp.	ν Theory	ν Exp.
ν_1 (σ_g)	3464	3489	3308	3332	2686	2701	2606	2605
ν_2 (σ_g)	2200	2178	2156	2146	2116	2097	2078	2067
ν_3 (σ_g)	879	867	852	854	865	851	837	839
ν_4 (σ_u)	2682	2696	2619	2600	2677	2693	2601	2598
ν_5 (σ_u)	1975	1967	1945	1938	1927	1917	1895	1890
ν_6 (π_g)	638	640	619	627	500	508	500	500
ν_7 (π_g)	477	478	476	471	468	466	463	459
ν_8 (π_u)	501	507	507	499	503	505	493	497
ν_9 (π_u)	212	213	210	210	203	205	201	202

[a] Symmetry labels and ordering correspond to the parent isotopolog. Experimental fundamental frequencies are from low resolution IR and liquid phase Raman studies performed by Owen, Smith, and Williams.[12] The corresponding harmonics are derived by assuming transferability of anharmonicities amongst related molecules, and have been assigned 1% error bars.[9]

Table 3.6. Vibrational anharmonicity constants and *l*-type doubling constants (cm^{-1}) for acetylene at the all electron CCSD(T) cc-pCVQZ level of theory.

x_{11}	–26.082	x_{41}	–13.063	x_{53}	–8.742
x_{21}	–11.156	x_{42}	–12.982	x_{54}	–1.435
x_{22}	–6.814	x_{43}	–7.280	x_{l4l4}	–5.946
x_{31}	–106.506	x_{44}	23.260	x_{l5l4}	6.621
x_{32}	–5.092	x_{51}	–10.560	x_{l5l5}	3.501
x_{33}	–27.269	x_{52}	–0.965	r_{54}	2.145

Table 3.7. Vibrational anharmonicity constants and *l*-type doubling constants (cm^{-1}) for diacetylene at the all electron CCSD(T) cc-pCVQZ level of theory.

x_{11}	–27.056	x_{71}	–2.817	x_{96}	–0.811
x_{21}	–2.609	x_{72}	–1.685	x_{97}	–1.752
x_{22}	–5.623	x_{73}	–26.362	x_{98}	–0.328
x_{31}	1.392	x_{74}	0.538	x_{99}	–0.227
x_{32}	–0.322	x_{75}	–5.264	x_{l6l6}	1.787
x_{33}	–2.753	x_{76}	3.834	x_{l7l6}	0.009
x_{41}	–105.257	x_{77}	8.825	x_{l7l7}	–7.111
x_{42}	–13.923	x_{81}	–7.822	x_{l8l6}	7.115
x_{43}	4.654	x_{82}	–10.402	x_{l8l7}	0.011
x_{44}	–26.490	x_{83}	3.193	x_{l8l8}	1.698
x_{51}	–4.098	x_{84}	–9.410	x_{l9l6}	0.494
x_{52}	–13.428	x_{85}	–5.143	x_{l9l7}	0.498
x_{53}	–2.036	x_{86}	–0.264	x_{l9l8}	0.823
x_{54}	–3.865	x_{87}	–1.318	x_{l9l9}	0.576
x_{55}	–4.311	x_{88}	1.410	r_{76}	4.479
x_{61}	–9.383	x_{91}	–0.189	r_{86}	–0.345
x_{62}	–5.024	x_{92}	–3.678	r_{87}	0.521
x_{63}	–5.134	x_{93}	4.511	r_{96}	1.961
x_{64}	–9.385	x_{94}	–0.300	r_{97}	0.249
x_{65}	–5.926	x_{95}	–1.611	r_{98}	2.145
x_{66}	1.773				

The zero point vibrational energy (ZPVE) correction is rather large, contributing –4.03 kcal mol^{-1} to the reaction energy. The corresponding correction within the harmonic oscillator approximation is –3.99 kcal mol^{-1}, so the contribution from anharmonicity is very small. The presence of the anomalous π_g modes raises concerns about the accuracy of any ZPVE contribution derived from these frequencies; however this is appeased by comparing our ZPVE for acetylene with the recommended value of Martin, Lee, and Taylor.[71] Their best computations reproduce all fundamental modes of acetylene within 6 cm^{-1}, and the corresponding ZPVE lowers our computed reaction energy by just 0.06 kcal mol^{-1}.

The thermal correction to this reaction enthalpy can be computed from the partition functions of the individual species. Using standard treatments, the electronic and translational contributions are equal for both reactants and products, leaving only a contribution from the

vibrational and rotational terms; the former is treated analytically in the harmonic approximation, while direct summation over rigid rotor energy levels provides the latter. The total resulting thermal contribution is 0.65 kcal mol^{-1} at 298.15 K.

By considering all of the above factors, we finally arrive at a 0 K reaction enthalpy of 0.03 kcal mol^{-1}, which becomes 0.68 kcal mol^{-1} at 298.15 K. Combining this purely *ab initio* reaction enthalpy with the enthalpies of formation for acetylene detailed above, we arrive at $\Delta_f H_0^\circ$ = 109.4 ± 0.3 kcal mol^{-1} and $\Delta_f H_{298}^\circ$ = 109.7 ± 0.3 kcal mol^{-1} for diacetylene. Our value is bracketed by the previously suggested enthalpies of formation, which were derived from chemical group increments, falling between 105 kcal mol^{-1} (Stein *et al.*)[39] and 111 kcal mol^{-1} (Kiefer *et al.*)[41] agreeing more favorably with the latter.

3.5 Conclusions

Using precise computational methodology, we have computed the thermally corrected enthalpy for the reaction 2 H–C≡C–H → H–C≡C–C≡C–H + H_2. This equation is remarkably close to thermoneutral, being endothermic by only 0.03 kcal mol^{-1} at 0 K. The vibrational contribution to this reaction energy was computed by the explicit computation of anharmonic vibrational frequencies, *i.e.*, no empirical scale factors were used; this is the first complete anharmonic force field diacetylene.

The resulting vibrational frequencies agree very favorably with experimentally observed modes, showing a deviation of no more than 2.9 cm^{-1} for all vibrational modes, excluding the troublesome π_g mode, which has been shown to be very sensitive to the basis set used and is consequently underestimated by 39 cm^{-1} for the acetylene molecule. The vibrational frequencies for diacetylene exhibit excellent agreement with experiment, deviating by no more than 6.9 cm^{-1}.

Combining our findings with previous determinations of the acetylene molecule's enthalpy of formation, we recommend enthalpies of formation of $\Delta_f H_0^o$ = 109.4 ± 0.3 kcal mol^{-1} and $\Delta_f H_{298}^o$ = 109.7 ± 0.3 kcal mol^{-1} for the diacetylene molecule.

3.6 Acknowledgments

ACS would like to thank Dr. S. E. Wheeler for discussions. The NERSC supercomputing facility of the US Department of Energy (DOE) was used to compute the quartic force fields described herein. This research was supported by the DOE Office of Basic Energy Sciences, Combustion Program (Grant number DE-FG02-97ER14748).

References

1 J. P. Senosiain, S. J. Klippenstein, and J. A. Miller, Proc. Comb. Inst. **31**, 185 (2007).

2 J. H. Kiefer, S. S. Sidhu, R. D. Kern, K. Xie, H. Chen, and L. B. Harding, Combust. Sci. Technol. **82**, 101 (1992).

3 C. S. McEnally, L. D. Pfefferle, A. G. Robinson, and T. S. Zwier, Combust. Flame **123**, 344 (2000).

4 C. S. McEnally, L. D. Pfefferle, B. Atakan, and K. Kohse-Höinghaus, Prog. Energy Combust. Sci. **32**, 247 (2006).

5 J. A. Miller and C. F. Melius, Combust. Flame **91**, 21 (1992).

6 J. H. Waite, D. T. Young, T. E. Cravens, A. J. Coates, F. J. Crary, B. Magee, and J. Westlake, Science **316**, 870 (2007).

7 R. E. Bandy, C. Lakshminarayan, R. K. Frost, and T. S. Zwier, Science **258**, 1630 (1992).

8 G. Fischer and I. G. Ross, J. Phys. Chem. A **107**, 10631 (2003).

[9] G. A. Williams and J. N. Macdonald, J. Mol. Struct. **320**, 217 (1994).

[10] P. Botschwina, Mol. Phys. **47**, 241 (1982).

[11] T. Koops, T. Visser, and W. M. A. Smit, J. Mol. Struct. **125**, 179 (1984).

[12] N. L. Owen, C. H. Smith, and G. A. Williams, J. Mol. Struct. **161**, 33 (1987).

[13] K. Nauta and R. E. Miller, J. Mol. Spectrosc. **223**, 101 (2004).

[14] G. Guelachvili, A. M. Craig, and D. A. Ramsay, J. Mol. Spectrosc. **105**, 156 (1984).

[15] L. Pasternack and J. R. McDonald, J. Mol. Spectrosc. **108**, 143 (1984).

[16] M. Tanimoto, K. Kuchitsu, and Y. Morino, Bull. Chem. Soc. Jpn. **44**, 386 (1971).

[17] J. L. Hardwick, D. A. Ramsay, J.-L. Garneau, J. Lavigne, and A. Cabana, J. Mol. Spectrosc. **76**, 492 (1979).

[18] J. E. Gambogi, R. Z. Pearson, Y. Xueming, K. K. Lehmann, and G. Scoles, Chem. Phys. **190**, 191 (1995).

[19] D. McNaughton and D. N. Bruget, J. Mol. Struct. **273**, 11 (1992).

[20] A. G. Robinson, P. R. Winter, and T. S. Zwier, J. Phys. Chem. A **106**, 5789 (2002).

[21] R. W. Wetmore and H. F. Schaefer, J. Chem. Phys. **69**, 1648 (1978).

[22] R. E. Bandy, C. Lakshminarayan, R. K. Frost, and T. S. Zwier, J. Chem. Phys. **98**, 5362 (1993).

[23] R. K. Frost, G. Zavarin, and T. S. Zwier, J. Phys. Chem. **99**, 9408 (1995).

[24] R. K. Frost, C. A. Arrington, C. Ramos, and T. S. Zwier, J. Am. Chem. Soc. **118**, 4451 (1996).

[25] C. A. Arrington, C. Ramos, A. D. Robinson, and T. S. Zwier, J. Phys. Chem. A **102**, 3315 (1998).

[26] X. Zhang, A. T. Maccarone, M. R. Nimlos, S. Kato, V. M. Bierbaum, G. B. Ellison, B. Ruscic, A. C. Simmonett, W. D. Allen, and H. F. Schaefer, J. Chem. Phys. **126**, 044312 (2007).

[27] J. H. Kiefer, L. J. Mizerka, M. R. Patel, and H. C. Wei, J. Phys. Chem. **89**, 2013 (1985).

[28] F. Goulay, D. L. Osborn, C. A. Taatjes, P. Zou, G. Meloni, and S. R. Leone, Phys. Chem. Chem. Phys. **9**, 4291 (2007).

[29] M. Weissman and S. W. Benson, Int. J. Chem. Kinet. **16**, 307 (1984).

[30] M. Frenklach, D. W. Clary, W. C. Gardiner, and S. E. Stein, Proc. Combust. Inst. **20**, 887 (1985).

[31] S. J. Klippenstein and J. A. Miller, J. Phys. Chem. A **109**, 4285 (2005).

[32] H. Wang and M. Frenklach, Combust. Flame **110**, 173 (1997).

[33] M. Hausmann and K.-H. Homann, Ber. Bunsen-Ges. Phys. Chem **101**, 651 (1997).

[34] R. I. Kaiser, W. Sun, A. G. Suits, and Y. T. Lee, J. Chem. Phys. **107**, 8713 (1997).

[35] M. Cowperthwaite and S. H. Bauer, J. Chem. Phys. **36**, 1743 (1962).

[36] M. J. S. Dewar and W. Thiel, J. Am. Chem. Soc. **99**, 4907 (1977).

[37] M. J. S. Dewar, E. G. Zoebisch, E. F. Healy, and J. J. P. Stewart, J. Am. Chem. Soc. **107**, 3209 (1985).

[38] D. R. Stull, E. F. Westrum, and S. G. C, *The Chemical Thermodynamics of Organic Compounds*. (Wiley, New York, 1969).

[39] S. E. Stein and A. Fahr, J. Phys. Chem. **89**, 3714 (1985).

[40] J. H. Kiefer and W. A. Von Drasek, Int. J. Chem. Kinet. **22**, 747 (1990).

[41] J. H. Kiefer, S. S. Sidhu, R. D. Kern, K. Xie, H. Chen, and L. B. Harding, Combust. Sci. Technol. **82**, 101 (1992).

[42] M. W. Chase, J. Phys. Chem. Ref. Data, Monograph 9, 675 (1998).

[43] S. Parthiban, J. M. L. Martin, and J. F. Liebman, Mol. Phys. **100**, 453 (2002).

[44] L. V. Gurvich, I. V. Veyts, C. B. Alcock, and V. S. Iorish, *Thermodynamic Properties of Individual Substances*, 4th ed. (Hemisphere, New York City, 1991).

[45] Y. J. Bomble, J. Vázquez, M. Kállay, C. Michauk, P. G. Szalay, A. G. Császár, J. Gauss, and J. F. Stanton, J. Chem. Phys. **125**, 064108 (2006).

[46] K. Raghavachari, G. W. Trucks, J. A. Pople, and M. Head-Gordon, Chem. Phys. Lett. **157**, 479 (1989).

[47] J. F. Stanton, Chem. Phys. Lett. **281**, 130 (1997).

[48] D. E. Woon and T. H. Dunning, J. Chem. Phys. **103**, 4572 (1995).

[49] K. L. Bak, J. Gauss, P. Jørgensen, J. Olsen, T. Helgaker, and J. F. Stanton, J. Chem. Phys. **114**, 6548 (2001).

[50] A. L. L. East and W. D. Allen, J. Chem. Phys. **99**, 4638 (1993).

[51] M. S. Schuurman, S. R. Muir, W. D. Allen, and H. F. Schaefer, J. Chem. Phys. **120**, 11586 (2004).

[52] J. M. Gonzales, C. Pak, R. S. Cox, W. D. Allen, H. F. Schaefer, A. G. Császár, and G. Tarczay, Chem. Eur. J. **9**, 2173 (2003).

[53] A. G. Császár, W. D. Allen, and H. F. Schaefer, J. Chem. Phys. **108**, 9751 (1998).

[54] T. Helgaker, W. Klopper, H. Koch, and J. Noga, J. Chem. Phys. **106**, 9639 (1997).

[55] D. Feller, J. Chem. Phys. **98**, 7059 (1993).

[56] Y. J. Bomble, J. F. Stanton, M. Kallay, and J. Gauss, J. Chem. Phys. **123**, 054101 (2005).

[57] T. H. Dunning, J. Chem. Phys. **90**, 1007 (1989).

[58] A. K. Wilson, T. van Mourik, and T. H. Dunning Jr., THEOCHEM **388**, 339 (1996).

[59] N. C. Handy, Y. Yamaguchi, and H. F. Schaefer, J. Chem. Phys. **84**, 4481 (1986).

[60] H. Sellers and P. Pulay, Chem. Phys. Lett. **103**, 463 (1984).

[61] R. D. Cowan and D. C. Griffin, J. Opt. Soc. Am. **66**, 1010 (1976).

[62] G. Strey and I. M. Mills, J. Mol. Spectrosc. **59**, 103 (1976).

[63] A. L. L. East, C. S. Johnson, and W. D. Allen, J. Chem. Phys. **98**, 1299 (1993).

[64] J. K. G. Watson, in *Vibrational Spectra and Structure*, edited by J. R. Durig (Elsevier, Amsterdam, 1977), Vol. 6, pp. 1.

[65] D. A. Clabo, W. D. Allen, R. B. Remington, Y. Yamaguchi, and H. F. Schaefer, Chem. Phys. **123**, 187 (1988).

[66] W. D. Allen, Y. Yamaguchi, A. G. Császár, D. A. Clabo, R. B. Remington, and H. F. Schaefer, Chem. Phys. **145**, 427 (1990).

[67] I. M. Mills, in *Molecular Spectroscopy: Modern Research*, edited by K. N. Rao and C. W. Mathews (Academic Press, New York, 1972), pp. 115.

[68] D. Papoušek and M. R. Aliev, *Molecular Vibrational-Rotational Spectra*. (Elsevier, Amsterdam, 1982).

[69] K. Aarset, A. G. Császár, E. L. Sibert, W. D. Allen, H. F. Schaefer, W. Klopper, and J. Noga, J. Chem. Phys. **112**, 4053 (2000).

[70] H. H. Nielsen, Reviews of Modern Physics **23**, 90 (1951).

[71] J. M. L. Martin, T. J. Lee, and P. R. Taylor, J. Chem. Phys. **108**, 676 (1998).

[72] J. M. L. Martin, P. R. Taylor, and T. J. Lee, Chem. Phys. Lett. **275**, 414 (1997).

[73] D. Moran, A. C. Simmonett, F. E. Leach, W. D. Allen, P. v. R. Schleyer, and H. F. Schaefer, J. Am. Chem. Soc. **128**, 9342 (2006).

[74] J. Almlöf and P. R. Taylor, J. Chem. Phys. **86**, 4070 (1987).

[75] A. G. Császár and W. D. Allen, J. Chem. Phys. **104**, 2746 (1996).

[76] Stanton, J.F.; Gauss, J.; Watts, J.D.; Szalay, P.G.; Bartlett R.J., with contributions from Auer, A.A.; Bernholdt, D.B.; Christiansen, O.; Harding, M.E.; Heckert, M.; Heun, O.; Huber, C.; Jonsson, D.; Jusélius, J.; Lauderdale, W.J.; Metzroth, T.; Michauk, C.; Price, D.R.; Ruud, K.; Schiffmann, F.;. Tajti, A; Varner, M.E.; Vázquez, J. and the integral packages: MOLECULE (Almlöf; J. and Taylor, P.R.), PROPS (Taylor, P.R.), and ABACUS (Helgaker, T.; Jensen, H.J. Aa.; Jørgensen, P. and Olsen, J.). Current version see http://www.aces2.de. .

[77] J. F. Stanton, J. Gauss, J. D. Watts, W. J. Lauderdale, and R. J. Bartlett, Int. J. Quantum Chem **44 (S26)**, 879 (1992).

[78] MOLPRO is a package of ab initio programs written by Werner, H.-J.; Knowles, P. J.; Lindh, R.; Manby, F. R.; Schütz, M.; Celani, P. ; Korona, T.; Rauhut, G. ; Amos, R. D.; Bernhardsson, A.; Berning, A.; Cooper, D. L.; Deegan, M. J. O.; Dobbyn, A. J.; Eckert, F.; Hampel, C.; Hetzer, G.; Lloyd, A. W.; McNicholas, S. J.; Meyer, W.; Mura, M. E.; Nicklaß, A.; Palmieri, P.; Pitzer, R.; Schumann, U.; Stoll, H.; Stone, A. J.; Tarroni, R. and Thorsteinsson, T. .

[79] T. D. Crawford, C. D. Sherrill, E. F. Valeev, J. T. Fermann, R. A. King, M. L. Leininger, S. T. Brown, C. L. Janssen, E. T. Seidl, J. P. Kenny, and W. D. Allen, J. Comput. Chem. **28**, 1610 (2007).

[80] *Mathematica*, Wolfram Research, Inc., Champaign, IL (2003).

[81] INTDIF2005 is an abstract program written by Wesley D. Allen for *Mathematica* to perform general numerical differentiations to high orders of electronic structure data.

[82] INTDER2005 is a general program written by Wesley D. Allen, which performs sundry vibrational analyses and higher order nonlinear transformations among force field representations.

[83] K. Sarka and J. Demaison, in *Computational Molecular Spectroscopy*, edited by P. Jensen and P. R. Bunker (Wiley, Chichester, 2000), pp. 255.

[84] ANHARM is a FORTRAN program written for VPT2 analysis written by Yukio Yamaguchi and Henry F. Schaefer (Center for Computational Chemistry, University of Georgia, Athens, GA, 30602, USA).

[85] F. Pawłowski, P. Jørgensen, J. Olsen, F. Hegelund, T. Helgaker, J. Gauss, K. L. Bak, and J. F. Stanton, J. Chem. Phys. **116**, 6482 (2002).

[86] K. P. Huber and G. Herzberg, *Molecular Spectra and Molecular Structure IV. Constants of Diatomic Molecules*. (Van Nostrand Reinhold, New York, 1979).

[87] Y. Kabbadj, M. Herman, G. Di Lonardo, L. Fusina, and J. W. C. Johns, J. Mol. Spectrosc. **150**, 535 (1991).

[88] G. Herzberg, *Spectra of Diatomic Molecules*. (Van Nostrand Reinhold, New York, 1950).

[89] M. A. Temsamani and M. Herman, J. Chem. Phys. **102**, 6371 (1995).

CHAPTER 4

SUMMARY AND CONCLUSIONS

4.1 Concluding Remarks

Using a range of highly accurate wavefunction-based methods, we have demonstrated how computational methods can aid in the description of intermediates and transition states commonly encountered in combustion chemistry. Vibrational frequencies can be computed without resorting to empirical scale factors and these can be of great utility in cases where synthesis and/or characterization of molecules is not trivial. These methods can also assist in the assignment of experimental vibrational spectra, which are often convoluted by the presence of overtone and combination bands. The focal point technique has been demonstrated to be a reliable and flexible way to obtain relative energies, whilst providing diagnostics of the final result. The combination of accurate experimental data and high-level theory is a pragmatic and accurate route to enthalpies of formation.

However, one important issue was only briefly discussed and warrants elaboration here: the issue of multi-reference character. In the case of ortho-benzyne, we saw that the wavefunction has ~10% diradical character, *i.e.* the wavefunction should be qualitatively written as a linear combination of two electron configurations; one with a 90% weight that doubly occupies the in plane π bond, and one with a 10% weight that has the in-plane π^* doubly occupied. The inclusion of high-order excitations allows us to start from a wavefunction that includes only the dominant component, but this would not be true if the ratio were higher, say 60:40. In this case, we would have severe multi-reference character and the concept of making small modifications to a wavefunction described by a single occupation does not work.

In combustion chemistry, many molecules with esoteric structure are created that simply could not exist in another environment. Multi-reference character is frequently observed in these systems and must be dealt with carefully. To this end, we have recently implemented an

extremely efficient multi-reference CCSD algorithm within the PSI3 program package, which is freely available to the academic community.[1,2] To allow multi-reference focal point analysis, we have also derived and implemented the multi-reference CCSDT analog to more completely treat the correlation.[3] Furthermore, we are working towards a multi-reference perturbation theory that will allow large basis sets to be used in order to extrapolate to the one-particle basis set limit. These methods can be applied in a manner analogous to the single-reference case to achieve highly accurate results for molecules that represent an incredibly tough subset of chemistry for theory and experiment alike.

REFERENCES

1 T. D. Crawford, C. D. Sherrill, E. F. Valeev, J. T. Fermann, R. A. King, M. L. Leininger, S. T. Brown, C. L. Janssen, E. T. Seidl, J. P. Kenny, and W. D. Allen, J. Comput. Chem. **28**, 1610 (2007).

2 F. A. Evangelista, W. D. Allen, and H. F. Schaefer, J. Chem. Phys. **127**, 024102 (2007).

3 F. A. Evangelista, A. C. Simmonett, W. D. Allen, H. F. Schaefer, and J. Gauss, J. Chem. Phys. **128**, 124104 (2008).

APPENDIX A

UNIMOLECULAR THERMAL FRAGMENTATION OF ORTHO-BENZYNE[†]

[†] X. Zhang, A. T. Maccarone, M. R. Nimlos, S. Kato, V. M. Bierbaum, G. B. Ellison, B. Ruscic, A. C. Simmonett, W. D. Allen, and H. F. Schaefer, J. Chem. Phys. **126**, 044312 (2007). Reprinted here with permission of the American Institute of Physics.

ABSTRACT

We have produced the ortho-benzyne diradical, *o*-C_6H_4, with a hyperthermal, supersonic nozzle and studied its subsequent thermal decomposition. As the temperature of the nozzle is increased, the benzyne molecule fragments: *o*-C_6H_4 + Δ → products. The thermal dissociation products were identified by three experimental methods: (i) time-of-flight photoionization mass spectrometry, (ii) matrix-isolation Fourier transform infrared absorption spectroscopy, and (iii) chemical ionization mass spectrometry. At the threshold dissociation temperature, *o*-benzyne cleanly decomposes into acetylene and diacetylene via an apparent retro-Diels-Alder process: *o*-C_6H_4 + Δ → HC≡CH + HC≡C-C≡CH. The experimental $\Delta_{rxn}H_{298}$(*o*-C_6H_4 → HC≡CH + HC≡C-C≡CH) is found to be 57 ± 3 kcal mol^{-1}. Further experiments with the substituted benzyne, 3,6-$(CH_3)_2$-*o*-C_6H_2, are consistent with a retro-Diels-Alder fragmentation. But at higher nozzle temperatures, the cracking pattern becomes more complicated. To interpret these experiments, the retro-Diels-Alder fragmentation of *o*-benzyne has been investigated by rigorous *ab initio* electronic structure computations. These calculations used basis sets as large as [C(7*s*6*p*5*d*4*f*3*g*2*h*1*i*)/H(6*s*5*p*4*d*3*f*2*g*1*h*)] (cc-pV6Z) and electron correlation treatments as extensive as full coupled cluster through triple excitations (CCSDT), in cases with a perturbative term for connected quadruples [CCSDT(Q)]. Focal point extrapolations of the computational data yield a 0 K barrier for the concerted, C_{2v}-symmetric decomposition of *o*-benzyne, E_b(*o*-C_6H_4 → HC≡CH + HC≡C-C≡CH) = 88.0 ± 0.5 kcal mol^{-1}. A barrier of this magnitude is consistent with the experimental results. A careful assessment of the thermochemistry for the high temperature fragmentation of benzene is presented: C_6H_6 → H + [C_6H_5] → H + [*o*-C_6H_4] → HC≡CH + HC≡C-C≡CH. Benzyne may be an important intermediate in the thermal decomposition of many alkylbenzenes (arenes). High engine temperatures above 1500 K may

crack these alkylbenzenes to a mixture of alkyl radicals and phenyl radicals. The phenyl radicals will then dissociate first to benzyne and then to acetylene and diacetylene.

INTRODUCTION

This is a combined experimental and theoretical study of the thermal fragmentation of benzyne. We have used a high temperature nozzle to observe the thermal fragmentation of benzyne (a C_6H_6 fragmentation product) to acetylene and diacetylene. The analysis of the pyrolysis products emerging from the hyperthermal nozzle is based on three analytical techniques: (i) Time of Flight Photoionization Mass Spectrometry (TOF-PIMS), (ii) Matrix-Isolation Fourier Transform Infrared Absorption Spectroscopy (Matrix-Isolation FTIR), and (iii) Chemical Ionization Mass Spectrometry (CIMS). To better interpret these experiments we have used high-level *ab initio* electronic structure computations [fully optimized structures and corresponding vibrational frequencies at the valence CCSD(T)/cc-pVTZ and composite all-electron CCSD(T)/cc-pCVQZ levels of theory with focal point extrapolations of the energetics to the complete basis set (CBS) CCSDT(Q) limit] to characterize the transition state for the C_{2v} symmetric, retro-Diels-Alder fragmentation: $[o\text{-}C_6H_4]^{\ddagger} \rightarrow HC{\equiv}CH + HC{\equiv}C\text{-}C{\equiv}CH$. Finally an analysis of thermochemistry of toluene and more complex arenes is presented. The high temperature thermochemistry of these arenes suggests that one might generalize the retro-Diels-Alder mechanism for benzene dissociation, (equations. A1 — A3), to include the high temperature (T > 1500 K) fragmentation of many alkybenzenes.

The thermal fragmentation of benzene has been extensively studied in shock tubes[1,2] and theoretically.[3-6] Most mechanisms have the C–H bond fission as the first step[2] to produce H atom and the phenyl radical:

$$C_6H_6 + M \rightarrow C_6H_5 + H + M \qquad (A1)$$

As noted by Kiefer et al.,[2] benzene decomposition at modest temperatures yields equal amounts of HCCH and HCC-CCH as the dominant products. However in all of these flow reactor, Knudsen cell, and shock tube studies there is a surprising absence of C_6H_5 signals.

The fate of the phenyl radical is of great interest[3-6] and much evidence suggests that the phenyl radicals further eliminate a second H atom to produce the 1, 2-diradical, ortho-benzyne (*o*-C_6H_4).

$$C_6H_5 + M \rightarrow o\text{-}C_6H_4 + H + M \qquad (A2)$$

A possible fate of *o*-C_6H_4 is fragmentation to acetylene and diacetylene:

$$o\text{-}C_6H_4 + D \rightarrow HC{\equiv}CH + HC{\equiv}C\text{-}C{\equiv}CH \qquad (A3)$$

We should consider several different dissociation pathways for o-benzyne to dissociate. Path A is a concerted, C_{2v} symmetric bond rupture of *o*-C_6H_4 and is a retro-didehydro Diels-Alder reaction. A concerted reaction implies that there are no bound intermediates between *o*-C_6H_4 and the acetylene/diacetylene fragments. Path B is a concerted asymmetric bond rupture of the *o*-C_6H_4 diradical. Or a final possibility is Path C, a nonconcerted, asymmetric bond rupture of the *o*-C_6H_4 diradical to produce an open-chain diradical intermediate. Subsequent decomposition of

this diradical intermediate produces acetylene/diacetylene: $[o\text{-}C_6H_4]^{\ddagger} \rightarrow$ [HC≐C⋯C=CH-CH=CH•] → HC≡CH + HC≡C-C≡CH.

There also exists the possibility that $o\text{-}C_6H_4$ may isomerize before it fragments. Instead of dissociating via (A3), $o\text{-}C_6H_4$ could rearrange first to m-benzyne and then to p-benzyne. At 1000 K it has been predicted that $o\text{-}C_6H_4$ overwhelmingly isomerizes to *p*-benzyne which could undergo[5] a Bergman fragmentation[7,8] to the endiyne, (Z)-HCC-CH=CH-CCH at higher temperatures. Scheme I shows these related reactions.

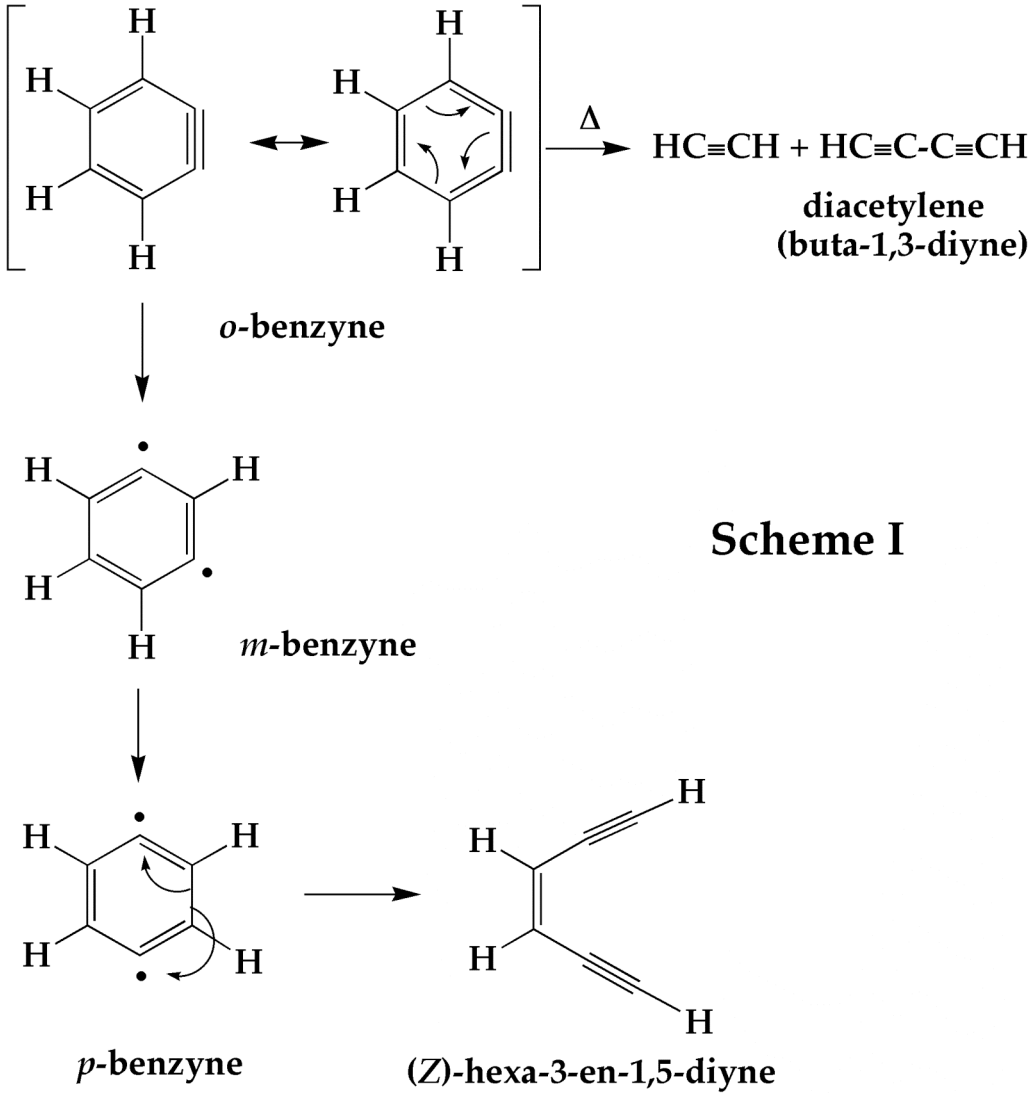

Scheme I

In order to understand (A1) — (A3), it is essential to have a firm grasp of the thermochemistry. We need accurate values for the following heats of formation: $\Delta_f H_{298}(C_6H_6)$, $\Delta_f H_{298}(C_6H_5)$, $\Delta_f H_{298}(o\text{-}C_6H_4)$, $\Delta_f H_{298}(m\text{-}C_6H_4)$, $\Delta_f H_{298}(p\text{-}C_6H_4)$, $\Delta_f H_{298}$(HCC-CH=CH-CCH), $\Delta_f H_{298}$(HCCH), and $\Delta_f H_{298}$(HCC-CCH). For the energies of closed shell species such as benzene and acetylene, we have used standard tables.[9] But the thermochemistry of phenyl radical, the benzynes, diacetylene, or the ene-diyne, (Z)-HCC-CH=CH-CCH, is not routinely tabulated.

In an experimental study[10] of the high temperature pyrolysis of acetylene, the heat of formation of diacetylene (HC≡C-C≡CH, buta-1,3-diyne) was quoted as $\Delta_f H_{298}$(HCC-CCH) = 111 kcal mol^{-1}. This paper used results from an earlier set of group additivity estimates[11] which placed $\Delta_f H_{298}$(HCC-CCH) in the range between 105 and 113 kcal mol^{-1}. There seems to be no reliable experimental thermochemistry for diacetylene, so we have used electronic structure computations to pinpoint $\Delta_f H_{298}$(diacetylene) by means of the isogyric reaction HC≡C-C≡CH + $H_2 \rightarrow$ 2 HCCH. Focal-point extrapolations conjoining MP2/cc-pV6Z, CCSD(T)/cc-pV5Z, and CCSDT(Q)/cc-pVDZ results (vide infra) yield $\Delta_f H_{298}$(diacetylene) = 109.4 ± 0.3 kcal mol^{-1}.

Calometric studies of the catalytic hydrogenation of the ene-diyne have been carried out and it is reported[12] that the solution heat of formation is $\Delta_f H_{298}$((Z)-HCC-CH=CH-CCH) = 129.5 kcal mol^{-1}. Most of the thermochemistry for the remaining aryl radicals and diradicals is available via the negative ion/acidity thermochemical cycle.[13,14]

The phenyl radical, C_6H_5, is known by EPR studies[15] and infrared absorption studies[16,17] to be a C_{2v} species with a $\tilde{X}\ ^2A_1$ ground state. The microwave spectrum of the C_6H_5 radical has been detected[18] but as yet the molecular structure has not been determined. Photoionization studies[19] of phenyl have reported IE(C_6H_5) = 8.32 ± 0.04 eV; however more recent photoelectron

spectroscopic studies[20] of beams of the phenyl radical find a slightly lower value; IE(C_6H_5) = 8.1 ± 0.1 eV. Negative ion photodetachment studies[21] established the electron affinity of the phenyl radical, EA(C_6H_5), to be 1.096 ± 0.006 eV. Use of the gas-phase enthalpy of deprotonation of benzene,[22,23] $\Delta_{acid}H_{298}(C_6H_5\text{-}H)$ = 401.2 ± 0.2 kcal mol^{-1}, and the EA(C_6H_5) in the acidity/EA thermochemical cycle[13,14] furnished the bond energy of benzene, $DH_{298}(C_6H_5\text{-}H)$ = 112.9 ± 0.5 kcal mol^{-1}. Since the heat of formation of benzene is known[9] to be $\Delta_fH_{298}(C_6H_6)$ = 19.7 ± 0.2 kcal mol^{-1}, the value of the C-H bond energy determines the heat of formation of the phenyl radical to be $\Delta_fH_{298}(C_6H_5)$ = 80.5 ± 0.5 kcal mol^{-1}.

Almost 50 years ago, a series of pioneering papers[24-26] clearly demonstrated that samples of gaseous benzyne could be generated. Rudimentary UV absorption spectra and EI mass spectra were reported[26-28] for all isomers of C_6H_4. The *o*-benzyne diradical, 1,2-dehydrobenzene, has been detected by microwave spectroscopy[29] and analyzed[30,31] to be a planar, C_{2v} ring. The ground state of *o*-C_6H_4 is $\tilde{X}\ ^1A_1$. The ionization potential of this diradical was measured[32] to be IE(*o*-C_6H_4) = 9.03 ± 0.05 eV. The ground state of the benzyne cation (*o*-$C_6H_4^+$) was assigned to be a "p-cation", $\tilde{X}\ ^2A_2$ and there is surely a second, nearly degenerate p-cation state, $\tilde{A}\ ^2B_1$. The term value of the excited "s-cation" state was found to be $T_0(\tilde{B}\ ^2A_1 — \tilde{X}\ ^2A_2)$ = 0.74 ± 0.06 eV.

The two lowest electronic states of *o*-C_6H_4 can be represented[33] by a pair of electrons in the lobe orbitals $\{l_a, l_b\}$ that are coupled singlet ($^1A_1$) or triplet ($^3B_2$).

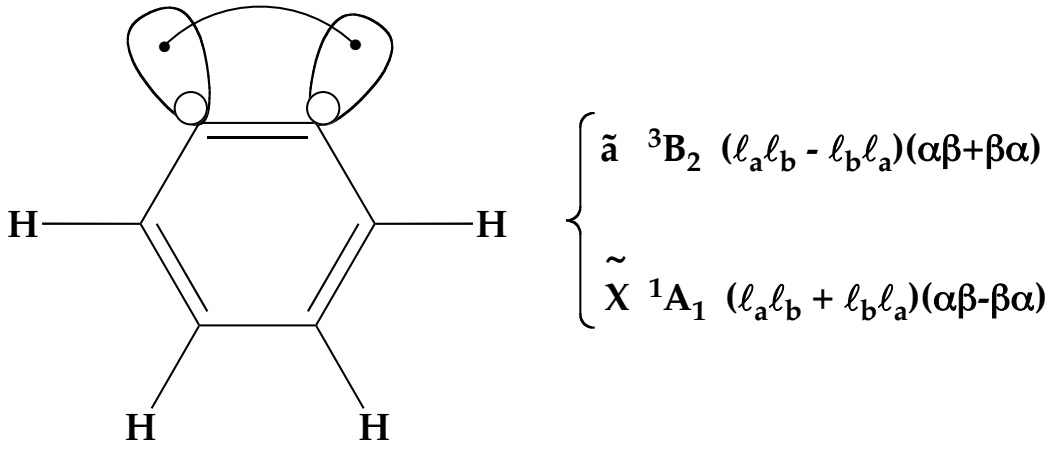

(A4)

Negative ion beams of the $C_6H_4^-$ anion were photodetached[34] and the electron affinity was measured to be EA(*o*-C_6H_4) = 0.560 ± 0.010 eV. Negative ion photoelectron spectroscopy established the intercombination gap, T_0(ã $^3B_2$ — $\tilde{X}$ $^1A_1$) = 1.637 ± 0.025 eV as well as the value of the vibrational frequency of the CC "triple bond", ν_3(*o*-C_6H_4) = 1860 ± 15 cm^{-1}. Subsequent infrared studies[35] in a Ne matrix confirm the assignment of the weak band, ν_3(*o*-C_6H_4), to be 1846 cm^{-1}.

If the gas phase acidity of the phenyl radical could be measured, the acidity/EA thermochemical cycle[13] could be applied to extract the C-H bond energy of the phenyl radical: $\Delta_{acid}H_{298}(C_6H_5) = DH_{298}(C_6H_4\text{-ortho-H}) + IE(H) - EA(o\text{-}C_6H_4)$. Measurement of the acidity of a radical such as C_6H_5 is not straightforward. Early flowing afterglow proton transfer studies[36] of the *o*-$C_6H_4^-$ anion were only able to bracket the acidity of the phenyl radical; $\Delta_{acid}H_{298}(C_6H_5) = 379^{+6}_{-3}$ kcal mol^{-1}. With this approximate acidity, the C-H bond energy of the phenyl radical a to the radical site becomes DH_{298}(C_6H_4-ortho-H) = 78 ± 6 kcal mol^{-1} and Δ_fH_{298}(*o*-C_6H_4) = 107 ± 6 kcal mol^{-1}.

The heat of formation of *o*-benzyne was improved by an FT-ICR study[37] of the energetics of the dehalogenation reaction: $OH^- + C_6H_5I \rightarrow (H_2O{\bullet}I)^- + o\text{-}C_6H_4$. By estimating the stability of the clustered halide ion, $(H_2O{\bullet}I)^-$, this study concluded that $\Delta_f H_{298}(o\text{-}C_6H_4) = 105 \pm 2$ kcal mol^{-1} and $DH_{298}(C_6H_4\text{-ortho-H}) = 77 \pm 2$ kcal mol^{-1}. Finally collision-induced threshold dissociation studies (CID) of deprotonated chlorobenzene[38] provided another independent route (A5) to establish the heat of formation of *o*-benzyne.

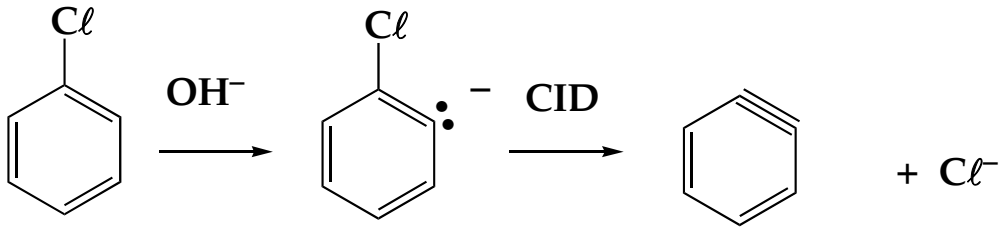

(A5)

These threshold dissociation studies reported $\Delta_f H_{298}(o\text{-}C_6H_4) = 107 \pm 3$ kcal mol^{-1} and $DH_{298}(C_6H_4\text{-ortho-H}) = 78 \pm 3$ kcal mol^{-1}. Parallel studies of the meta and para chlorophenide anions could be analyzed[39] to find the other C-H bond energies of the phenyl radical: $DH_{298}(C_6H_4\text{-meta-H}) = 94 \pm 3$ kcal mol^{-1} and $DH_{298}(C_6H_4\text{-para-H}) = 109 \pm 3$ kcal mol^{-1}. These experimental benzene and benzyne bond energies[9,14] are summarized in Scheme II.

Scheme II

Arene Bond Dissociation Enthalpies, DH_{298}, kcal mol^{-1}

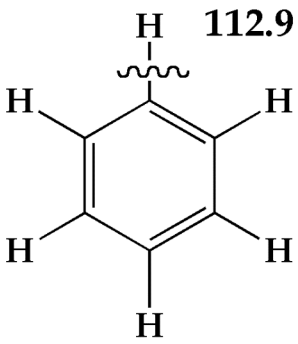

112.9 ± 0.5

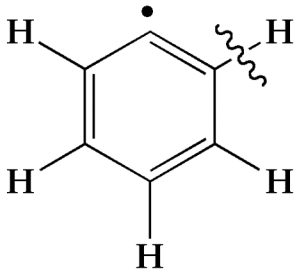

78 ± 3

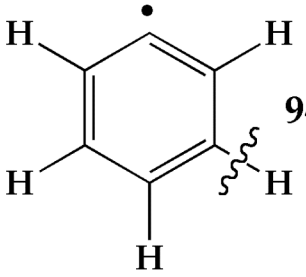

94 ± 3

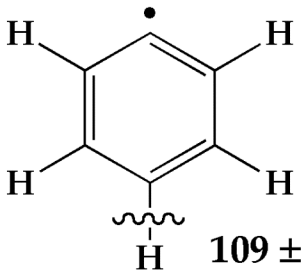

109 ± 3

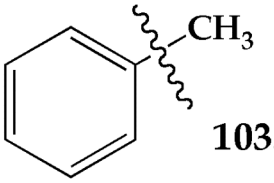

103.5 ± 0.6

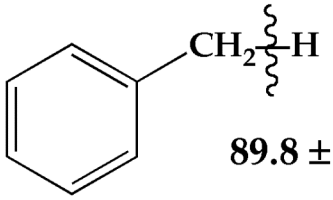

89.8 ± 0.6

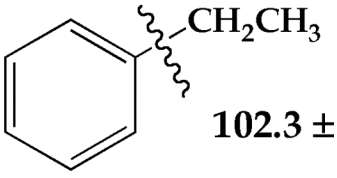

102.3 ± 0.7

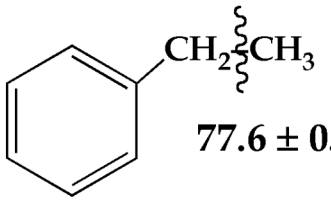

77.6 ± 0.7

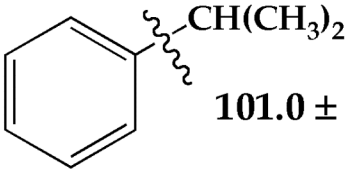

101.0 ± 0.7

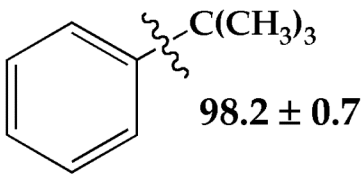

98.2 ± 0.7

EXPERIMENTAL METHODS

Molecular beams of *o*-benzyne (*o*-C_6H_4) and 3,6-dimethyl-o-benzyne were prepared in a hyperthermal nozzle that has been described previously.[40] To simplify the discussion in this paper, the nozzle temperature will be categorized by room temperature, low heat, medium heat and high heat, instead of the specific temperature (in K or ºC) used previously.[41] In general, the following temperature ranges apply to these heating categories: room temperature implies 300 K, low heat implies 1200-1400 K, medium heat implies 1400-1600 K, high heat implies 1600-1800 K.

Benzoyl chloride (C_6H_5COCl) is a convenient source of *o*-benzyne.

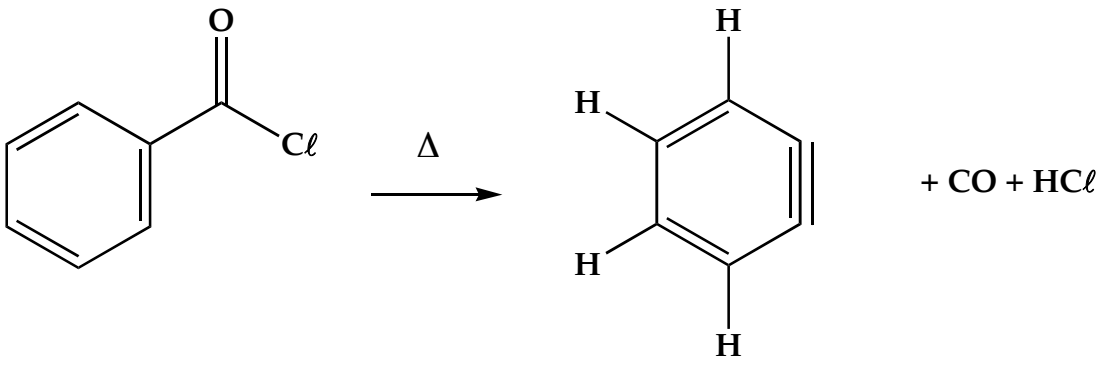

(A6)

The reaction enthalpy[9,14] is measured to be $\Delta_{rxn}H_{298}$(A6) = 83 ± 3 kcal mol^{-1}. In addition to benzoyl chloride, 1,2-diiodobenzene ($C_6H_4I_2$) is an effective *o*-benzyne precursor.

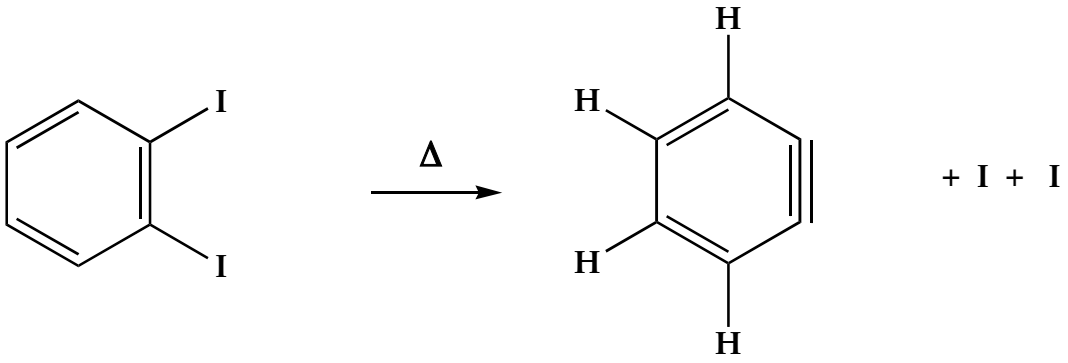

(7)

Diiodobenzene probably decomposes by sequential cracking of the C-I bonds since the bond energy of iodobenzene is $\Delta H_{298}(C_6H_5\text{-I}) = 67 \pm 2$ kcal mol^{-1}. The enthalpy[9,14] is measured to be $\Delta_{rxn}H_{298}(A7) = 97 \pm 3$ kcal mol^{-1}.

The diketone, benzocyclobutene-1,2-dione [$C_6H_4(CO)_2$], is an elegant source[20,42] of o-benzyne. The thermochemistry of (A8) is unknown.

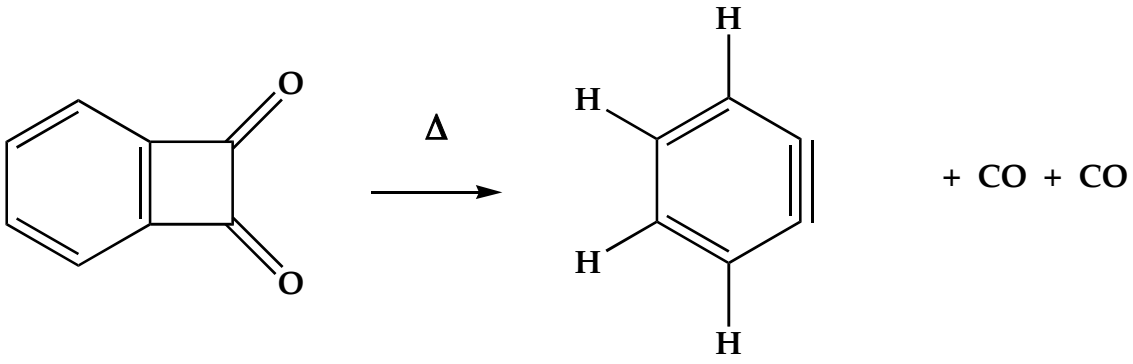

(A8)

Bromobenzene (C_6H_5Br) was used to generate the phenyl radical (C_6H_5), which further fragments to *o*-benzyne.

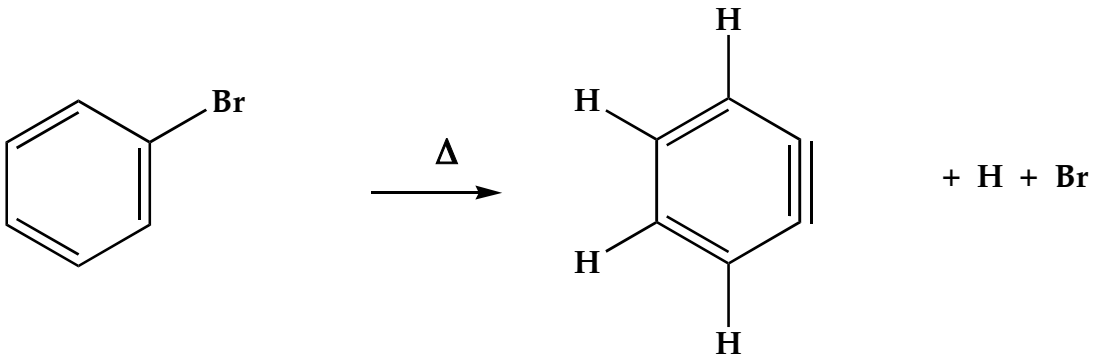

(A9)

Bromobenzene fragments by rupture of the C-Br bond [$DH_{298}(C_6H_5\text{-Br}) = 82 \pm 1$ kcal mol^{-1}] followed by H expulsion from the phenyl radical (see Scheme A2). The enthalpy[9,14] is $\Delta_{rxn}H_{298}(A9) = 160 \pm 3$ kcal mol^{-1}.

Finally we have used 2,5-dimethylbenzoyl chloride, $(CH_3)_2C_6H_3COCl$, as an *o*-benzyne precursor (A10) to study the regiochemistry of benzyne cracking.

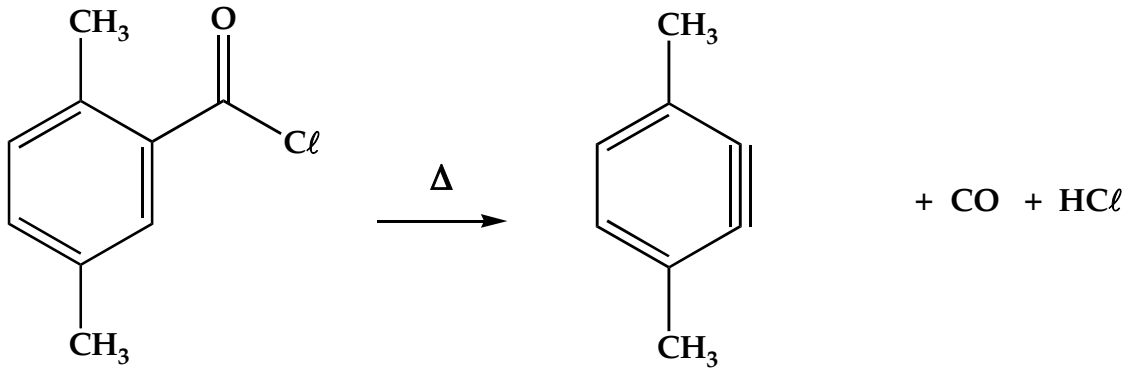

(A10)

All precursors were purchased from Sigma-Aldrich, with the exception of benzocyclobutene-1,2-dione and 2,5-dimethylbenzoyl chloride which were purchased from Molecular Diversity Preservation International and Advanced Synthesis Technologies, respectively. All compounds had the purity of 95% or higher and were used as prepared by their respective companies.

To identify the pyrolysis products emerging from the hyperthermal nozzle, we have employed three analytical techniques: (i) Time of Flight Photoionization Mass Spectrometry, (ii) Matrix-Isolation Fourier Transform Infrared Absorption Spectroscopy, and (iii) Chemical Ionization Mass Spectrometry. Each will be briefly described below.

(i) TOF-PIMS

The Photoionization Mass Spectrometer we have employed is housed at the DOE's National Renewable Energy Laboratory in Golden, CO. A description of this instrument has been previously reported.[40,43] In brief, the 9th harmonic of a Nd:YAG laser (Continuum PL8010) at λ= 118.2 nm is generated by frequency tripling the 355 nm output (10 Hz, 40 mJ/pulse) from

the laser in a xenon cell (roughly 4 Torr Xe mixed with 40 Torr Ar). After exiting the tripling cell, the VUV photons cross a molecular beam of organic radicals. Most organics have ionization energies less than 10 eV and will be photoionized by the 10.487 eV laser photon. The photoions travel through a reflectron Time of Flight Mass Spectrometer (R.M. Jordan Co.), where the signal is detected and sent to a computer for collection.

The supersonic molecular beam of organic radicals is generated in a supersonic hyperthermal nozzle.[40] A SiC tube (2.5 cm length, 1 mm ID, 2 mm OD) sits on top of a solenoid pulsed valve (Parker Hannifin Corp.) and is resistively heated. In one configuration, a gas mixture of 0.1% precursor in helium (roughly 2 atm total pressure) is prepared in a manifold that is connected to the valve; this works for relatively volatile precursors. In another configuration, for non-volatile precursors such as those used in this study, the precursor is placed in a glass tube (2.5 cm length, 1 mm ID, 2 mm OD) that is put behind the body of the valve. The valve is wrapped with nichrome wire for resistive heating to increase the vapor pressure of the precursor. Helium is passed over the heated sample to carry the vapor through the valve and into the SiC tube, where it undergoes thermal decomposition. The product radicals reside in the SiC tube for roughly 30 μs. This short residence time dramatically reduces side reactions and increases radical yield. After exiting the SiC tube, the radicals supersonically expand into a region near 5 x 10^{-6} Torr and the beam is skimmed on its way into the laser photoionization region. Photoions are extracted into the time-of-flight tube, which is mutually orthogonal to the radical beam and the laser beam.

(ii) Matrix-Isolation FTIR

Matrix-Isolation FTIR is used to study the vibrational behavior of organic radicals generated in the supersonic, hyperthermal nozzle.[40,44] The experimental components involved in the matrix studies are very similar to those used in the TOF-PIMS experiments except for the use of argon instead of helium as the carrier gas. After supersonically expanding from the nozzle into a region on the order of 5 x 10^{-5} Torr, the radical/argon beam travels about 25 mm (25 nozzle ID) where it is deposited onto a CsI window (2.5 cm diameter, 5 mm thick) at 15 K. The CsI window is cooled by a helium cryostat (APD Cryogenics Inc.). The argon atoms surround the radicals, forming a matrix that prevents the radicals from undergoing further reactions. After deposition over a period of several hours, the matrix is analyzed using an FTIR Spectrometer (Nicolet Magna 550) interfaced to a computer for signal processing. The spectra are recorded with either a MCT-A (8000 – 550 cm^{-1}) or a MCT-B (5000 – 400 cm^{-1}) detector.

(iii) Chemical Ionization Mass Spectrometry

The CIMS experiments were carried out in a flowing afterglow selected ion flow tube (FA-SIFT) instrument coupled with the supersonic hyperthermal nozzle.[45,46] The reagent ions, H_3O^+ or HO^-, are generated in the source flow tube by electron ionization and ion-molecule reactions. The ions are then mass selected with the SIFT quadrupole mass filter and injected into the reaction flow tube (7.3 cm inner diameter and roughly 1 m long) containing a helium buffer gas (0.5 Torr, 300 K) flowing at a velocity of about 95 m s^{-1}. The SIFT injection produces a continuous flow of ions (approximately 10^5 particles cm^{-3}) in a stream of helium. The radical source is mounted to the flow tube after the SIFT quadrupole mass filter. Streams of *o*-C_6H_4

diradicals are generated through pyrolysis of C_6H_5COCl. Benzoyl chloride seeded in helium (roughly 0.5 Torr in 600 Torr) passes through a pulsed valve (20-40 Hz) into the resistively heated SiC nozzle. The pyrolysis products along with the He carrier gas expand supersonically through the nozzle into the flow tube. The gas transit time from the radical source to the detection sampling orifice is approximately 10 ms. The ionic species (both the reactant and products) are detected using the quadrupole mass spectrometer at the end of the flow tube.

ELECTRONIC STRUCTURE METHODS

The cc-pV*X*Z (*X* = D, T, Q, 5, 6) family of correlation-consistent, atomic-orbital basis sets[47-49] was employed in this study. The contracted Gaussian orbitals in these [C/H] sets extend from [3*s*2*p*1*d*/2*s*1*p*] (DZ) to [7*s*6*p*5*d*4*f*3*g*2*h*1*i*/6*s*5*p*4*d*3*f*2*g*1*h*] (6Z), the latter comprising 1204 functions for the C_6H_4 system. Core correlation effects were accounted for by all-electron (AE) computations with the cc-pCVTZ and cc-pCVQZ basis sets.[50] All polarization manifolds contained only pure spherical harmonics.

Reference electronic wave functions were primarily determined by the single-configuration, self-consistent-field, restricted Hartree–Fock (RHF) method,[51-54] but test computations were also performed with the complete-active-space self-consistent-field (CASSCF) approach.[55] The CASSCF procedures involved an active space of 12 electrons in 12 orbitals, selected by the criterion of lowest orbital energy. Dynamical electron correlation was accounted for by second-order Møller–Plesset perturbation theory (MP2),[54,56-58] by the coupled cluster singles and doubles method (CCSD),[57,59-64] and by CCSD theory augmented with either a perturbative[65,66] or full[67-69] inclusion of connected triple excitations. Final energetic determinations incorporated computations with the recently implemented CCSDT(Q) method[70]

for the treatment of connected quadruple excitations. Unless otherwise stated, the carbon 1s core electrons were frozen in all correlation treatments.

Basis set extrapolations, an integral feature of the focal-point analysis method[71-75] for inferring ab initio limits, utilized the asymptotic formulas $E_X = E_{CBS} + a \exp(-bX)$ and $E_X = E_{CBS} + aX^{-3}$ for Hartree-Fock[76] and correlation energies,[77] respectively, where X is the cardinal number of the cc-pVXZ series and CBS denotes the complete basis set limit.

Geometric structures were optimized to at least 10^{-6} Å and 0.0001° using analytic gradient[78] techniques at the RHF, MP2, CCSD,[79] and CCSD(T)[80] levels of theory. Final structures were obtained by gradient-driven, full energy (E) minimizations of a composite approximation (c~) to CCSD(T)-AE/cc-pCVQZ:

E[c~CCSD(T)-AE/cc-pCVQZ] ≡

$$E[CCSD(T)/cc\text{-}pVTZ] + E[MP2\text{-}AE/cc\text{-}pCVQZ] - E[MP2/cc\text{-}pVTZ] \quad (A11)$$

Quadratic force constants for harmonic vibrational frequency analyses were generally obtained via analytic second derivatives,[78,81-83] except in the CCSD(T)/cc-pVTZ case, where force fields were determined by numerical differentiation of analytic first derivatives,[84,85] and in selected c~CCSD(T)-AE/cc-pCVQZ benchmark runs, where energy points were used in careful double finite-difference procedures. Zero-point vibrational energies (ZPVEs) were computed from unscaled CCSD(T)/cc-pVTZ harmonic frequencies.

All electronic structure computations were performed with either a local version of the ACESII package,[86] the MOLPRO suite,[87] NWCHEM,[88,89] or MRCC.[90]

EXPERIMENTAL RESULTS

DETECTION AND THERMAL DECOMPOSITION OF *O*-BENZYNE

a) TOF-PIMS of C_6D_5COCl

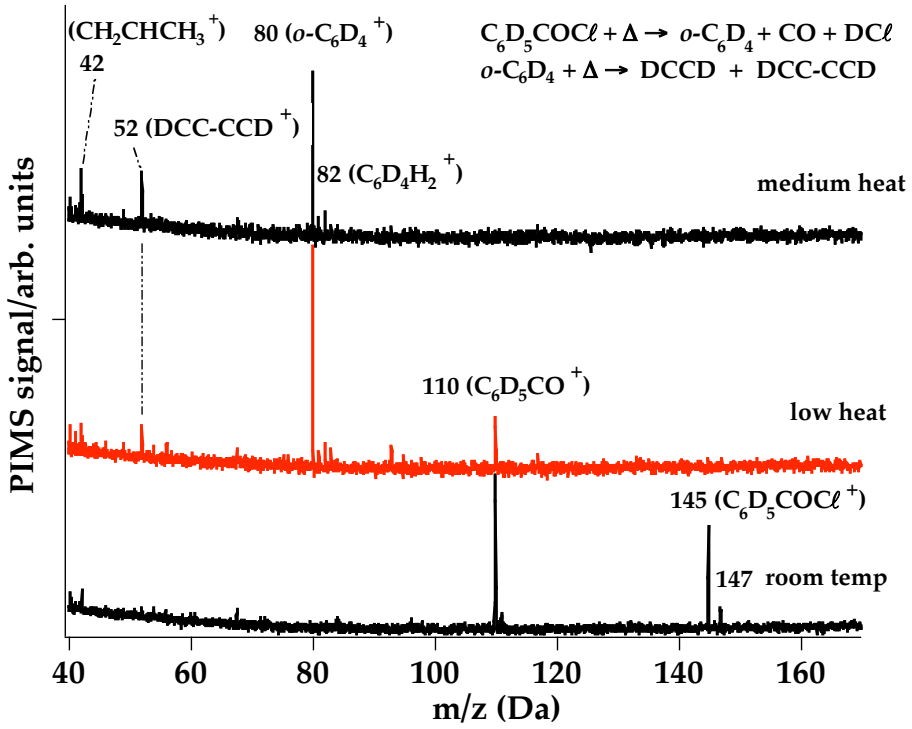

Figure A1. TOF photoionization mass spectra from supersonic hyperthermal nozzle decomposition of benzoyl-d_5 chloride, with nozzle temperatures at *Room Temperature, Low Heat and High Heat*. *o*-Benzyne-d_4 is detected at m/z 80 (*o*-$C_6D_4^+$). At room temperature, ions resulting from ionization of benzoyl-d_5 chloride are detected: m/z 145 and 147 ($C_6D_5COC\ell^+$) and m/z 110 ($C_6D_5CO^+$ from ionization-dissociation of $C_6D_5COC\ell$). At low heat, the precursor has largely decomposed to form *o*-benzyne shown at m/z 80 (*o*-$C_6D_4^+$). The signal at m/z 110 is attributed to residual precursor. The small peak at m/z 52 corresponds to ionized diacetylene $(DC{\equiv}C\text{-}C{\equiv}CD)^+$. At medium heat, the peak at m/z 52 increases, indicating more thermal cracking of *o*-benzyne. The small signal at m/z 82 might be benzene ($C_6D_4H_2^+$) which may result from secondary reactions of *o*-benzyne (*o*-C_6D_4). The signals from the precursor are absent, and the feature at m/z 42 belongs to an added mass marker, propene ($C_3H_6^+$).

Earlier we used benzoyl chloride as a convenient source of o-benzyne.[45,46] Fig. A1 illustrates the TOF-PIMS spectrum of the thermal decomposition of deuterated benzoyl chloride, C_6D_5COCl. It demonstrates the production of *o*-C_6D_4, which subsequently fragments to produce DC≡CD and DC≡C-C≡CD. The bottom trace shows the background ions resulting from ionization of room temperature C_6D_5COCl. Peaks at m/z 145 and 147 belong to the precursor, $C_6D_5COCl^+$. The acyl cation $C_6D_5CO^+$ at m/z 110 arises from ionization-dissociation of C_6D_5COCl. At low heat, the precursor has largely decomposed to form *o*-benzyne shown at m/z 80 (*o*-$C_6D_4^+$), carbon monoxide and hydrogen chloride; the latter two products have high ionization energies[91] [IE(CO) = 14.014 ± 0.003 eV and IE(HCl) = 12.744 ± 0.009 eV] that are beyond the range of the 118.2 nm laser. The small feature at m/z 52 corresponds to ionized diacetylene $(DC{\equiv}C\text{-}C{\equiv}CD)^+$. PIMS detection of acetylene is not possible with the 10.487 eV laser due to its high[92] ionization energy, IE(HCCH) = 11.4006 ± 0.0006 eV. The ion signal at m/z 52 suggests that a small amount of *o*-C_6D_4 has fragmented to form DC≡C-C≡CD and DC≡CD. At medium heat more *o*-C_6D_4 decomposes, as demonstrated by the increased peak intensity of m/z 52 and decreased peak intensity of m/z 80. The PIMS spectra cannot distinguish the *o*-C_6D_4 species from its isomers (*m*-C_6D_4, *p*-C_6D_4, and DCC-CD=CD-CCD).

b) Matrix FTIR of C_6D_5COCl

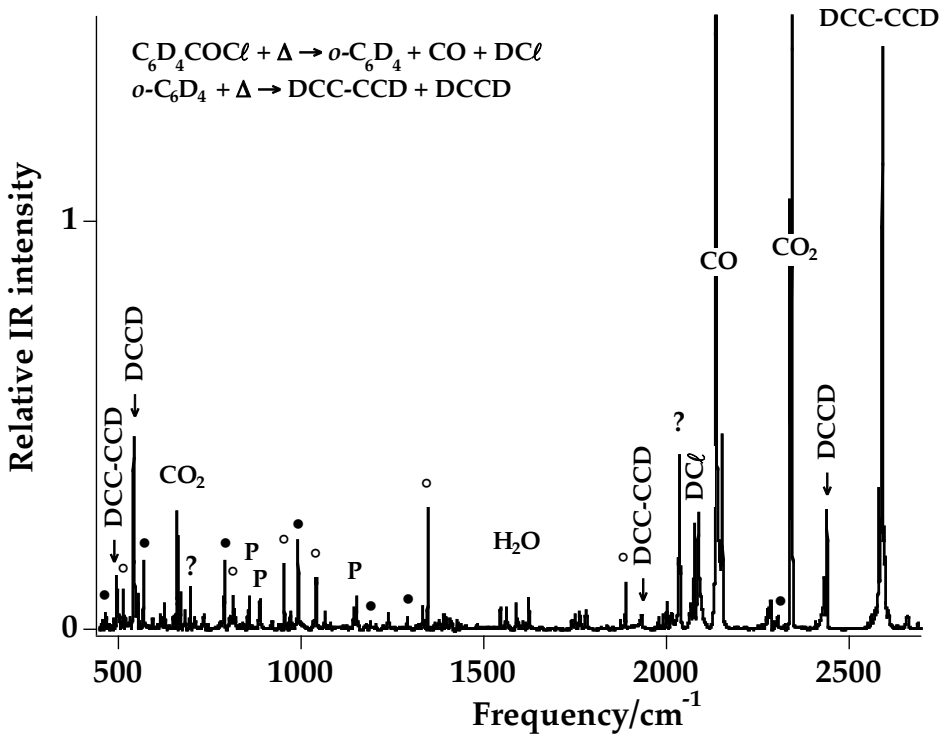

Figure A2. Matrix-Isolation IR spectrum from thermal decomposition of benzoyl-d_5 chloride at medium heat. The thermal decomposition products of benzoyl-d_5 chloride, *o*-benzyne, DCℓ, and CO, are observed. Also present in the spectrum are DC≡C-C≡CD and DC≡CD, which are derived from *o*-C_6D_4 thermal fragmentation. A small amount of residual precursor is detected in the spectrum. Benzene-d_4 ($C_6H_2D_4$) which may arise from secondary reactions of *o*-benzyne-d_4 is also observed. The peak assignments (in cm^{-1}) follow. The unknown bands (indicated with ?) may result from impurities in the sample line or from the hot nozzle itself.

o-C_6D_4 (●) : 466, 569, 792, 993, 1191, 1292, 2307;

DC≡C-C≡CD : 496, 1935, 2593;

DC≡CD : 543, 2442;

$C_6H_2D_4$ (❍) : 513, 816, 955, 1042, 1349, 1891;

Unknown species (?): 699, 2037.

Figure A2 is the IR absorption spectrum of the benzoyl chloride (C_6D_5COCl) pyrolysis products at medium heat (similar condition to the top trace of Fig. A1), which shows the generation[35] of *o*-C_6D_4 (marked by the bullets, •). Diacetylene and acetylene, which arise from further thermal cracking of *o*-C_6D_4, are prominent in the spectrum. There is still a small amount of the precursor remaining (C_6D_5COCl, marked by P), along with the benzene ($C_6D_4H_2$, marked by °) which may be produced from secondary reactions of *o*-C_6D_4. Signals from DCl and CO (byproducts) are also detected as well as H_2O and CO_2 (from impurities).

c) Positive ion CIMS of benzoyl chloride pyrolysis

We have used a FA-SIFT device to study the reactions[45,46] of ions with *o*-benzyne. Fig. A3 shows the reaction of H_3O^+ ions with the benzoyl chloride pyrolysis products at low and medium heat. The bottom trace is a reference spectrum resulting from reaction of mass-selected H_3O^+ and benzoyl chloride at room temperature; peaks at m/z 141, 143 are the protonated benzoyl chloride, $[C_6H_5COCl, H]^+$, at natural chlorine abundance. Fragmentation of these parent ions affords the acyl cation, $C_5H_5CO^+$ m/z 105 and HCl. At low heat, the major product is observed at m/z 77 ($C_6H_5^+$) which is derived from protonation of *o*-benzyne, *o*-$C_6H_4 + H^+ \rightarrow [C_6H_4, H]^+$. A small amount of *o*-benzyne further fragments: *o*-$C_6H_4 \rightarrow$ HC≡CH and HC≡C-C≡CH. Acetylene (proton affinity[91] PA = 153.3 kcal mol^{-1}) will not proton transfer with H_3O^+ but diacetylene[91] will (PA = 176.2 kcal mol^{-1}) to produce the observed cation [HC≡C-C≡CH, H^+] at m/z 51. At medium heat, the precursor benzoyl chloride is completely depleted, while *o*-benzyne (m/z 77) and diacetylene (m/z 51) increase in intensity.

d) Negative ion CIMS of benzoyl chloride pyrolysis

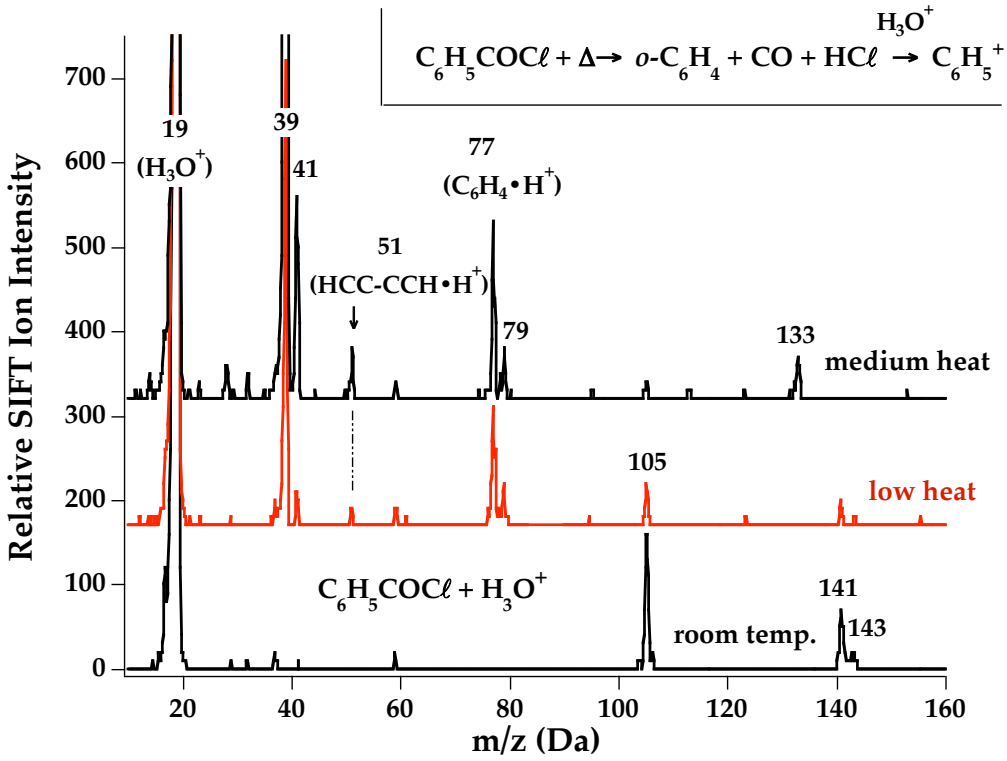

Figure A4. SIFT mass spectrum for reaction of HO^- with thermal decomposition products of benzoyl chloride at low and medium heat (top 2 trace). The signal at m/z 75 ($C_6H_3^-$) results from deprotonation of *o*-benzyne. The peaks at m/z 49 and m/z 25 belong to the deprotonated diacetylene ($HCCCC^-$) and acetylene (HCC^-). The inset is an expanded view of the top trace from m/z 24 to 76. The bottom trace is a reference spectrum showing ions resulting from reaction of HO^- and the precursor, benzoyl chloride.

Fig. A4 displays the SIFT mass spectra for the reaction of HO^- with benzoyl chloride pyrolysis products at low and medium heat. Hydroxide ion is very reactive since the gas phase enthalpy of deprotonation[93,94] of water is $\Delta_{acid}H_{298}$(HO-H) = 390.20 ± 0.07 kcal mol^{-1}. The bottom trace is the reference spectrum resulting from reaction of mass-selected HO^- and the precursor, benzoyl chloride, at room temperature. Features at m/z 139, 141 are the deprotonated benzoyl chloride: $C_6H_5COCl + HO^- \rightarrow C_6H_4COCl^- + H_2O$. The large signal of Cl^- (m/z 35, 37) results from reaction of benzoyl chloride with HO^-.

At low heat, the signal at m/z 75 ($C_6H_3^-$, 15 counts) is reproducibly observed, which is assigned to the deprotonated *o*-benzyne [*o*-C_6H_3]$^-$. At medium heat, benzoyl chloride is depleted, while deprotonated acetylene $HC{\equiv}C^-$ (m/z 25), diacetylene $HC{\equiv}C\text{-}C{\equiv}C^-$ (m/z 49) and *o*-benzyne $C_6H_3^-$ (m/z 75) are detected (see green inset). Both acetylene [gas-phase enthalpy of deprotonation[23] $\Delta_{acid}H_{298}$ (HCC-H) = 378.3 ± 0.1 kcal mol^{-1}] and diacetylene[95] [$\Delta_{acid}H_{298}$(HCCCC-H) = 359 ± 2 kcal mol^{-1}] are thermal cracking products of *o*-C_6H_4.

e) TOF-PIMS of *o*-$C_6H_4I_2$

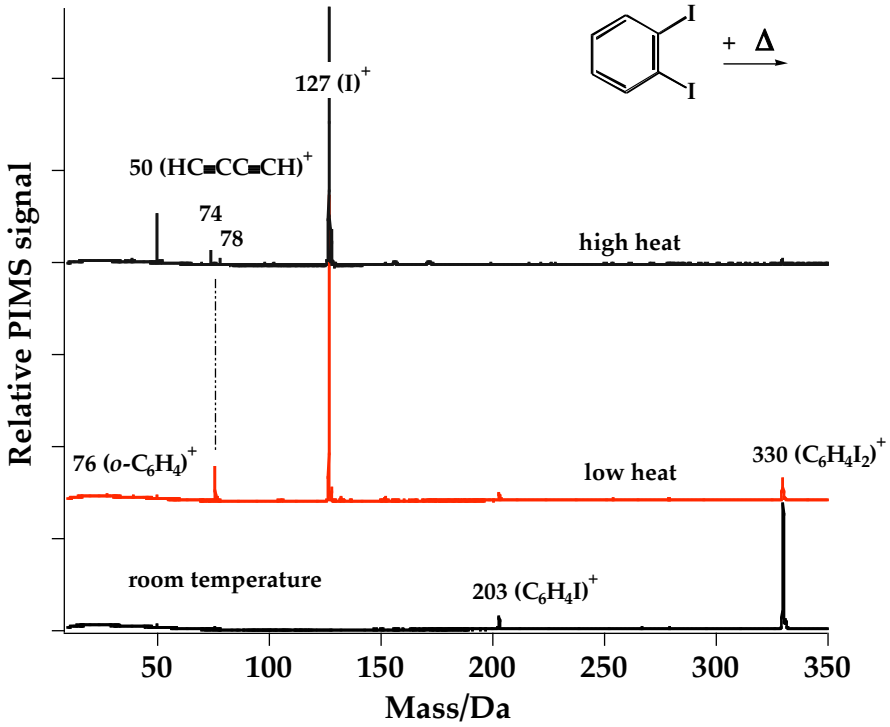

Figure A5. TOF photoionization mass spectra from thermal decomposition of $C_6H_4I_2$. The reference spectrum with the nozzle unheated (room temperature) is also shown in the bottom trace. At room temperature, ions resulting from ionization of $C_6H_4I_2$ are detected: m/z 330 ($C_6H_4I_2^+$) and m/z 203 ($C_6H_4I^+$ from ionization-dissociation of $C_6H_4I_2$). At low heat, ions from thermal decomposition products are shown: *o*-benzyne at m/z 76 (*o*-$C_6H_4^+$) and iodine atom at m/z 127 (I^+). The signal at m/z 330 is attributed to residual precursor. At high heat, the peak at m/z 76 disappears while the peak at m/z 50 appears in which corresponds to ionized diacetylene $(HC{\equiv}C\text{-}C{\equiv}CH)^+$, indicating thermal cracking of *o*-benzyne. Small signals at m/z 74 and 78 most likely belong to $C_6H_2^+$ and $C_6H_6^+$ which may result from secondary reactions of *o*-C_6H_4.

Fig. A5 illustrates the TOF-PIMS spectrum of *o*-$C_6H_4I_2$ thermal decomposition. It demonstrates the production of *o*-C_6H_4, followed by cracking of *o*-C_6H_4 to form HCCH and HCC-CCH. The room temperature trace shows ions resulting from ionization of *o*-$C_6H_4I_2$; the peak at m/z 330 is $C_6H_4I_2^+$. The ion $C_6H_4I^+$ at m/z 203 arises from ionization-dissociation of $C_6H_4I_2$. At low heat, the precursor has largely decomposed to form *o*-benzyne shown at m/z 76 (*o*-$C_6H_4^+$) and iodine atom shown at m/z 127 (I^+). At high heat, *o*-C_6H_4 thermally decomposes to produce HCC-CCH and HCCH; the peak at m/z 50 corresponds to the diacetylene cation $(HC{\equiv}C\text{-}C{\equiv}CH)^+$.

f) TOF-PIMS of $C_6H_4(CO)_2$

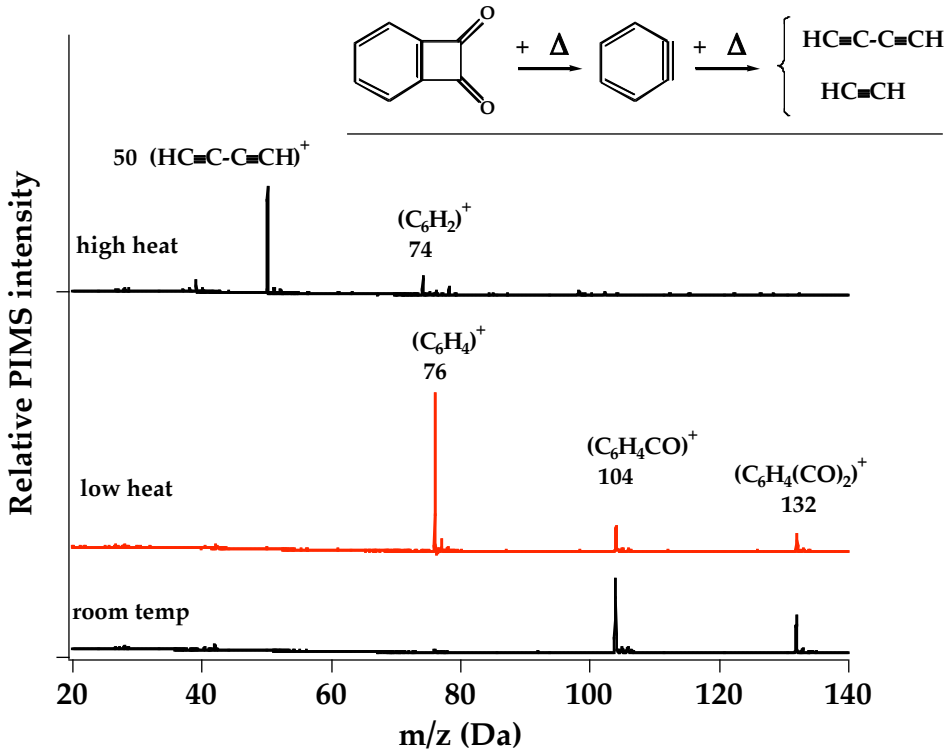

Figure 6. TOF photoionization mass spectra from thermal decomposition of $C_6H_4(CO)_2$. The reference spectrum with the nozzle unheated (room temperature) is also shown in the bottom trace. At room temperature, ions resulting from ionization of $C_6H_4(CO)_2$ are detected: m/z 132 ($C_6H_4(CO)_2^+$) and m/z 104 ($C_6H_4(CO)^+$ from ionization-dissociation of $C_6H_4(CO)_2$). At low heat, thermal decomposition product *o*-benzyne shown at m/z 76 (*o*-$C_6H_4^+$) is observed. The signals at m/z 132 and 104 are attributed to residual precursor. At high heat, the peak at m/z 76 disappears while the peak at m/z 50 appear in which corresponds to ionized diacetylene $(HC{\equiv}C\text{-}C{\equiv}CH)^+$, indicating thermal cracking of *o*-benzyne. Two small signals at m/z 74 and 78 most likely belong to $C_6H_2^+$ and $C_6H_6^+$, which may result from secondary reaction of *o*-C_6H_4.

Fig. A6 displays the TOF-PIMS spectrum of the products of benzocyclobutene-1, 2-dione thermal decomposition. It demonstrates the clean production of *o*-C_6H_4, followed by fragmentation of *o*-C_6H_4 to form HCC-CCH and HCCH. At room temperature, two peaks

appear: m/z 132 C_6H_4 $(CO)_2^+$ belongs to the precursor and m/z 104 (C_6H_4 $(CO)^+$) arises from ionization-dissociation of precursor $C_6H_4(CO)_2$. At low heat, the precursor has largely decomposed to form *o*-benzyne shown at m/z 76 (*o*-$C_6H_4^+$). At high heat, *o*-C_6H_4 is fragmented to form C_4H_2 and C_2H_2; the peak at m/z 50 corresponds to ionized diacetylene $(HC{\equiv}C\text{-}C{\equiv}CH)^+$.

g) TOF-PIMS of C_6H_5Br

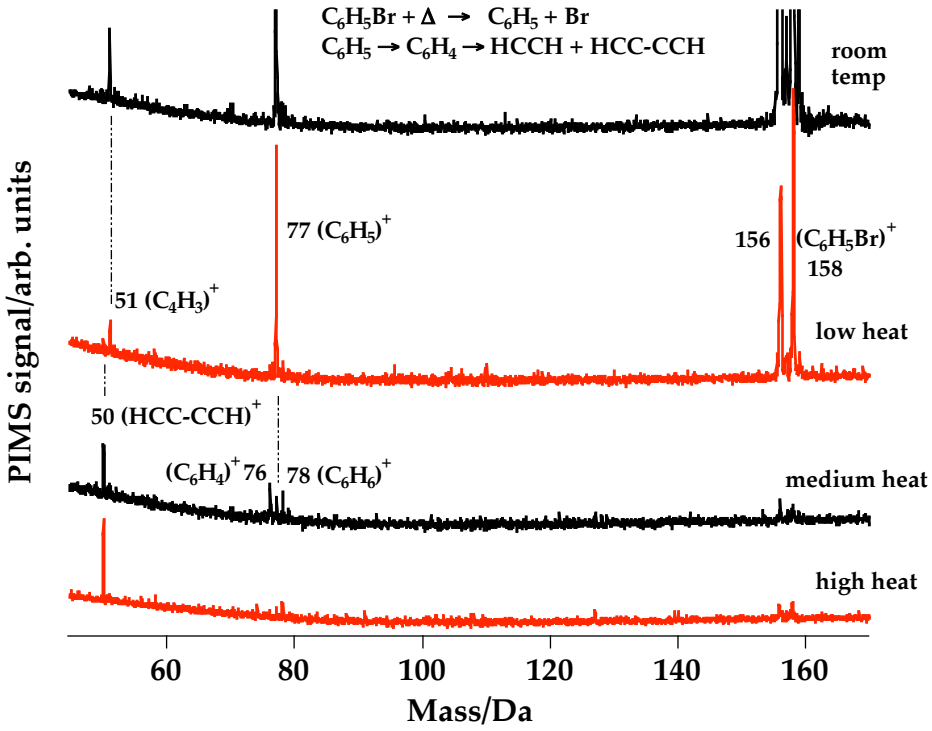

Figure A7. TOF photoionization mass spectra from thermal decomposition of C_6H_5Br. The reference spectrum with the nozzle unheated (room temperature) is also shown in the top trace. At room temperature, ions resulting from ionization of C_6H_5Br are detected: m/z 156 and 158 ($C_6H_5Br^+$) as well as at m/z 77 and 51 ($C_6H_6^+$ and $C_4H_3^+$ respectively, from ionization-dissociation of C_6H_5Br). The intensities of the peaks at m/z 156 and 158 are about 20 times of the intensities shown, and the peak height of m/z 77 is about twice as big as it is shown. At low heat, the thermal decomposition product, phenyl radical, is shown at m/z 77 ($C_6H_5^+$). The signals at m/z 156 and 158 are attributed to residual precursor. At medium heat, the peak at m/z 77 decreases while a new peak appears at m/z 50 corresponding to ionized diacetylene $(HC{\equiv}C\text{-}C{\equiv}CH)^+$, indicating thermal cracking of *o*- C_6H_4. *o*-Benzyne shown at m/z 76 can be generated by thermal dissociation of phenyl radical (C_6H_5). A small signal at 78 most likely belongs to $C_6H_6^+$ which may result from secondary reaction of C_6H_5. Both *o*-C_6H_4 and C_6H_6 may also be generated through disproportionation of C_6H_5. At high heat, the only peak remaining is m/z 50 $(HC{\equiv}C\text{-}C{\equiv}CH)^+$, indicating a complete thermal cracking of *o*-C_6H_4.

Bromobenzene was used to generate the phenyl radical (C_6H_5), which subsequently decomposes to *o*-benzyne. The *o*-C_6H_4 was observed to fragment further to acetylene and diacetylene.

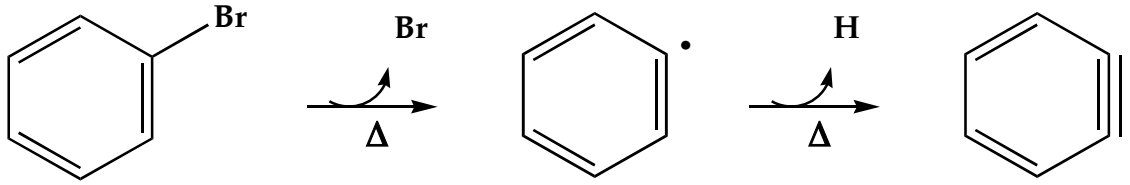

(A12)

Fig. A7 illustrates the TOF-PIMS spectrum of C_6H_5Br thermal decomposition. The room temperature spectrum at the top of Fig. A7 shows ions resulting from ionization of the precursor C_6H_5Br. The signals at m/z 156 and 158 belong to the precursor, $C_6H_5Br^+$. The features at m/z 77 ($C_6H_5^+$) and 51 ($C_4H_3^+$) arise from ionization-dissociation of C_6H_5Br. At low heat, the precursor has decomposed to form the phenyl radical shown at m/z 77 ($C_6H_5^+$) while bromine atom[96] has too high an ionization energy to be ionized by the 118.2 nm laser; IE(Br) = 11.81381 ± 0.00006 eV. The precursor C_6H_5Br still remains as shown at m/z 156, 158 and 51 (It is likely that a small amount of signal at m/z 77 results from the precursor's ionization dissociation.) At medium heat, the signal at m/z 77 ($C_6H_5^+$) decreases while new peaks at m/z 76 ($C_6H_4^+$) and 50 ($HCCCCH^+$) appear, indicating that phenyl radical further dissociates to form *o*-C_6H_4 which then fragments to HCC-CCH and HCCH. The bottom trace in Fig. A7 is at high heat and the only peak remaining is m/z 50 which corresponds to diacetylene ($HCC\text{-}CCH^+$). Matrix-isolation FTIR spectra of C_6H_5Br thermal decomposition were also collected and revealed signals from both HCCH and HCC-CCH, thus confirming the assignments for the TOF-PIMS experiment in Fig. A7. These IR spectra are not shown in this paper but are similar to Fig. A2.

a) PIMS of 2,5-$(CH_3)_2C_6H_3COCl$

The mechanism for the fragmentation of *o*-benzyne to produce acetylene and diacetylene in eq (A3) and Scheme I is an apparent retro-Diels-Alder reaction which has been exhaustively studied.[97-100] It is believed that retro-Diels-Alder fragmentations are rapid, direct processes. This implies that the chemically activated *o*-benzyne fragments to acetylene and diacetylene without scrambling: $[o\text{-}C_6H_4]^* \rightarrow HC{\equiv}CH + HC{\equiv}C\text{-}C{\equiv}CH$.

In an attempt to test for a retro-Diels-Alder mechanism, we have examined the regiochemistry of the fragmentation of a substituted o-benzyne. If we use 2,5-dimethylbenzoyl chloride [2,5-$(CH_3)_2C_6H_3COCl$] as a precursor to generate 3,6-dimethyl-*o*-benzyne (A13), Scheme III indicates that this *o*-benzyne should fragment to form only acetylene ($HC{\equiv}CH$) and dimethyldiacetylene ($CH_3\text{-}C{\equiv}C\text{-}C{\equiv}C\text{-}CH_3$) (A14).

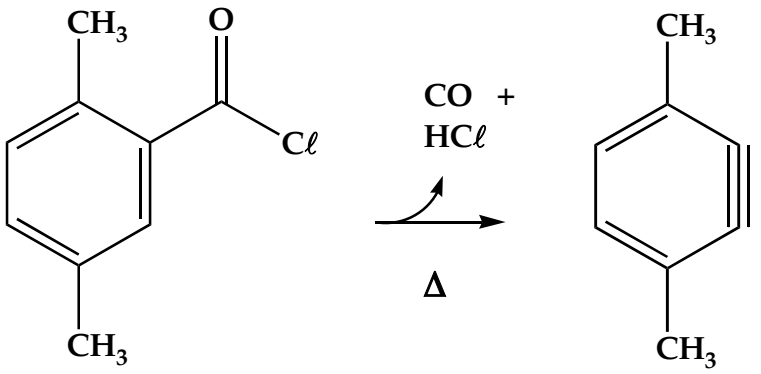

[3,6-$(CH_3)_2$-*o*-C_6H_2]

(A13)

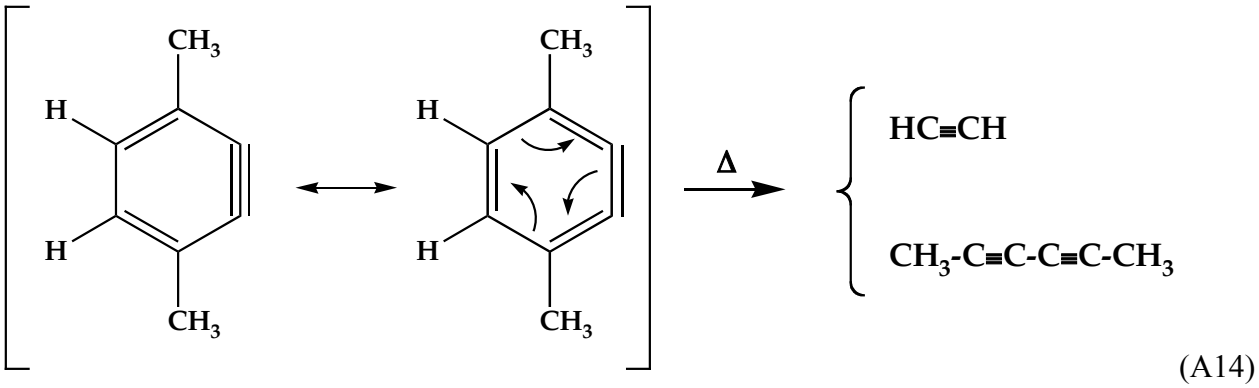

(A14)

Before discussing the experimental spectra, it is helpful to consider the implications from Scheme I which are sketched in Scheme III for the dimethylbenzynes.

Scheme III

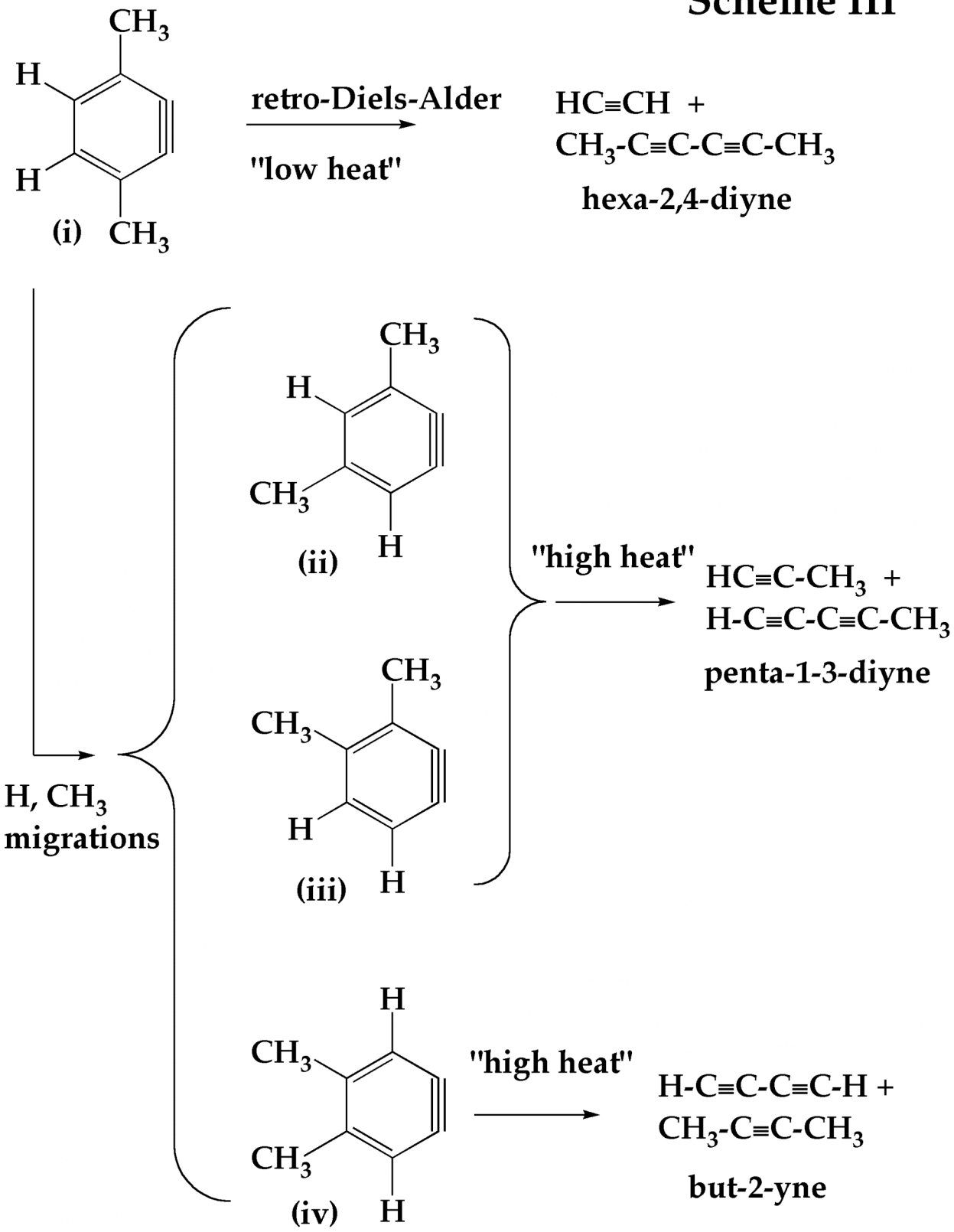
CH3
H
H
(i) CH3
retro-Diels-Alder
"low heat"
HC≡CH +
CH3-C≡C-C≡C-CH3
hexa-2,4-diyne
H, CH3
migrations
CH3
H
CH3
(ii)
H
CH3
CH3
H
(iii)
H
"high heat"
HC≡C-CH3 +
H-C≡C-C≡C-CH3
penta-1-3-diyne
H
CH3
CH3
(iv)
H
"high heat"
H-C≡C-C≡C-H +
CH3-C≡C-CH3
but-2-yne

The nascent 3,6-$(CH_3)_2$-*o*-C_6H_2 (i, Scheme A3) could directly fragment to HCCH + CH_3CC-$CCCH_3$. Alternatively 3,6-$(CH_3)_2$-*o*-C_6H_2 might rearrange to the less stable isomers, *m*-benzyne and *p*-benzyne, which cascade to a set of isomeric *o*-benzynes (ii, iii, and iv, Scheme III). Retro-Diels-Alder fragmentation of ii, iii, or iv would generate a different set of acetylene and diacetylene isomers.

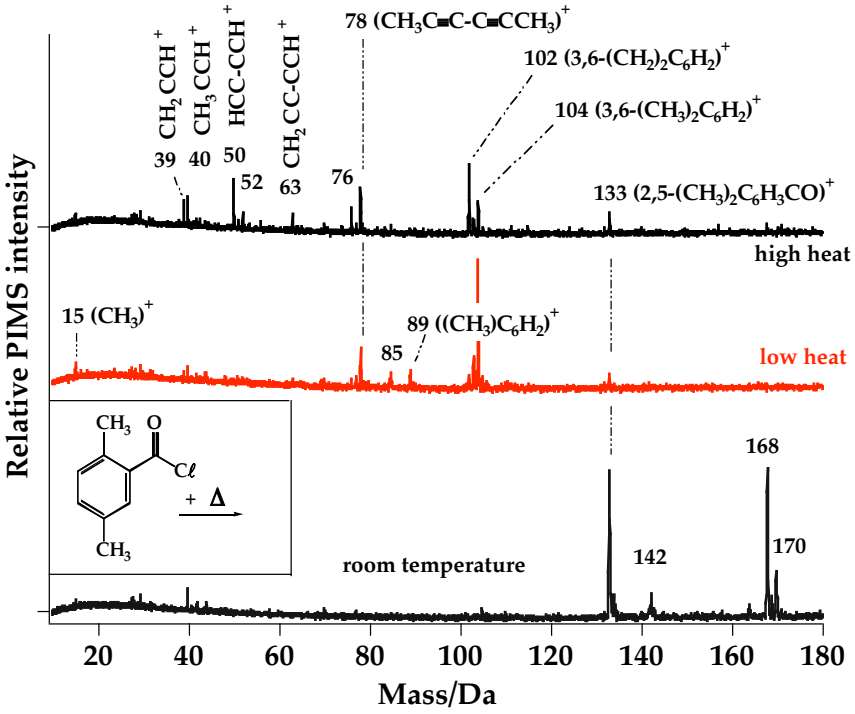

Figure A8. TOF photoionization mass spectra from supersonic hyperthermal nozzle decomposition of 2,5-$(CH_3)_2C_6H_3COCl$. The reference spectrum with the nozzle unheated (room temperature) is also shown in the bottom trace. At room temperature, ions resulting from ionization of 2,5-$(CH_3)_2C_6H_3COCl$ are detected: m/z 168 and 170 (2,5-$(CH_3)_2C_6H_3COCl^+$) as well as m/z 133 (2,5-$(CH_3)_2C_6H_3CO^+$ from ionization-dissociation of 2,5-$(CH_3)_2C_6H_3COCl$). At low heat thermal decomposition products are observed: m/z 104 (3,6-$(CH_3)_2$-*o*-$C_6H_2^+$), m/z 78 $(CH_3C{\equiv}C\text{-}C{\equiv}CCH_3)^+$, m/z 15 ($CH_3^+$), m/z 89 (6-$(CH_3)$-*o*-$C_6H_2^+$), m/z 103 (3-$(CH_2)$-6-$(CH_3)$-*o*-$C_6H_2^+$). The small feature at m/z 85 is unknown. At high heat most of 3,6-$(CH_3)_2$-*o*-C_6H_2 at m/z 104 further fragments to form 3,6-$(CH_2)_2$-*o*-C_6H_2 shown at m/z 102, or acetylene and dimethyldiacetylene ($CH_3C{\equiv}C\text{-}C{\equiv}CCH_3$) at m/z 78 which can further dissociate to $CH_2{=}C{=}C{=}C{=}CH_2$ shown at m/z 76. The peaks at m/z 39, 40 and 63 correspond to $HCCCH_2$, methylacetylene and $HCCCCCH_2$ respectively. The signals at m/z 50 and 52 correspond to diacetylene and H_2CCCCH_2.

Fig. A8 plots the TOF-PIMS spectrum of 2,5-$(CH_3)_2C_6H_3COCl$ thermal decomposition products. It shows the production of 3,6-$(CH_3)_2$-*o*-C_6H_2, followed by its fragmentation to $CH_3C{\equiv}C\text{-}C{\equiv}CCH_3$ and $HC{\equiv}CH$. The bottom trace shows ions resulting from ionization of the precursor via a room temperature nozzle. Peaks at m/z 168 and 170 belong to the precursor $(2,5\text{-}(CH_3)_2C_6H_3COCl)^+$, while the ion $(2,5\text{-}(CH_3)_2C_6H_3CO)^+$ at m/z 133 arises from ionization-dissociation of the precursor. At low heat, the precursor has largely decomposed to form $(3,6\text{-}(CH_3)_2\text{-}o\text{-}C_6H_2)^+$ shown at m/z 104. Some cation further dissociates to form $(CH_3C{\equiv}C\text{-}C{\equiv}CCH_3)^+$ shown at m/z 78, and acetylene. A small amount of 3,6-$(CH_3)_2$-*o*-C_6H_2 also decomposes (see eq. A15) into $(CH_3)^+$ and $(6\text{-}(CH_3)\text{-}o\text{-}C_6H_2)^+$, which appear at m/z 15 and 89, respectively. The small peak at m/z 85 is unknown. The signal at m/z 103 results from the decomposition of 3,6-$(CH_3)_2$-*o*-C_6H_2 to H and 3-(CH_2)-6-(CH_3)-*o*-C_6H_2.

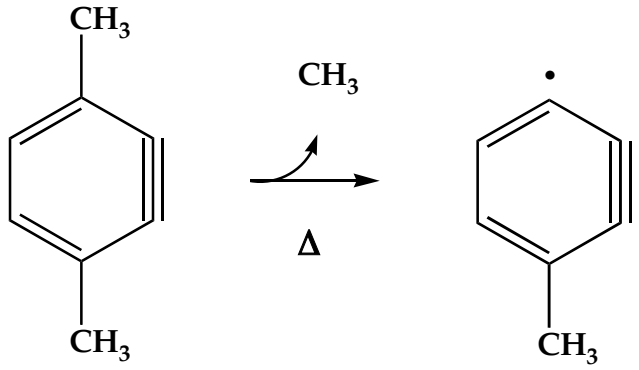

(A15)

At high heat the cracking pattern of 3,6-$(CH_3)_2$-*o*-C_6H_2 becomes much more complex. The compound appears to fragment as shown in (A16) to form the conjugated species 3,6-$(CH_2)_2$-*o*-C_6H_2.

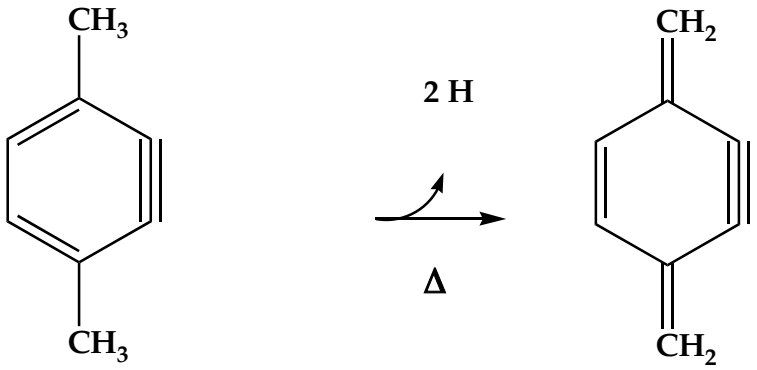

(A16)

Retro-Diels-Alder fragmentation of the benzyne, 3,6-$(CH_3)_2$-*o*-C_6H_2, to acetylene and dimethyldiacetylene produces the $(CH_3\text{-}C{\equiv}C\text{-}C{\equiv}C\text{-}CH_3)^+$ ion at m/z 78. Dimethylacetylene can lose an additional pair of H atoms to generate the cumulated species, $CH_2{=}C{=}C{=}C{=}CH_2$. These mechanisms are consistent with the decreased peak intensity of m/z 104 (3,6-$(CH_3)_2$-*o*-$C_6H_2)^+$ and increased peak intensities of m/z 76 $(CH_2CCCCCH_2)^+$ and 102 (3,6-$(CH_2)_2$-*o*-$C_6H_2)^+$.

In addition to the retro-Diels-Alder cracking of the 3,6-$(CH_3)_2$-*o*-C_6H_2 benzyne, more complicated fragmentations are evident in the top trace of Fig. A8. As suggested in Scheme III, H and CH_3 migrations around the benzyne ring could form different benzyne isomers[5] which can further fragment to several products. The peaks at m/z 39, 40 and 63 belong to propargyl $(HCCCH_2)^+$, methylacetylene $(HC{\equiv}CCH_3)^+$ and $(HC{\equiv}C\text{-}C{\equiv}C\text{-}CH_2)^+$, respectively, which are fragmentation products of 3,4-dimethyl-*o*-benzyne and 3,5-dimethyl-*o*-benzyne. The signals at m/z 50 and 52 belong to $HC{\equiv}C\text{-}C{\equiv}CH$ and $CH_2{=}C{=}C{=}CH_2$ which are fragmentation products of 4,5-dimethyl-*o*-benzyne.

b) IR of 2,5-$(CH_3)_2C_6H_3COCl$

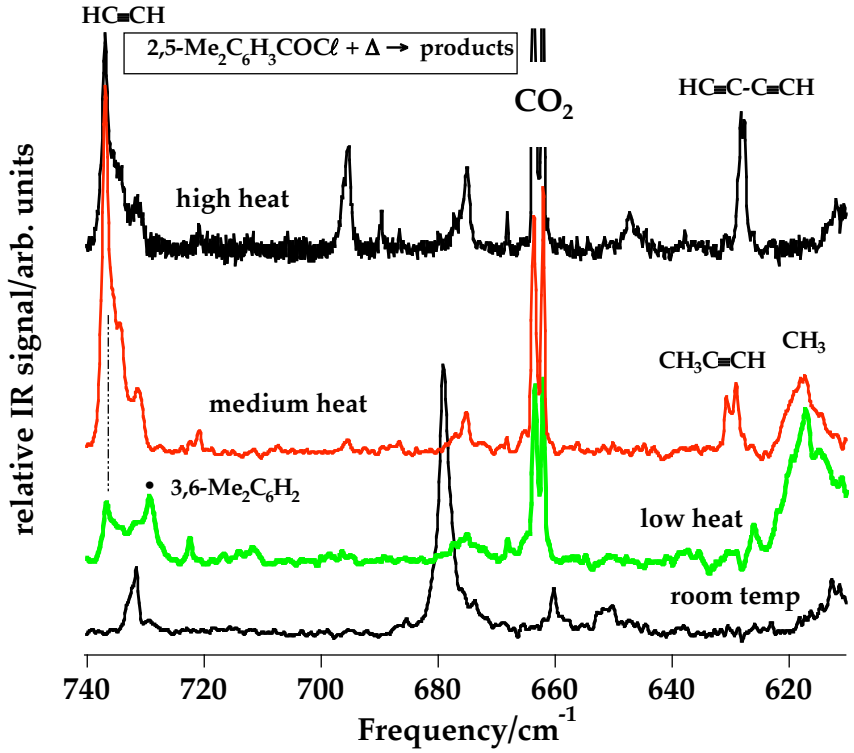

Figure A9a. IR spectra of 2,5-$(CH_3)_2C_6H_3COCl$ pyrolysis in the low frequency fingerprint region. At room temperature, the signals correspond to the precursor. At low heat HCCH and CH_3 are observed as well as 3,6-$(CH_3)_2$-*o*-C_6H_2. At medium heat, the HCCH peak increases while CH_3 decrease and new peak (CH_3CCH) appears. At high heat signals of methyl radical and methylacetylene disappear, the acetylene peak decreases and a new peak corresponding to HCC-CCH appears.

Figures A9a and A9b are the IR spectra of 2,5-dimethylbenzoyl chloride pyrolysis. Fig. A9a shows the IR spectra at the low frequency fingerprint region. At room temperature, the signals belong to the precursor. At low heat, HC≡CH and CH_3 are observed as well as 3,6-$(CH_3)_2$-*o*-C_6H_2. This demonstrates that retro-Diels-Alder reaction of 3,6-dimethyl-*o*-benzyne occurs at relatively lower temperature. At medium heat, the acetylene peak increases while the

methyl peak decreases and a feature which belongs to $CH_3C{\equiv}CH$ grows in. This is evidence for H or CH_3 migrations. At high heat the signals of CH_3, $HC{\equiv}CH$, and $CH_3C{\equiv}CH$ all disappear. However a new peak which is assigned to $HC{\equiv}C\text{-}C{\equiv}CH$ appears; this is consistent with further H and CH_3 migrations.

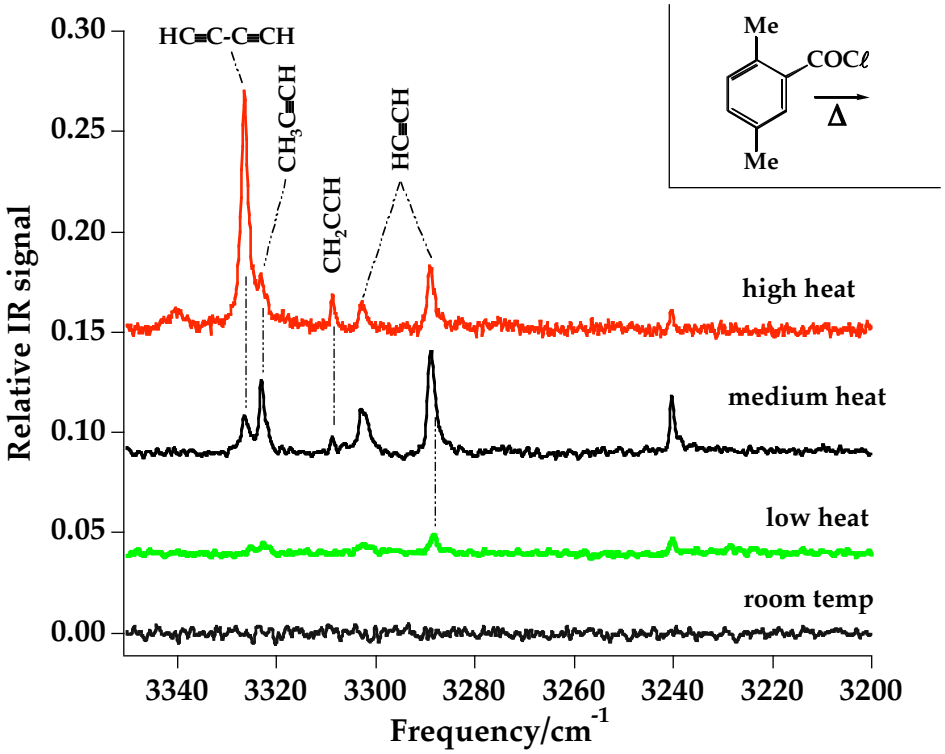

Figure A9b. IR spectra of 2,5-$(CH_3)_2C_6H_3COCl$ pyrolysis at relatively high frequency C-H stretching region. At low heat, there are small signals that correspond to acetylene and methylacetylene. At medium heat, both of these peaks increase, and signals that correspond to diacetylene and propargyl radical ($HCCCH_2$) appear. At high heat, both the acetylene peak and the methylacetylene peak decrease, while signals that correspond to diacetylene and propargyl radical increase.

Fig. A9b displays the IR spectra in the high frequency C-H stretching region. At low heat, there are small signals that belong to $HC{\equiv}CH$ and $HC{\equiv}CCH_3$. At medium heat, both the acetylene peak and the methylacetylene peak increase, and signals that belong to $HC{\equiv}C\text{-}C{\equiv}CH$

and $HCCCH_2$ grow in. At high heat, both the acetylene peak and the methylacetylene peak decrease, while signals that belong to HC≡C-C≡CH and $HCCCH_2$ continue to increase. These results are in agreement with the findings obtained from the IR spectra in Fig. A9a and the PIMS spectrum in Fig. A8.

THEORETICAL ASSESSMENT OF BENZYNE FRAGMENTATION

We have used rigorous *ab initio* electronic structure computations to characterize the retro-Diels-Alder fragmentation of *o*-C_6H_4 to acetylene + diacetylene. Geometric structures fully optimized at our highest level of theory [explicit or composite CCSD(T)-AE/cc-pCVQZ] for *o*-benzyne, acetylene, diacetylene, and the retro-Diels-Alder transition state are shown in Figs. A10-A13. A more extensive tabulation of r_e parameters for all these species at the RHF, MP2, CCSD, and CCSD(T) levels with the cc-pVDZ, cc-pVTZ, and cc-pCVQZ basis sets is provided as Supplementary Material in Appendix D.

To complete the assessment of the thermochemistry of reaction (A3), we require the heat of formation of diacetylene. A valence focal-point analysis of

$$2\ HCCH \rightarrow HCC\text{-}CCH + H_2 \qquad \text{(A17)}$$

was executed with cc-pV*X*Z basis sets and explicit electronic energies computed at the RHF (*X* = 2-6), MP2 (*X* = 2-6), CCSD (*X* = 2-5), CCSD(T) (*X* = 2-5), CCSDT(*X* = 2) and CCSDT(Q) (*X* = 2) levels of theory. Core correlation was accounted for with the CCSD(T)/cc-pCVTZ method; CCSD(T)/cc-pVTZ structures and harmonic vibrational frequencies were employed. The final result for the reaction enthalpy of (A17) at 298 K is +0.6 ± 0.3 kcal mol^{-1}. Adopting the

experimental[101] $\Delta_f H_{298}$(HCCH) = 54.4 ± 0.2 kcal mol^{-1}, we thus obtain $\Delta_f H_{298}$(diacetylene) = 109.4 ± 0.3 kcal mol^{-1}.

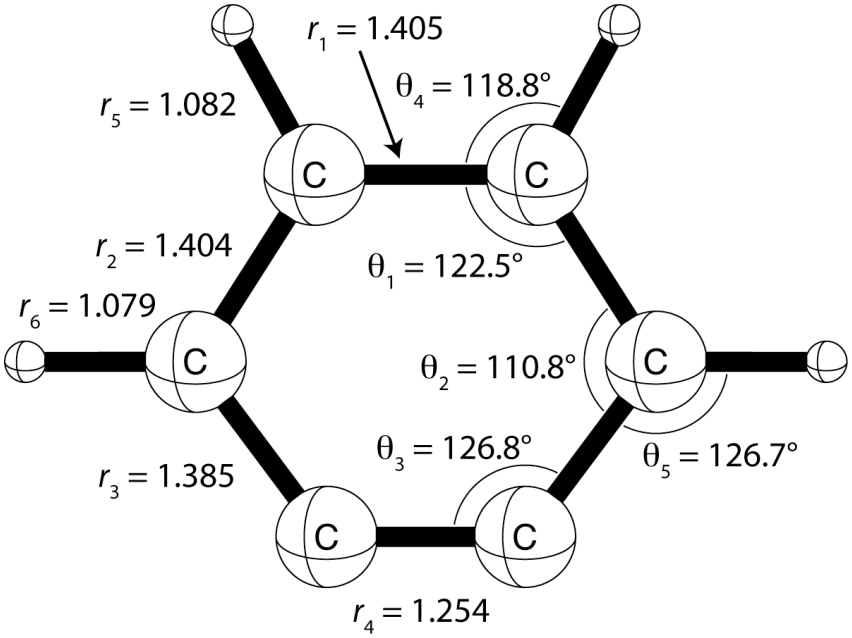

Figure A10. c~CCSD(T)-AE/cc-pCVQZ optimum geometry (Å or deg) of *o*-benzyne. Experimental microwave values[30,31] are: r_1 = 1.405 ± 0.003 Å, r_2 = 1.403 ± 0.002 Å, r_3 = 1.383 ± 0.002 Å, r_4 = 1.255 ± 0.003 Å, r_5 = 1.082 ± 0.001 Å, r_6 = 1.080 ± 0.001 Å; θ_1 = 122.36º ± 0.08º, θ_2 = 111.0º ± 0.1º, θ_3 = 126.66º ± 0.09º, θ_4 = 118.73º ± 0.08º, θ_5 = 127.40º ± 0.11º.

The best computed [c~CCSD(T)-AE/cc-pCVQZ] equilibrium structure for *o*-C_6H_4 is displayed in Fig. A10. In *o*-benzyne the C≡C distance is shortened by 0.14 Å from the bond distance in benzene upon dehydrogenation. The precise equilibrium structure[102] for gas-phase C_6H_6 is: r_e(CC) = 1.391 ± 0.001 Å and r_e(CH) = 1.080 ± 0.002 Å. The other C-C distances in *o*-benzyne are within 0.014 Å of the benzene value. An r_e structure derived from microwave spectra of *o*-benzyne isotopologs has recently been reported,[29-31] and the experimental structural parameters are listed in the caption of Fig. A10. The agreement between c~CCSD(T)-AE/cc-

pCVQZ theory and experiment is on the order of 0.001 Å for bond distances and 0.1° for bond angles. The lone outlier is θ_5, for which theory predicts an angle 0.7° less than the empirical value. The size of this disparity might suggest a re-examination of the microwave data for those isotopologs that fix the hydrogen closest to the strained triple bond. The electric dipole moment computed for o-benzyne with CCSD(T)/cc-pVTZ theory is $\mu_e(o\text{-}C_6H_4) = 1.54$ Debye.

The C–C≡C angle in *o*-benzyne is greater by almost 7° relative to benzene but is still more than 53° smaller than the idealized angle (180°) for sp hybridization. The resulting ring strain engenders diradical character in *o*-benzyne, amounting to about 10% of the ground-state singlet electronic wavefunction.[103] Nonetheless, this degree of multireference character can be readily described by single-reference coupled-cluster methods extended through connected triple excitations. This conclusion was confirmed by evaluation of a common T_1 coupled-cluster diagnostic[104] for *o*-benzyne, yielding 0.0130, comfortably below the recommended threshold of 0.020 for invoking multireference methods. The largest doubles (T_2) amplitude in the CCSD/cc-pVTZ wave function is 0.154, corresponding to the in-plane $\pi^2 \rightarrow \pi^{*2}$ excitation in the C≡C bond. No other T_2 amplitude exceeds 0.09.

For the acetylene + diacetylene fragmentation products (Fig. A12), the C≡C distances (1.204 and 1.209 Å) are now fully contracted to prototypical triple-bond lengths. The C-H distances in the products are about 0.02 Å shorter than in the *o*-benzyne reactant. Electron delocalization in diacetylene is evident in the unusually[105] short central C-C bond length of 1.374 Å as well as a surprisingly strong C-C bond. With our best computed $\Delta_f H_{298}$(HCC-CCH) of 109.4 ± 0.3 kcal mol^{-1}, one finds DH_{298}(HCC-CCH) = 161.9 ± 0.6 kcal mol^{-1}. Recall[14] that a typical "sp^3 C-C bond strength" is $DH_{298}(CH_3CH_2\text{-}CH_2CH_3)$ = 88.0 ± 0.6 kcal mol^{-1} while a

common "sp^2 C-C bond strength" is $DH_{298}(CH_2CH\text{-}CHCH_2)$ = 116 ± 1 kcal mol^{-1}. The normal >C=C< bond energy is 174 kcal mol^{-1} (from ethylene)[14] and a typical –C≡C- bond energy is 230 kcal mol^{-1} (from acetylene).[14] However, the DH_{298}(HCCCC-H) has been measured[95] to be identical to that of DH_{298}(HCC-H).

A comparison of the explicit CCSD(T)-AE/cc-pCVQZ bond distances for acetylene with r_e parameters derived from high-resolution IR spectroscopy [r_e(C≡C) = 1.20292 ± 0.00013 Å, r_e(C-H) = 1.06138 ± 0.00035 Å][106] shows remarkable accord, with disparities of only +0.0008 Å and +0.0007 Å, respectively. This impressive performance of the CCSD(T)-AE/cc-pCVQZ method is a general occurrence.[107] As documented in the Supplementary Material, the composite c~CCSD(T)-AE/cc-pCVQZ approach is able to reproduce the explicit CCSD(T)-AE/cc-pCVQZ results for all bond distances in acetylene and diacetylene to 0.0002 Å or better. This comparison places a high degree of confidence in the c~CCSD(T)-AE/cc-pCVQZ structures of *o*-benzyne and the retro-Diels-Alder transition state. The (CCSD/cc-pVTZ) T_1 diagnostics for acetylene and diacetylene are 0.0132 and 0.0139, respectively. By this measure, the overall multireference character in the *o*-benzyne reactant is very nearly the same (actually slightly smaller) as in the fragmentation products.

The retro-Diels-Alder fragmentation of *o*-benzyne is formally allowed by conservation of orbital symmetry,[108] as the number of (a_1, a_2, b_1, b_2) doubly-occupied valence orbitals is (7, 1, 2, 4) in both the reactant and products for the C_{2v} Path A. The principal orbital transformation is σ(C-C) (a_1, b_2) o-benzyne → π(a_1) acetylene + π(b_2) diacetylene. From a frontier orbital perspective, the reverse reaction is driven by the interaction of [π (a_1) C_2H_2, π *(a_1) C_4H_2] and [π *(b_2) C_2H_2, π (b_2) C_4H_2] occupied/virtual orbital pairs.

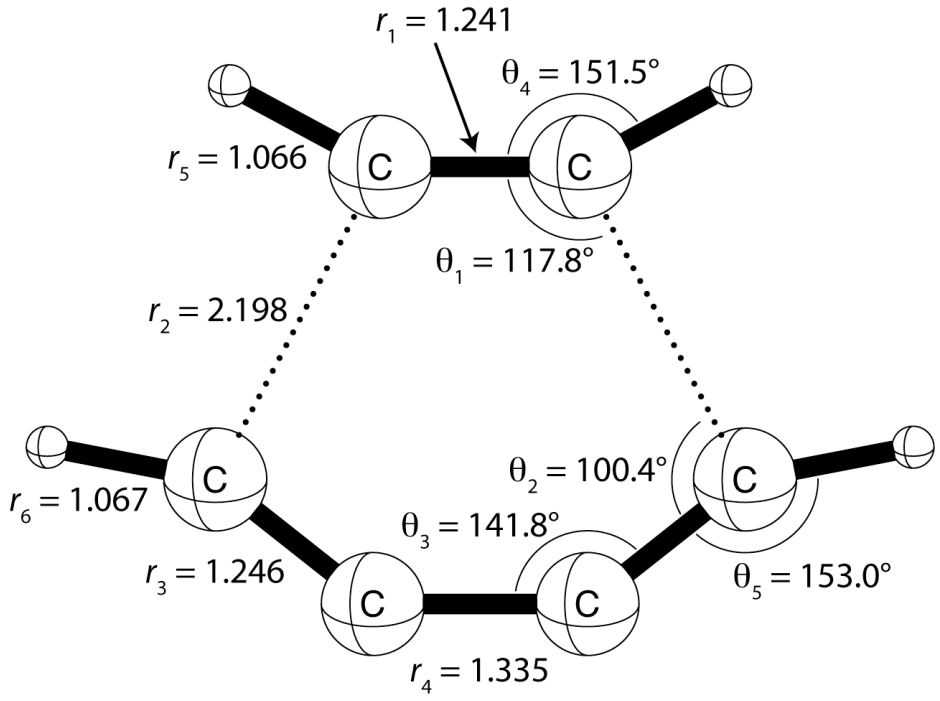

Figure A11. c~CCSD(T)-AE/cc-pCVQZ optimum geometry (Å or deg) of C_{2v}-symmetric, retro-Diels-Alder transition state for concerted fragmentation of *o*-benzyne to acetylene + diacetylene.

In the C_{2v} transition state for concerted *o*-benzyne decomposition (Fig. A11), the C-C bond being broken has a distance of 2.198 Å at the c~CCSD(T)-AE/cc-pCVQZ level. As shown below, the transition state and products lie 94.5 and 59.8 kcal mol^{-1}, respectively, above *o*-benzyne, without inclusion of zero-point vibrational energy (ZPVE). Our best calculations place the transition state farther out in the product channel than in previous theoretical work: HF/6-31G(d), r(C···C) = 2.148 Å; CASSCF(12,12)/6-31G(d,p), r(C···C) = 2.147 Å;[5] and MP2/6-31G(d), r(C···C) = 2.195 Å.[5] From the tabulations in Supplementary Material, the [RHF, MP2, CCSD, CCSD(T)] series of r(C···C) distances (in Å) is (2.149, 2.221, 2.197, 2.233) and (2.132, 2.205, 2.171, 2.207) with the cc-pVDZ and cc-pVTZ basis sets, respectively. Thus, the transition state

migrates outward in an oscillatory fashion with improvements in the electron correlation treatment but moves inward as the basis set is enlarged.

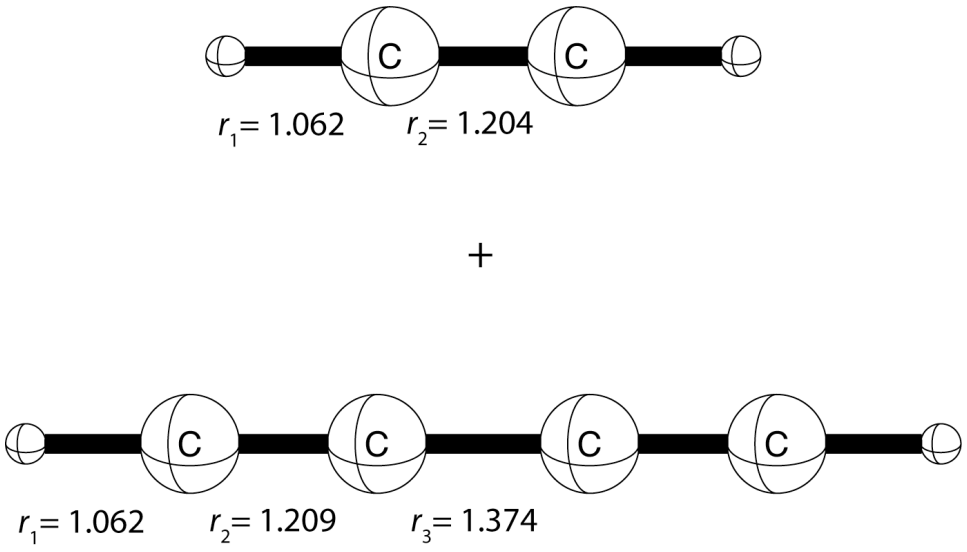

Figure A12. CCSD(T)-AE/cc-pCVQZ optimum geometries (Å) of acetylene and diacetylene. From an analysis of high resolution infrared absorption spectra,[107] the structure of acetylene is known to be: r_e(HCC-H) = 1.06138 ± 0.00035 Å and r_e(HC≡CH) = 1.20292 ± 0.00013 Å. Alternative[108] empirical r_e parameters are r_e(C≡C) = 1.2026 Å, r_e(C-H) = 1.0622 Å.

As expected for an endoergic reaction, the concerted retro-Diels-Alder reaction has a rather late transition state. As quantified by the (monotonic) progression of the C-C and C-H bonds distances, the transition state occurs when the reaction is 75 ± 7 % complete. However, the geometric relaxation necessary to yield the products is still substantial; for example, the C–C≡C angle must increase by 38.2° to reach linear diacetylene. If free acetylene and diacetylene are distorted to the conformations taken by the corresponding fragments in the transition state, then the monomer energies are raised by 12.7 and 25.8 kcal mol^{-1}, respectively, giving a total

deformation energy of 38.5 kcal mol^{-1}, all at the CCSD(T)/cc-pVTZ level. In the process, the HOMO/LUMO gaps of HCCH and HCC-CCH are reduced by 34.9 and 34.7 kcal mol^{-1} (respectively), preparing the frontier orbitals for bonding vis-à-vis the reverse reaction. The total deformation energy of the acetylene and diacetylene fragments is remarkably close to the corresponding CCSD(T)/cc-pVTZ barrier height (35.3 kcal mol^{-1}) for the reverse reaction, revealing that only 3.3 kcal mol^{-1} of electronic stabilization is gained in the transition state by interfragment orbital interactions.

The concerted (C_{2v}) retro-Diels-Alder transition state exhibits little multireference character, a conclusion critical for establishing the reliability of our computations. The [CCSD(T)/cc-pVTZ] T_1 diagnostic is 0.0148, only 6% larger than the value for diacetylene. The largest doubles (T_2) amplitude is only 0.089, comparable to those in acetylene and diacetylene and substantially smaller than that in o-benzyne. In our CASSCF(12,12)/cc-pVDZ computations at the CCSD(T)/cc-pVTZ geometry, the four largest CI coefficients ranged from 0.102 to 0.131, and the natural orbital occupation numbers in the Hartree-Fock virtual space never exceeded 0.112. Such CI coefficients are typical of CASSCF computations on single-reference systems. In brief, a number of measures show that there are no secondary reference configurations of importance for the transition state, and the CCSD(T) method should provide a highly accurate description in this region of the potential energy surface.

To obtain final energetics for the retro-Diels-Alder decomposition of *o*-benzyne, focal-point analyses were executed for the reaction energy and the fragmentation barrier. The layout of the dual approach to the one- and *n*-particle limits is provided in Table A1. There is very little uncertainty in achieving the CBS limit of each electronic structure method, as the extrapolated increments are all within 0.25 kcal mol^{-1} of the largest explicitly computed values. On the other

hand, the approach to the full configuration interaction (FCI) limits is oscillatory and more demanding to converge. With the cc-pVDZ basis set, the [MP2, CCSD, CCSD(T), CCSDT(Q)] correlation increments for the reaction energy are (+23.00, –7.98, +4.41, –0.17) kcal mol^{-1}, and those for the barrier height are (–13.26, +5.39, –2.49, –0.28) kcal mol^{-1}. Based on these trends, we conservatively ascribe uncertainties of ±0.5 kcal mol^{-1} to the CCSDT(Q) values for the reaction energy and barrier height as estimates of the FCI limit. The valence focal-point analyses yield final results of (59.9, 94.2) kcal mol^{-1} for (ΔE_{rxn}, ΔE_b), whereas all-electron computations at the CCSD(T)/cc-pCVTZ level give core-correlation shifts of (–0.08, +0.26) kcal mol^{-1}. With addition of the large effect of zero-point vibrations (evaluated from unscaled CCSD(T)/cc-pVTZ harmonic vibrational frequencies), our final predictions from Table A1 of the *ab initio* limits are $\Delta E_{rxn,0}$ = 52.4 ± 0.5 kcal mol^{-1} and $\Delta E_{b,0}$ = 88.0 ± 0.5 kcal mol^{-1}, both quantities corresponding to 0 K. With CCSD(T)/cc-pVTZ thermal corrections, the reaction energy at 298 K becomes 55.2 ± 0.5 kcal mol^{-1}. Using our computed $\Delta_f H_{298}$(diacetylene) from above and experimental values for *o*-C_6H_4 and HCCH, the "experimental" $\Delta_{rxn}H_{298}$(o-C_6H_4 → HC≡CH + HC≡C-C≡CH) becomes 57 ± 3 kcal mol^{-1}. The purely *ab initio* and experimental reaction energies for *o*-benzyne decomposition are in satisfactory accord.

Table A1. Valence focal-point analysis of the reaction energy and concerted retro-Diels-Alder barrier for the fragmentation of *o*-benzyne to acetylene and diacetylene[a]

Basis Set	ΔE_e [RHF]	$+\delta$ [MP2]	$+\delta$ [CCSD]	$+\delta$ [CCSD(T)]	$+\delta$ [CCSDT(Q)]	ΔE_e[CCSDT(Q)]
			Fragmentation energy (ΔE_{rxn} , kcal mol^{-1})			
cc-pVDZ	44.27	+23.00	–7.98	+4.41	–0.17	63.52
cc-pVTZ	38.45	+24.80	–9.11	+4.66	[–0.17]	[58.63]
cc-pVQZ	38.47	+25.34	–9.13	+4.78	[–0.17]	[59.28]
cc-pV5Z	38.59	+25.55	[–9.16]	[+4.82]	[–0.17]	[59.63]
cc-pV6Z	38.62	+25.59	[–9.12]	[+4.84]	[–0.17]	[59.76]
CBS limit	[38.63]	[+25.71]	[–9.13]	[+4.87]	[–0.17]	**[59.91]**
$\Delta E_{rxn,0}$ (final) = ΔE_e[CBS CCSDT(Q)] +ΔZPVE[CCSD(T)/cc-pVTZ]+ Δcore[CCSD(T)/cc-pCVTZ] = 59.91 – 7.46 –0.08 = **52.4 ± 0.5 kcal mol^{-1}**						
			Barrier (ΔE_b, kcal mol^{-1})			
cc-pVDZ	108.43	–13.26	+5.39	–2.40	–0.28	97.88
cc-pVTZ	104.83	–14.28	+6.41	–2.89	[–0.28]	[93.79]
cc-pVQZ	104.87	–14.40	+6.86	–3.05	[–0.28]	[94.01]
cc-pV5Z	104.98	–14.42	[+6.99]	[–3.10]	[–0.28]	[94.17]
cc-pV6Z	104.99	–14.42	[+7.04]	[–3.13]	[–0.28]	[94.21]
CBS limit	[104.99]	[–14.43]	[+7.11]	[–3.16]	[–0.28]	**[94.24]**
$\Delta E_{b,0}$ (final) = ΔE_e[CBS CCSDT(Q)] +ΔZPVE[CCSD(T)/cc-pVTZ]+ Δcore[CCSD(T)/cc-pCVTZ] = 94.24 – 6.52 + 0.26 = **88.0 ± 0.5 kcal mol^{-1}**						
Fit	$a + bc^{-cX}$	$a + bX^{-3}$	$a + bX^{-3}$	$a + bX^{-3}$	additive	
Points (X)	4,5,6	4,5,6	3,4	3,4		

[a]The symbol δ denotes the *increment* in the energy difference (ΔE) with respect to the previous level of theory. Bracketed numbers are the result of basis set extrapolations or additivity assumptions (as specified at the bottom of the table), while unbracketed numbers were explicitly computed. The reference structures were the CCSD(T)-AE/cc-pCVQZ optimized geometries depicted in Figs. A10-A12. The use of CCSD(T)/cc-pVTZ structures changes the final energetics by no more than 0.01 kcal mol^{-1}.

In 1999, Moskaleva, Madden, and Lin[5] studied the decomposition and isomerization of *o*-benzyne with the composite G2M(rcc,MP2) method.[109] The highest-level single-point energies in this scheme are determined from RCCSD(T)/6-311G(d,p) and MP2/6-311+G(3df,2p) computations. In the standard G2M(rcc,MP2) approach, the geometries and vibrational frequencies are determined from B3LYP/6-311G(d,p) density functional theory; however, there is no C_{2v}-symmetric retro-Diels-Alder transition state for this method, and thus MP2/6-31G(d) was substituted for the geometry optimizations. With inclusion of ZPVE, the G2M(rcc,MP2) results for the 0 K retro-Diels-Alder (fragmentation energy, barrier height) were (50.2, 87.4) kcal mol^{-1}. An earlier 1998 study[4] at the less reliable B3LYP/6-31G*//HF/6-31G* level placed the barrier height at 88.6 kcal mol^{-1}. The previous theoretical data of Refs.[4,5] agree with our new results within 2.5 kcal mol^{-1}. In contrast, the barrier height reported in 2000 by Wang et al.[6] is 4-5 kcal mol^{-1} smaller than our final value.[110]

Vibrational frequencies at the CCSD(T)/cc-pVTZ level for *o*-benzyne, acetylene, and diacetylene, and the concerted (C_{2v}) retro-Diels-Alder transition state are compiled in Table A2. Corresponding CCSD(T)/cc-pVDZ frequencies are given in Supplementary Material. The frequencies of 20 of the 24 internal vibrations transform monotonically along the path, including the modes correlating to C≡C stretches in acetylene and diacetylene, i.e., [$\omega_9(a_1)$: 1904 → 2015 → 2233 cm^{-1}]; [$\omega_4(a_1)$: 1477 → 1750 → 2201 cm^{-1}]; and [$\omega_{19}(b_2)$: 1488 → 1854 → 2051 cm^{-1}] The most salient frequencies in Table A2 are $\omega_9(a_1) = 621i$ cm^{-1} and $\omega_{24}(b_2) = 40$ cm^{-1} in the transition state, the associated normal modes being depicted in Fig. A13. The $\omega_9(a_1)$ eigenvector gives positive identification of the retro-Diels-Alder transition state, whereas the $\omega_{24}(b_2)$ eigenvector is a distortion toward a stepwise carbon-carbon bond fragmentation path.

Table A2. CCSD(T)/cc-pVTZ vibrational frequencies (in cm^{-1}) along the retro-Diels-Alder fragmentation path of *o*-benzyne[a]

mode	*o*-benzyne	transition state	products
$\omega_1(a_1)$	3220	3418	3511 (σ_g C_2H_2)
$\omega_2(a_1)$	3191	3380	3458 (σ_g C_4H_2)
$\omega_3(a_1)$	1904	2015	2233 (σ_g C_4H_2)
$\omega_4(a_1)$	1477	1750	2001 (σ_g C_2H_2)
$\omega_5(a_1)$	1318	1113	887 (σ_g C_4H_2)
$\omega_6(a_1)$	1154	850	746 (π_u C_2H_2)
$\omega_7(a_1)$	1055	699	633 (π_u C_4H_2)
$\omega_8(a_1)$	996	404	227 (π_u C_4H_2)
$\omega_9(a_1)$	606	621*i*	0
$\omega_{10}(a_2)$	949	624	623 (π_g C_4H_2)
$\omega_{11}(a_2)$	862	597	578 (π_g C_2H_2)
$\omega_{12}(a_2)$	592	487	474 (π_g C_4H_2)
$\omega_{13}(a_2)$	440	254	0
$\omega_{14}(b_1)$	914	658	746 (π_u C_2H_2)
$\omega_{15}(b_1)$	746	622	633 (π_u C_4H_2)
$\omega_{16}(b_1)$	387	228	227 (π_u C_4H_2)
$\omega_{17}(b_2)$	3216	3380 (3385)	3454 (σ_u C_4H_2)
$\omega_{18}(b_2)$	3174	3355 (3357)	3410 (σ_u C_2H_2)
$\omega_{19}(b_2)$	1488	1854 (1866)	2051 (σ_u C_4H_2)
$\omega_{20}(b_2)$	1418	838 (838)	623 (π_g C_4H_2)
$\omega_{21}(b_2)$	1261	746 (757)	578 (π_g C_2H_2)
$\omega_{22}(b_2)$	1107	483 (489)	0
$\omega_{23}(b_2)$	849	435 (442)	474 (π_g C_4H_2)
$\omega_{24}(b_2)$	462	40 (42)	0

[a] For the b_2 normal modes, c~CCSD(T)-AE/cc-pCVQZ frequencies are given in parentheses.

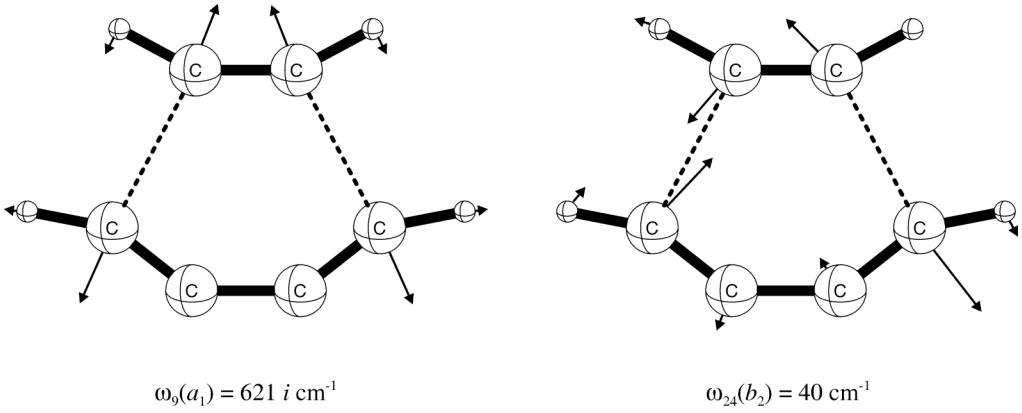

$\omega_9(a_1) = 621\ i\ cm^{-1}$ $\omega_{24}(b_2) = 40\ cm^{-1}$

Figure A13. Normal-mode eigenvectors [$Q_9(a_1)$ and $Q_{24}(b_2)$] for the retro-Diels-Alder transition state for *o*-benzyne fragmentation (Path A). Corresponding vibrational frequencies are listed from the CCSD(T)/cc-pVTZ level of theory.

The potential energy curve along the $\omega_{24}(b_2)$ normal mode is extremely flat. Indeed, some lower levels of theory give imaginary values of $\omega_{24}(b_2)$, a fact observed for B3LYP/6-311G(d,p) theory by Moskaleva et al.[5] but whose significance was not pursued. With the cc-pVDZ basis set, we find $\omega_{24}(b_2)$ = (177, 178, 39, 93*i*) cm^{-1} at the [RHF, MP2, CCSD, CCSD(T)] levels. To gain more confidence that the concerted, retro-Diels-Alder process (Path A) has a true transition state in C_{2v} symmetry with a single imaginary frequency corresponding to $\omega_9(a_1)$, we recomputed the b_2 vibrational frequencies of the critical structure at the c~CCSD(T)-AE//cc-pCVQZ level. As a test of our procedure, we obtained the following frequencies (in cm^{-1}) for acetylene: $[\omega_1(\sigma_g), \omega_3(\sigma_u), \omega_2(\sigma_g), \omega_5(\pi_u), \omega_4(\pi_g)]$ = (3509, 3417, 2012, 747, 605) from explicit CCSD(T)-AE//cc-pCVQZ; and (3508, 3415, 2012, 746, 600) from c~CCSD(T)-AE//cc-pCVQZ; as compared to (3501.5, 3417.6, 2013.3, 746.8, 621.5) from experiment.[111] The *o*-benzyne transition state frequencies given in parentheses in Table A2 show no asymmetric b_2 normal modes of negative curvature at the c~CCSD(T)-AE//cc-pCVQZ level, and $\omega_{24}(b_2)$ has increased slightly to 42 cm^{-1}. In conclusion, we believe that the C_{2v} structure of Fig. A11 is stable with respect to all asymmetric distortions of the nuclear framework and is a genuine transition state for the C_{2v} symmetric, concerted retro-Diels-Alder decomposition of *o*-benzyne (Path A).

Notwithstanding the existence of Path A, the remarkably flat $\omega_{24}(b_2)$ potential energy profile in the C_{2v} transition state raises the specter of more convoluted routes and complex dynamics for *o*-benzyne fragmentation. The qualitative energy contour sketches of Figs. A14 and A15 illustrate the most viable possibilities. Hypothetical Path B is an asymmetric, but concerted, retro-Diels-Alder route having degenerate planar transition states of C_s symmetry. Path B might exist regardless of whether Path A exhibits a true transition state. However, the scenario shown in Fig. A14 is more likely, whereby Path A directly bifurcates into a degenerate

Path B pair when a mound (shown with a dashed contour) on the potential energy surface obstructs the C_{2v} route. We examined the possibility of Path B by following the $\omega_{24}(b_2)$ normal mode with CCSD/cc-pVDZ theory. What we found was not a Path B transition state, but one leading from *o*-benzyne to an open-chain, open-shell singlet intermediate HC≡C···C=CH-CH=CH• which could subsequently undergo C-C bond scission to yield acetylene and diacetylene. Therefore, our computations do not support the existence of Path B, but rather the nonconcerted Path C depicted in Fig. A15, which might be a legitimate alternative for producing acetylene + diacetylene from *o*-benzyne.

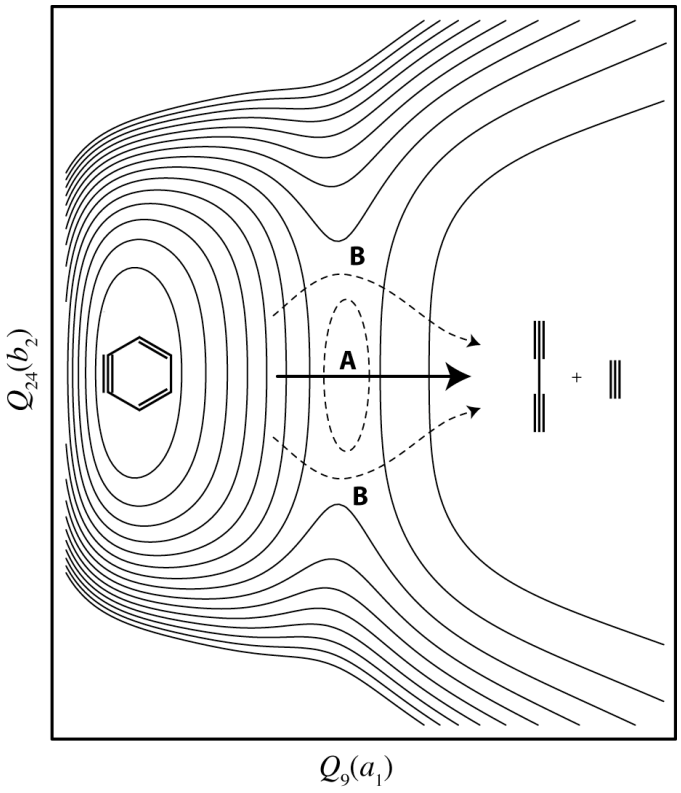

Figure A14. Schematic energy contours of concerted pathways for *o*-benzyne fragmentation to acetylene + diacetylene. Path A is the classic, concerted retro-Diels-Alder route (C_{2v} symmetry). Shown by dashed lines is a hypothetical Path B, which is asymmetric but concerted; it does not pass through a chemical intermediate. The qualitative energy surface is represented in the $Q_9(a_1)$ and $Q_{24}(b_2)$ normal coordinates of the Path A transition state, as depicted in Fig. A13.

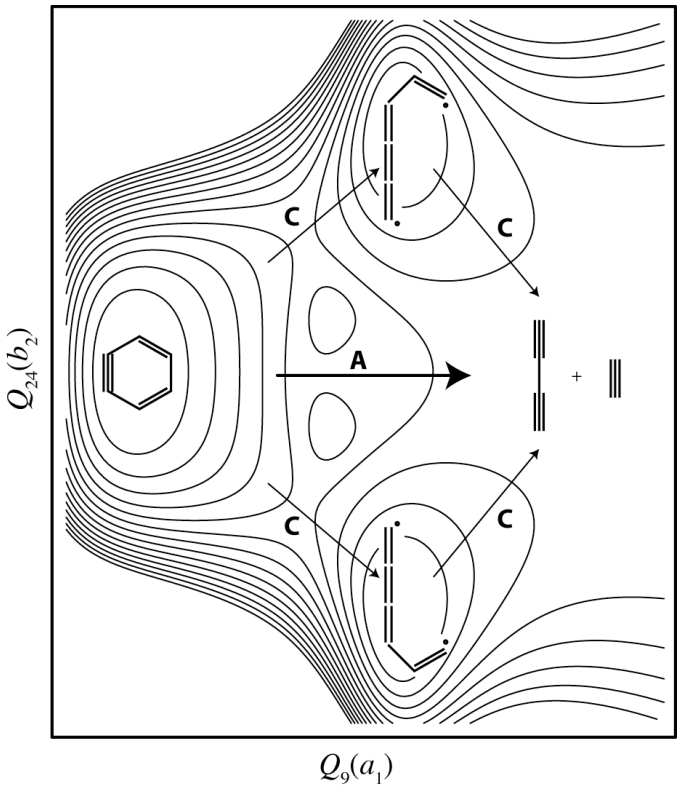

Figure A15. Schematic energy contours of possible competitive pathways for *o*-benzyne fragmentation to acetylene + diacetylene. Path A is the classic, concerted retro-Diels-Alder route (C_{2v} symmetry). In contrast, Path C is an asymmetric, nonconcerted route through an open-chain diradical intermediate. See Fig. A13 and the caption of Fig. A14 for definitions of the $Q_9(a_1)$ and $Q_{24}(b_2)$ geometric coordinates.

The possible competition between Paths A and C cannot be probed by any of the experiments reported in this paper. Furthermore the accurate theoretical characterization of Path C is a formidable task that will require much additional computational effort. The severe multireference electronic character encountered along Path C is an acute problem. Not only is the open-chain intermediate a large singlet diradical, but it is connected smoothly to closed-shell reactants and products via homolytic bond fission processes. We confirmed the difficulty of applying single-reference electron correlation methods to Path C in locating the CCSD/cc-pVDZ

transition state connecting o-benzyne to HC≒C⋯C=CH-CH=CH•. The T_1 diagnostic (0.0585) for this transition state is enormous. The corresponding barrier for the first step of Path C was almost 10 kcal mol^{-1} lower than the barrier for Path A, but this prediction is likely dubious. Even if the first step of Path C has a lower barrier than Path A, the second step leading from the intermediate to acetylene + diacetylene fragments might be energetically prohibitive. Careful work with multireference and perhaps spin-flip coupled-cluster methods will be required to reliably investigate the possibility of a competitive, stepwise fragmentation path to acetylene and diacetylene.

Constructing multiconfigurational reference wave functions for characterization of Paths A and C is also problematic. The σ(C-C) bonds in o-benzyne that are broken in the retro-Diels-Alder fragmentation have molecular orbitals buried below a σ(C-H) orbital. The correlating σ*(C-C) virtual orbitals in o-benzyne have 8 other virtual orbitals lower in energy, and in particular there are 4 σ*(C-H) orbitals underneath. Accordingly, there are numerous avoided crossings in the orbital stacking as one proceeds from *o*-benzyne to the products via Path A or C. Because of the cascading effect in the orbital transformations, there is no clear choice of a CASSCF scheme to describe the fragmentation process uniformly from reactant to products.

We have considered whether triplet electronic states might play a role in *o*-benzyne pyrolysis. The measured[34] singlet-triplet splitting in *o*-benzyne is 37.8 ± 0.6 kcal mol^{-1}, whereas the lowest triplet electronic states in acetylene[112] and diacetylene[113,114] have adiabatic excitation energies of 88 and 62 kcal mol^{-1}, respectively. At the retro-Diels-Alder transition state, UMP2/cc-pVTZ theory places the lowest triplet state 134 kcal mol^{-1} above the ground-state singlet. Therefore, as long as the reaction dynamics proceed along the C_{2v} concerted path, rather

than through open-chain intermediates, intersystem crossing to triplet surfaces is not a concern. However, the intermediate region of Path C is certainly complicated by an intermingling of close-lying singlet and triplet states.

A pathway competitive to the decomposition of *o*-benzyne to acetylene and diacetylene is successive isomerization to *m*- and *p*-benzyne followed by a retro-Bergman[7,8] ring opening to hex-3-ene-1,5-diyne (HCC-CH=CH-CCH); see Scheme A1. With G2M(rcc,MP2) theory[5] the transition states for *o*-benzyne → *m*-benzyne, *m*-benzyne → *p*-benzyne, and *p*-benzyne → hex-3-ene-1,5-diyne were computed to lie 71, 75, and 43 kcal mol^{-1}, respectively, above *o*-benzyne. While these energetics should be confirmed with higher levels of theory, it appears that the stepwise *o*-benzyne isomerization route has an overall barrier at least 10 kcal mol^{-1} below that for decomposition to acetylene + diacetylene via Path A. Multichannel RRKM calculations[5] using G2M(rcc,MP2) potential energy surface data predict that the isomerization process accounts for as much as 99% of *o*-benzyne depletion at 1000 K. However, at temperatures above 2000 K concerted decomposition to acetylene and diacetylene dominates. Because our experiments are performed at temperatures between these two extremes, the isomerization and decomposition routes should be in strong competition. The crux is that the observed acetylene and diacetylene products cannot be produced by the HCC-CH=CH-CCH intermediate, because the necessary carbon-carbon bond fragmentation must also be accompanied by an unfavorable hydrogen shift. Our preliminary CCSD(T)/cc-pVDZ computations indicated that this process would have to overcome an overall barrier of at least 100 kcal mol^{-1}.

If HCC-CH=CH-CCH is being formed in our experiments, it should be detectable. The IE(HCC-CH=CH-CCH) is certainly below 10.487 eV so the 118.2 nm laser line in the PIMS experiment could ionize this species. Likewise the proton affinity or gas phase acidity of HCC-

CH=CH-CCH implies that hex-3-ene-1,5-diyne could react with H_3O^+ or OH^- in the CIMS apparatus. And hex-3-ene-1,5-diyne will have characteristic C-H stretching frequencies for the H-C≡C- and =C-H bonds. The experimental infrared spectra (Figs. 2, 9a, 9b) are the most persuasive data that indicate the absence of the hex-3-ene-1,5-diyne.

DISCUSSION

The decomposition of benzene at high temperatures has been studied in shock tubes.[1,2] From the thermochemistry of Scheme A2, it is clear that conditions harsh enough to break the C-H bond in benzene[2] (113 kcal mol^{-1}) can also easily break the remaining C-H bonds to produce any of the isomeric benzynes: *o*-C_6H_4, *m*-C_6H_4, *p*-C_6H_4. The experiments from this paper (Figs. A1-A7) clearly demonstrate that our hyperthermal nozzle generates *o*-C_6H_4. At higher temperatures, the most facile path for *o*-benzyne decomposition is fragmentation to acetylene and diacetylene. Thus we have demonstrated the occurrence of reaction (A3). Our study with 3,6-$(CH_3)_2$-*o*-C_6H_2 in Figs A8, A9a, and A9b, demonstrates that at the threshold decomposition temperature, the 3,6-dimethyl-*o*-benzyne does not isomerize but fragments to HCCH and CH_3-CC-CC-CH_3.

We conclude that at high temperatures, the fragmentation path for benzene is exactly that outlined by the reactions (1) → (2) → (3). According to our high-level *ab initio* computations, the concerted, retro-Diels-Alder route (Path A) of reaction (A3) is completely consistent with the experimental observations. However, there may also be a competitive, nonconcerted route (Path C) through an open-chain singlet diradical intermediate, a problem that awaits elucidation by arduous multireference electronic structure studies.

The retro-Diels-Alder cracking of *o*-benzyne may be of greater importance than simply describing the decomposition of benzene. In a shock tube study of the fragmentation of toluene it was discovered that there are two important, parallel reactions.[115] Scheme A2 indicates that the lowest toluene fragmentation route (90 kcal mol^{-1}) is formation of hydrogen atom and the benzyl radical (A18a). In contrast, C-C bond scission is higher in energy (104 kcal mol^{-1}) but it produces a pair of polyatomic radicals (A18b).

$$C_6H_5CH_3 \rightarrow C_6H_5CH_2 + H \qquad \text{(A18a)}$$

$$C_6H_5CH_3 \rightarrow C_6H_5 + CH_3 \qquad \text{(A18b)}$$

Scheme A2 summarized these enthalpy changes. However the entropy increase will be more important for (A18b) because it produces a pair of polyatomic radicals. As the temperatures increases the free energy, $\Delta G = \Delta H - T\Delta S$, will increasingly favor (A18b) over (A18a). At some high temperature, the C-C bond cleaving reaction will become the favored decomposition route of toluene: $\Delta_{rxn}G(C_6H_5CH_3 \rightarrow C_6H_5CH_2 + H) > \Delta_{rxn}G(C_6H_5CH_3 \rightarrow C_6H_5 + CH_3)$. The validity of this expectation has been explored using Active Thermochemical Tables (ATcT) resulting in Fig. A16.[116-118]

The pertinent details of ATcT and its underlying Thermochemical Network (TN) approach are given elsewhere.[116] The thermochemical data needed to construct Fig. A16 has been obtained by a statistical analysis and simultaneous solution of the Core (Argonne) Thermochemical Network, C(A)TN, which currently (ver. 1.052) contains more than 700 chemical species interconnected by roughly 6500 thermochemically-relevant experimental and computational determinations, and is growing on a daily basis.[119] The detailed description of the intricacies of C(A)TN is beyond the scope of the present paper. Suffices it to say here that the

determinations influencing the ATcT result for the bond dissociation enthalpy of toluene into benzyl and H (Reaction A18a) are those listed in the recent IUPAC recommendation for the thermochemistry of benzyl.[94] The manifold of C(A)TN interdependencies determining the bond dissociation enthalpy of toluene into phenyl and methyl (Reaction A18b) is substantially more complex, but the ATcT sensitivity analysis indicates that the current result is heavily dominated by the negative-ion-cycle determination of the bond dissociation energy of benzene,[21,22] the positive-ion-cycle determinations of the bond dissociation energy of methane,[120-123] and the calorimetric determinations of the combustion enthalpies of methane,[124-131] and liquid benzene[132-134] and toluene,[132,134,135] coupled to the determinations of the vaporization enthalpies of benzene[136-139] and toluene.[136-140] The entropy changes of Reactions 18a and 18b, needed to relate reaction enthalpies to corresponding free energies, and the temperature dependences of the enthalpy and free energy of both reactions are based on the partition functions (and their various derivatives) for toluene, benzyl, phenyl, methyl, and hydrogen atom, contained in ATcT. The partition-function related thermochemical quantities for H are trivially obtained by level-counting, and are in ATcT the same as in standard thermochemical compilations.[141-144] In the absence of more elaborate information (e.g. full complement of anharmonicities), the partition-function related thermochemical quantities for the other four species was computed internally by ATcT using a rigid-rotor harmonic-oscillator (RRHO) approach, including an explicit treatment of internal rotors (for toluene and benzyl, see discussion for these two species in Ref.[94]) as implemented by McBride and Gordon in the NASA approach.[145] The spectroscopic constants for toluene,[139,146] phenyl,[17,147] and methyl[148] were taken from the literature, and those for benzyl from the recent IUPAC review.[94]

Though the difference in the enthalpies of Reactions A18a and A18b is obtained by ATcT quite accurately and reliably at room temperature (based on the thermochemical knowledge content of C(A)TN described above), the accuracy of extrapolation of the relevant thermochemistry to high temperatures is highly dependent on the applicability of the inherently approximate RRHO approach. Nevertheless, the combined ATcT results shown in Fig. A16 are sufficiently accurate to explicitly demonstrate the point that at a sufficiently high temperature $\Delta_{rxn}G(C_6H_5CH_3 \rightarrow C_6H_5CH_2 + H)$ becomes larger than $\Delta_{rxn}G(C_6H_5CH_3 \rightarrow C_6H_5 + CH_3)$. Both the enthalpy (■) and the free energy (•••) change for benzyl radical formation, ΔH(A18a) and ΔG(A18a), are plotted as a function of temperature and compared to the enthalpy (□) and the free energy (°°°) change for C-C bond scission, ΔH(A18b) and ΔG(A18b). At roughly 1500 K the free energies of (A18a) and (A18b) become equivalent; $\Delta_{rxn}G(C_6H_5CH_3 \rightarrow C_6H_5CH_2 + H) \approx \Delta_{rxn}G(C_6H_5CH_3 \rightarrow C_6H_5 + CH_3)$.

The kinetics of toluene decomposition[149] follows the thermochemistry of Fig. A16. As predicted earlier,[115] rate constants for fragmentation of a polyatomic molecule to a stable radical (like $C_6H_5CH_2$ in A18a) and an H atom are characterized by A factors in the range of 10^{15} s^{-1}, but dissociation to a pair of complex radicals (as in A18b) could have A factors in excess of 10^{17} sec^{-1}. The conclusion of Fig. A16 is that at decomposition temperatures of 1600 K or greater, arenes like toluene will begin to shed their alkyl groups and produce phenyl radicals. As indicated in (A2) these C_6H_5 radicals will decompose to *o*-C_6H_4 and thence via (A3) to HC≡CH + HC≡C-C≡CH. Since gasoline contains[150] an appreciable fraction of aromatic hydrocarbons, high engine temperatures may crack these alkylbenzenes to a mixture of alkyl radicals and phenyl radicals. The phenyl radicals will then dissociate first to benzyne and then to acetylene and diacetylene.

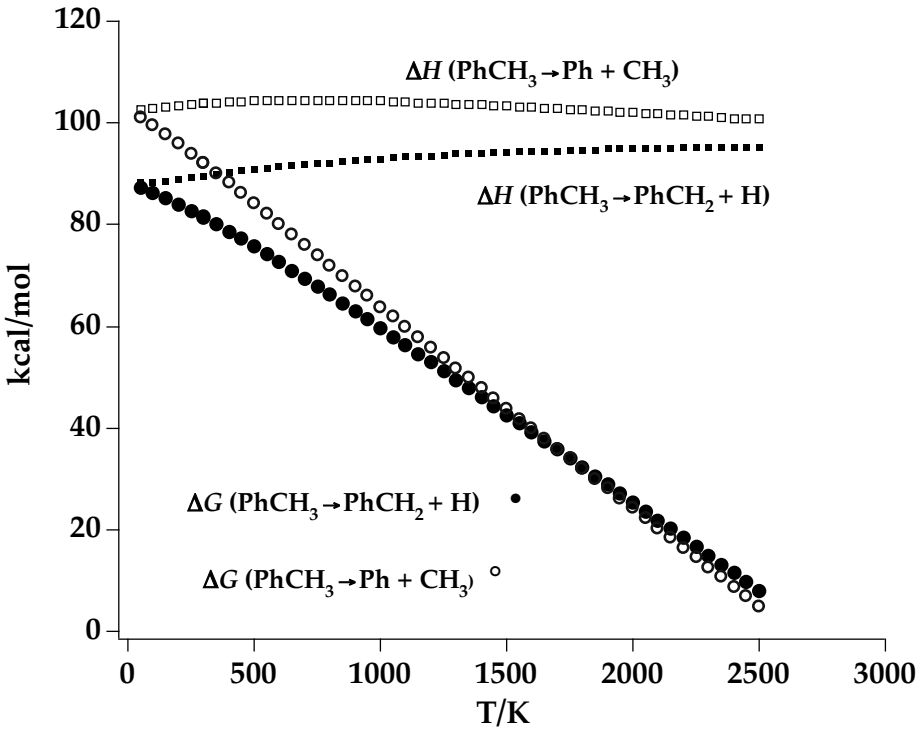

Figure A16. Variation of the enthalpy of reaction for $\Delta_{rxn}H_T(C_6H_5CH_3 \rightarrow C_6H_5CH_2 + H)$ and $\Delta_{rxn}H_T(C_6H_5CH_3 \rightarrow C_6H_5 + CH_3)$ as a function of Temperature. Both plots are relatively flat out to 2500 K. In contrast the free energies, $\Delta_{rxn}G_T(C_6H_5CH_3 \rightarrow C_6H_5CH_2 + H)$ and $\Delta_{rxn}G_T(C_6H_5CH_3 \rightarrow C_6H_5 + CH_3)$, both steadily decline. Around 1600 K $\Delta_{rxn}G_T(C_6H_5CH_3 \rightarrow C_6H_5CH_2 + H)$ becomes greater than $\Delta_{rxn}G_T(C_6H_5CH_3 \rightarrow C_6H_5 + CH_3)$.

ACKNOWLEDGMENTS

The research at the University of Georgia was supported by the U. S. Department of Energy, Office of Basic Energy Sciences, Combustion Program (Grant No. DE-FG02-00ER14748). Experiments at the University of Colorado were supported by grants from the Chemical Physics Program, United States Department of Energy (DE-FG02-87ER13695) and the National Science Foundation (CHE-9813659) to GBE. VMB and SK thank the National Science Foundation (CHE-0349937) for support.

The work at Argonne National Laboratory, together with the underlying fundamental thermochemical development of the ATcT approach, was supported by the U.S. Department of Energy, Division of Chemical Sciences, Geosciences, and Biosciences of the Office of Basic Energy Sciences, under Contract No. W-31-109-ENG-38. Development of inherent computer-science aspects of ATcT and the underpinning data management technologies were supported by the U.S. Department of Energy, Division of Mathematical, Information, and Computational Science of the Office of Advanced Scientific Computing Research, under Contract No. W-31-109-ENG-38 (Argonne) as part of the multi-institutional Collaboratory for Multi-Scale Chemical Science (CMCS), which is a project within the National Collaboratories Program of the U.S. Department of Energy. This work has benefited from the support and effort of numerous past and present CMCS Team members. Portions of the research described are related to the effort of a Task Group of the International Union of Pure and Applied Chemistry (2003-024-1-100).

We thank Drs. Larry B. Harding, John F. Stanton, and Alexander Laskin for several enlightening discussions. Barry K. Carpenter spent part of his 2005 sabbatical in Boulder and we have benefited a great deal from our conversations with Prof. Carpenter. This story about the formation of benzyne from phenyl radicals and its subsequent Diels-Alder fragmentation was first presented by GBE in Jan. 2006 at Yale University's Wiberg Lecture.

REFERENCES

[1] S. H. Bauer and C. F. Aten, J. Chem. Phys. **39**, 1253 (1963).

[2] J. H. Kiefer, L. J. Mizerka, M. R. Patel, and H. C. Wei, J. Phys. Chem. **89**, 2013 (1985).

[3] P. R. Westmoreland, A. M. Dean, J. B. Howard, and J. P. Longwell, J. Phys. Chem. **93**, 8171 (1989).

[4] W. Q. Deng, K. L. Han, J. P. Zhan, and G. Z. He, Chem. Phys. Lett. **288**, 33 (1998).

[5] L. V. Moskaleva, L. K. Madden, and M. C. Lin, Phys. Chem. Chem. Phys. **1**, 3967 (1999).

[6] H. Wang, A. Laskin, N. W. Moriarty, and M. Frenklach, Proc. Combust. Inst. **28**, 1545 (2000).

[7] R. R. Jones and R. G. Bergman, J. Am. Chem. Soc. **94**, 660 (1972).

[8] R. G. Bergman, Acc. Chem. Res. **6**, 25 (1973).

[9] J. B. Pedley, R. D. Naylor, and S. P. Kirby, *Thermochemistry of Organic Compounds*, 2nd ed. (Chapman and Hall, New York, 1986).

[10] J. H. Kiefer, S. S. Sidhu, R. D. Kern, K. Xie, H. Chen, and L. B. Harding, Comb. Sci. Tech. **82**, 101 (1992).

[11] S. E. Stein and A. Fahr, J. Phys. Chem. **89**, 3714 (1985).

[12] W. R. Roth, O. Adamczak, R. Breuckmann, H. W. Lennartz, and R. Boese, Chem. Ber. **124**, 2499 (1991).

[13] J. Berkowitz, G. B. Ellison, and D. Gutman, J. Phys. Chem. **98**, 2744 (1994).

[14] S. J. Blanksby and G. B. Ellison, Acc. Chem. Res. **36**, 255 (2003).

[15] P. H. Kasai, E. Hedaya, and P. H. Kasai, J. Am. Chem. Soc. **91**, 4364 (1969).

[16] J. G. Radziszewski, M. R. Nimlos, P. R. Winter, and G. B. Ellison, J. Am. Chem. Soc. **118**, 7400 (1996).

[17] A. V. Friderichsen, J. G. Radziszewski, M. R. Nimlos, P. R. Winter, D. C. Dayton, D. E. David, and G. B. Ellison, J. Am. Chem. Soc. **123**, 1977 (2001).

[18] R. J. McMahon, M. C. McCarthy, C. A. Gottlieb, J. B. Dudek, J. F. Stanton, and P. Thaddeus, Astrophysical Journal **590**, L61 (2003).

[19] V. Butcher, M. L. Costa, J. M. Dyke, A. R. Ellis, and A. Morris, Chem. Phys. **115**, 261 (1987).

[20] X. Zhang, PhD, Harvard University, 1995.

[21] R. F. Gunion, M. K. Gilles, M. L. Polak, and W. C. Lineberger, Int. J. Mass Spectrom. **117**, 601 (1992).

[22] G. E. Davico, V. M. Bierbaum, C. H. Depuy, G. B. Ellison, and R. R. Squires, J. Am. Chem. Soc. **117**, 2590 (1995).

[23] K. M. Ervin and V. F. DeTuri, J. Phys. Chem. A **106**, 9947 (2002).

[24] R. S. Berry, G. N. Spokes, and R. M. Stiles, J. Am. Chem. Soc. **82**, 5240 (1960).

[25] R. S. Berry, G. N. Spokes, and R. M. Stiles, J. Am. Chem. Soc. **84**, 3570 (1962).

[26] R. S. Berry, J. Clardy, and M. E. Schafer, J. Am. Chem. Soc. **86**, 2738 (1964).

[27] R. S. Berry, J. Clardy, and M. E. Schafer, Tetrahedron Lett. **15**, 1003 (1965).

[28] R. S. Berry, J. Clardy, and M. E. Schafer, Tetrahedron Lett. **15**, 1011 (1965).

[29] R. D. Brown, P. D. Godfrey, and M. Rodler, J. Am. Chem. Soc. **108**, 1296 (1986).

[30] S. G. Kukolich, C. Tanjaroon, M. C. McCarthy, and P. Thaddeus, J. Chem. Phys. **119**, 4353 (2003).

[31] S. G. Kukolich, M. C. McCarthy, and P. Thaddeus, J. Phys. Chem. A **108**, 2645 (2004).

[32] X. Zhang and P. Chen, J. Am. Chem. Soc. **114**, 3147 (1992).

[33] W. A. Goddard III, T. H. Dunning Jr., W. J. Hunt, and P. J. Hay, Acct. Chem. Res. **6**, 368 (1973).

[34] D. G. Leopold, A. E. S. Miller, and W. C. Lineberger, J. Am. Chem. Soc. **108**, 1379 (1986).

[35] J. G. Radziszewski, B. A. Hess, and R. Zahradnik, J. Am. Chem. Soc. **114**, 52 (1992).

[36] Y. L. Guo and J. J. Grabowski, J. Am. Chem. Soc. **113**, 5923 (1991).

[37] J. M. Riveros, S. Ingemann, and N. M. M. Nibbering, J. Am. Chem. Soc. **113**, 1053 (1991).

[38] P. G. Wenthold and R. R. Squires, J. Am. Chem. Soc. **116**, 6401 (1994).

[39] P. G. Wenthold, J. Hu, and R. R. Squire, J. Am. Chem. Soc. **116**, 6961 (1994).

[40] X. Zhang, A. V. Friderichsen, S. Nandi, G. B. Ellison, D. E. David, J. T. McKinnon, T. G. Lindeman, D. C. Dayton, and M. R. Nimlos, Rev. Sci. Instrum. **74**, 3077 (2003).

[41] E. B. Jochnowitz, X. Zhang, M. R. Nimlos, M. E. Varner, J. F. Stanton, and G. B. Ellison, J. Phys. Chem. A **109**, 3812 (2004).

[42] O. L. Chapman, K. Mattes, C. L. McIntosh, J. Pacansky, G. V. Calder, and G. Orr, J. Am. Chem. Soc. **95**, 6134 (1973).

[43] A. L. Brown, D. C. Dayton, M. R. Nimlos, and J. W. Daily, Chemosphere **42**, 663 (2001).

[44] S. Nandi, P. A. Arnold, B. K. Carpenter, M. R. Nimlos, D. C. Dayton, and G. B. Ellison, J. Phys. Chem. A **105**, 7514 (2001).

[45] X. Zhang, V. M. Bierbaum, G. B. Ellison, and S. Kato, J. Chem. Phys. **120**, 3531 (2004).

[46] X. Zhang, S. Kato, V. M. Bierbaum, M. R. Nimlos, and G. B. Ellison, J. Phys. Chem. A **108**, 9733 (2004).

[47] T. H. Dunning, Jr., J. Chem. Phys. **90**, 1007 (1989).

[48] A. K. Wilson, T. van Mourik, and T. H. Dunning, Jr., J. Mol. Struct. - Theochem **388**, 339 (1996).

[49] E. C. C. E. B. S. Database, (2006).

[50] D. E. Woon and T. H. Dunning, Jr., J. Chem. Phys. **103**, 4572 (1995).

[51] C. C. J. Roothaan, Reviews of Modern Physics **23**, 69 (1951).

[52] W. J. Hehre, L. Radom, P. v. R. Schleyer, and J. A. Pople, *Ab Initio Molecular Orbital Theory*. (Wiley-Interscience, New York, 1986).

[53] J. A. Pople and R. K. Nesbet, J. Chem. Phys. **22**, 571 (1954).

[54] A. Szabo and N. S. Ostlund, *Modern Quantum Chemistry: Introduction to Advanced Electronic Structure Theory*, 1st edition, revised ed. (McGraw-Hill, New York, 1989).

[55] B. O. Roos, in *Ab Initio Methods in Quantum Chemistry, Part II*, edited by K. P. Lawley (Wiley & Sons, New York, 1987), pp. 399.

[56] D. Cremer, in *The Encyclopedia of Computational Chemistry*, edited by P. v. R. Schleyer, N. L. Allinger, T. Clark, J. Gasteiger, P. A. Kollmann, H. F. Schaefer III, and P. R. Schreiner (Wiley, Chichester, 1998), Vol. 3, pp. 1706.

[57] T. Helgaker, P. Jørgensen, and J. Olsen, *Molecular Electronic-Structure Theory*. (John Wiley & Sons, Chichester, 2000).

[58] J. A. Pople, J. S. Binkley, and R. Seeger, Int. J. Quantum Chem. **10**, 1 (1976).

[59] R. J. Bartlett, Annu. Rev. Phys. Chem. **32**, 359 (1981).

[60] G. D. Purvis III and R. J. Bartlett, J. Chem. Phys. **76**, 1910 (1982).

[61] J. Paldus, in *New Horizons of Quantum Chemistry*, edited by P.-O. Löwdin and B. Pullmann (Reidel, Dordrecht, 1983), pp. 31.

[62] R. J. Bartlett, C. E. Dykstra, and J. Paldus, in *Advanced Theories and Computational Approaches to the Electronic Structure of Molecules*, edited by C. E. Dykstra (Reidel, Dordrecht, 1984), pp. 127.

[63] G. E. Scuseria, A. C. Scheiner, T. J. Lee, J. E. Rice, and H. F. Schaefer, J. Chem. Phys. **86**, 2881 (1987).

[64] J. Gauss, in *The Encyclopedia of Computational Chemistry*, edited by P. v. R. Schleyer, N. L. Allinger, T. Clark, J. Gasteiger, P. A. Kollmann, H. F. Schaefer III, and P. R. Schreiner (Wiley, Chichester, 1998), Vol. 1, pp. 615.

[65] K. Raghavachari, G. W. Trucks, J. A. Pople, and M. Head-Gordon, Chem. Phys. Lett. **157**, 479 (1989).

[66] G. E. Scuseria and T. J. Lee, J. Chem. Phys. **93**, 5851 (1990).

[67] J. Noga and R. J. Bartlett, J. Chem. Phys. **86**, 7041 (1987).

[68] J. Noga and R. J. Bartlett, J. Chem. Phys. **89**, 3401 (1988).

[69] G. E. Scuseria and H. F. Schaefer III, Chem. Phys. Lett. **152**, 382 (1988).

[70] Y. J. Bomble, J. F. Stanton, M. Kallay, and J. Gauss, J. Chem. Phys. **123** (2005).

[71] A. G. Császár, A. D. W D Allen, and H. F. Schaefer III, J. Chem. Phys. **108**, 9751 (1998).

[72] A. L. L. East and W. D. Allen, J. Chem. Phys. **99**, 4638 (1993).

[73] A. G. Császár, G. Tarczay, M. L. Leininger, O. L. Polyansky, J. Tennyson, and W. D. Allen, in *Spectroscopy from Space*, edited by J. Demaison and K. Sarka (Kluwer, Dordrecht, 2001), pp. 317.

[74] J. M. Gonzales, C. Pak, R. S. Cox, W. D. Allen, H. F. Schaefer, A. G. Csaszar, and G. Tarczay, Chemistry-A European Journal **9**, 2173 (2003).

[75] M. S. Schuurman, S. R. Muir, W. D. Allen, and H. F. Schaefer III, J. Chem. Phys. **120**, 11586 (2004).

[76] D. Feller, J. Chem. Phys. **98**, 7059 (1993).

[77] T. Helgaker, W. Klopper, H. Koch, and J. Noga, J. Chem. Phys. **106**, 9639 (1997).

[78] Y. Yamaguchi, Y. Osamura, J. D. Goddard, and H. F. Schaefer III, *A New Dimension to Quantum Chemistry: Analytic Derivative Methods in Ab Initio Molecular Electronic Structure Theory*. (Oxford Univ. Press, New York, 1994).

[79] J. Gauss, W. J. Lauderdale, J. F. Stanton, J. D. Watts, and R. J. Bartlett, Chem. Phys. Lett. **182**, 207 (1991).

[80] J. D. Watts, J. Gauss, and R. J. Bartlett, J. Chem. Phys. **98**, 8718 (1993).

[81] N. C. Handy, R. D. Amos, J. F. Gaw, J. E. Rice, and E. D. Simandiras, Chem. Phys. Lett. **120**, 151 (1985).

[82] E. D. Simandiras, N. C. Handy, and R. D. Amos, Chem. Phys. Lett. **133**, 324 (1987).

[83] J. Gauss and J. F. Stanton, Chem. Phys. Lett. **276**, 70 (1997).

[84] J. D. Watts, J. Gauss, and R. J. Bartlett, Chem. Phys. Lett. **200**, 1 (1992).

[85] T. J. Lee and A. P. Rendell, J. Chem. Phys. **94**, 6229 (1991).

[86] J. F. Stanton, J. Gauss, J. D. Watts, W. J. Lauderdale, and R. J. Bartlett, Int. J. Quantum Chem. **26S**, 879 (1992).

[87] H.-J. Werner, P. J. Knowles, M. Schütz, R. D. Amos, A. Bernhardsson, A. Berning, P. Celani, D. L. Cooper, M. J. O. Deegan, A. J. Dobbyn, F. Eckert, C. Hampel, G. Hetzer, T. Korona, R. Lindh, A. W. Lloyd, S. J. McNicholas, F. R. Manby, W. Meyer, M. E.

Mura, A. Nicklass, P. Palmieri, R. Pitzer, G. Rauhut, U. Schumann, H. Stoll, A. J. Stone, R. Tarroni, and T. Thorsteinsson, MOLPRO (2002).

[88] E. Aprà, T. L. Windus, T. P. Straatsma, E. J. Bylaska, W. de Jong, S. Hirata, M. Valiev, M. Hackler, L. Pollack, K. Kowalski, R. Harrison, M. Dupuis, D. M. A. Smith, J. Nieplocha, V. Tipparaju, M. Krishnan, A. A. Auer, E. Brown, G. Cisneros, G. Fann, H. Fruchtl, J. Garza, K. Hirao, R. Kendall, J. Nichols, K. Tsemekhman, K. Wolinski, J. Anchell, D. Bernholdt, P. Borowski, T. Clark, D. Clerc, H. Dachel, M. Deegan, K. Dyall, D. Elwood, E. Glendening, M. Gutowski, A. Hess, J. Jaffe, B. Johnson, J. Ju, R. Kobayashi, R. Kutteh, Z. Lin, R. Littlefield, X. Long, B. Meng, T. Nakajima, S. Niu, M. Rosing, G. Sandrone, M. Stave, H. Taylor, G. Thomas, J. van Lenthe, A. Wong, Z. Zhang, M. A. list, H.-J. Werner, P. J. Knowles, M. Schütz, R. D. Amos, A. Bernhardsson, A. Berning, P. Celani, D. L. Cooper, M. J. O. Deegan, A. J. Dobbyn, F. Eckert, C. Hampel, G. Hetzer, T. Korona, R. Lindh, A. W. Lloyd, S. J. McNicholas, F. R. Manby, W. Meyer, M. E. Mura, A. Nicklass, P. Palmieri, R. Pitzer, G. Rauhut, U. Schumann, H. Stoll, A. J. Stone, R. Tarroni, and T. Thorsteinsson, NWChem, A Computational Chemistry Package for Parallel Computers (Pacific Northwest National Laboratory, Richland, Washington 99352-0999, USA., 2005).

[89] R. A. Kendall, E. Apra, D. E. Bernholdt, E. J. Bylaska, M. Dupuis, G. I. Fann, R. J. Harrison, J. Ju, J. A. Nichols, J. Nieplocha, T. P. Straatsma, T. L. Windus, and A. T. Wong, Comput. Phys. Comm. **128**, 260 (2000).

[90] M. Kállay and J. Gauss, J. Chem. Phys. **123**, 214105 (2005).

[91] S. G. Lias, J. E. Bartmess, J. F. Liebman, J. L. Holmes, R. D. Levin, and W. G. Mallard, J. Phys. Chem. Ref. Data **17 (supplement 1)**, 1 (1988).

[92] K.-C. Lau and C.-Y. Ng, Acc. Chem. Res., (submitted) (2006).

[93] B. Ruscic, A. F. Wagner, L. B. Harding, R. L. Asher, D. Feller, D. A. Dixon, K. A. Peterson, Y. Song, X. M. Qian, C. Y. Ng, J. B. Liu, and W. W. Chen, J. Phys. Chem. A **106**, 2727 (2002).

[94] B. Ruscic, J. E. Boggs, A. Burcat, A. G. Csaszar, J. Demaison, R. Janoschek, J. M. L. Martin, M. L. Morton, M. J. Rossi, J. F. Stanton, P. G. Szalay, P. R. Westmoreland, F. Zabel, and T. Berces, J. Phys. Chem. Ref. Data **34**, 573 (2005).

[95] Y. Shi and K. M. Ervin, Chem. Phys. Lett. **318**, 149 (2000).

[96] C. E. Moore, *Atomic Energy Levels*. (Nat. Bur. Stand., Washington, DC 20402, 1971).

[97] W. T. Borden, R. J. Loncharich, and K. N. Houk, Annu. Rev. Phys. Chem. **39**, 213 (1988).

[98] K. N. Houk, R. J. Loncharich, J. F. Blake, and W. L. Jorgensen, J. Am. Chem. Soc. **111**, 9172 (1989).

[99] K. N. Houk, Y. Li, and J. D. Evanseck, Angewandte Chemie-International Edition In English **31**, 682 (1992).

[100] H. H. Wenk, M. Winkler, and W. Sander, Angewandte Chemie-International Edition **42**, 502 (2003).

[101] L. V. Gurvich, I. V. Veyts, C. B. Alcock, and V. S. Iorish, *Thermodynamic Properties of Individual Substances*, 4th ed. (Hemisphere, New York City, 1991).

[102] J. Gauss and J. F. Stanton, J. Phys. Chem. A **104**, 2865 (2000).

[103] A. C. Scheiner, H. F. Schaefer, and B. Liu, J. Am. Chem. Soc. **111**, 3118 (1989).

[104] T. J. Lee and P. R. Taylor, Int. J. Quantum Chem. **23**, 199 (1989).

[105] P. D. Jarowski, M. D. Wodrich, C. S. Wannere, P. v. R. Schleyer, and K. N. Houk, J. Am. Chem. Soc. **126**, 15036 (2004).

[106] M. Herman, A. Campargue, M. I. El Idrissi, and J. Vander Auwera, J. Phys. Chem. Ref. Data **32**, 921 (2003).

[107] K. L. Bak, J. Gauss, P. Jørgensen, J. Olsen, T. Helgaker, and J. F. Stanton, J. Chem. Phys. **114**, 6548 (2001).

[108] R. B. Woodward and R. Hoffmann, *The Conservation of Orbital Symmetry*. (Academic, New York, 1970).

[109] A. M. Mebel, K. Morokuma, and M. C. Lin, J. Chem. Phys. **103**, 3440 (1995).

[110] H. Wang, (2000).

[111] M. A. Temsamani and M. Herman, J. Chem. Phys. **102**, 6371 (1995).

[112] C. D. Sherrill, E. F. C. Byrd, and M. Head-Gordon, J. Chem. Phys. **113**, 1447 (2000).

[113] M. Allan, J. Chem. Phys. **80**, 6020 (1984).

[114] F. Vila, P. Borowski, and K. D. Jordan, J. Phys. Chem. A **104**, 9009 (2000).

[115] K. M. Pamidimukkala, R. D. Kern, M. R. Patel, H. C. Wei, and J. H. Kiefer, J. Phys. Chem. **91**, 2148 (1987).

[116] B. Ruscic, R. E. Pinzon, M. L. Morton, G. von Laszevski, S. J. Bittner, S. G. Nijsure, K. A. Amin, M. Minkoff, and A. F. Wagner, J. Phys. Chem. A **108**, 9979 (2004).

[117] B. Ruscic, R. E. Pinzon, G. von Laszewski, D. Kodeboyina, A. Burcat, D. Leahy, D. Montoya, and A. F. Wagner, J. Phys. Conf. Ser. **16**, 561 (2005).

[118] B. Ruscic, in *McGraw-Hill Encyclopedia of Science and Technology* (McGraw-Hill, New York, 2004), pp. 3.

[119] B. Ruscic, R. E. Pinzon, M. L. Morton, N. K. Srinivasan, M. C. Su, J. W. Sutherland, and J. V. Michael, J. Phys. Chem. A **110**, 6592 (2006).

[120] B. Ruscic, M. Litorja, and R. L. Asher, J. Phys. Chem. A **103**, 8625 (1999).

[121] M. Litorja and B. Ruscic, J. Chem. Phys. **107**, 9852 (1997).

[122] J. A. Blush, P. Chen, R. T. Wiedmann, and M. G. White, J. Chem. Phys. **98**, 3557 (1993).

[123] G. Herzberg, Proc. R. Soc. London Ser. A **262**, 291 (1961).

[124] F. D. Rossini, J. Res. Nat. Bur. Stand. **6**, 37 (1931).

[125] F. D. Rossini, J. Res. Nat. Bur. Stand. **7**, 329 (1931).

[126] W. A. Roth and H. Banse, Arch. Eisenhuttenw. **6**, 43 (1932).

[127] F. D. Rossini, Chem. Rev. **27**, 1 (1940).

[128] D. A. Pittam and G. Pilcher, Journal Of The Chemical Society-Faraday Transactions I **68**, 2224 (1972).

[129] A. Dale, C. Lythall, J. Aucott, and C. Sayer, Thermochimica Acta **382**, 47 (2002).

[130] Y. I. Alexsandrov, E. N. Korchagina, and A. G. Chunovkina, Measurement Techniques **45**, 268 (2002).

[131] Y. I. Alexandrov, Thermochimica Acta **382**, 55 (2002).

[132] E. J. Prosen, R. Gilmont, and F. D. Rossini, J. Res. Natl. Bur. Stand. **34**, 65 (1945).

[133] W. H. Johnson, E. J. Prosen, and F. D. Rossini, J. Res. Natl. Bur. Stand. **39**, 49 (1947).

[134] W. D. Good and N. K. Smith, J. Chem. Eng. Data **14**, 102 (1969).

[135] J. Coops, D. Mulder, J. W. Dienske, and J. Smittenberg, Rev. Trav. Chim. **65**, 128 (1946).

[136] V. Majer and V. Svoboda, *Enthalpies of Vaporization of Organic Compounds: A Critical Review and Data Compilation*. (Blackwell, Oxford, 1985).

[137] N. S. Osborne and D. C. Ginnings, J. Res. Natl. Bur. Stand. **39**, 453 (1947).

[138] N. L. Yarym-Agaev, N. N. Feodosev, and K. G. Skorikov, Zh Oxford. Fiz. Khim. **24**, 1061 (1950).

[139] R. J. L. Andon, J. D. Cox, E. F. G. Herington, and J. F. Martin, Trans. Faraday Soc. **53**, 1074 (1957).

[140] D. W. Scott, G. B. Guthrie, J. F. Messerly, S. S. Todd, W. T. Berg, I. A. Hossenlopp, and J. P. McCullough, J. Phys. Chem. **66**, 911 (1962).

[141] J. D. Cox, D. D. Wagman, and V. A. Medvedev, *CODATA Key Values for Thermodynamics*. (Hemisphere, New York City, 1989).

[142] L. V. Gurvich, I. V. Veyts, and C. B. Alcock, *Thermodynamic Properties of Individual Substances*, 4th Ed. ed. (Hemisphere, New York City, 1989).

[143] M. W. Chase, C. A. Davies, J. R. Downey Jr., D. J. Frurip, R. A. McDonald, and A. N. Syverud, J. Phys. Chem. Ref. Data **14**, Suppl. 1 (1985).

[144] M. W. Chase, C. A. Davies, J. R. Downey Jr., D. J. Frurip, R. A. McDonald, and A. N. Syverud, *JANAF Thermochemical Tables*. (1998).

[145] B. J. McBride and S. Gordon, Properties and Coefficients: Computer Program for Calculating and Fitting Thermodynamic Functions (NASA, 1999).

[146] A. P. Hitchcock and J. D. Laposa, J. Mol. Spectrosc. **54**, 223 (1975).

[147] M. E. Jacox, J. Phys. Chem. Ref. Data **32**, 1 (2003).

[148] M. E. Jacox, *Vibrational and Electronic Energy Levels of Polyatomic Transient Molecules*. (J. Phys. Chem. Ref. Data, 1994).

[149] S. J. Klippenstein, L. B. Harding, and Y. Georgievskii, Proc. Combust. Inst. **(submitted)** (2006).

[150] T. L. Conner, W. A. Lonneman, and R. L. Seila, J. Air Waste Manage. Assoc. **45**, 383 (1995).

APPENDIX B

SUPPLEMENTARY MATERIAL FOR CHAPTER 2

Table B1 Quadratic force constants F_{ij} and harmonic vibrational frequencies (cm^{-1}) for NCCO at the CCSD(T)/cc-pCVQZ optimized geometry.[a]

ij	RHF	CCSD	CCSD(T)
11	18.6825	17.8153	17.5194
21	0.2774	0.3090	0.3414
22	5.3237	4.7026	4.5342
31	0.0330	0.0003	–0.03879
32	1.0091	1.0281	1.0639
33	15.4463	15.1300	14.9111
41	0.1661	0.1826	0.1904
42	0.0896	0.0956	0.0982
43	–0.05963	–0.08911	–0.09566
44	0.3982	0.3237	0.3058
51	–0.11208	–0.18819	–0.20712
52	0.5181	0.5929	0.6044
53	0.3142	0.3636	0.3795
54	0.1417	0.1357	0.1372
55	0.8958	0.7269	0.6987
66	0.2646	0.2021	0.1833
$\omega_1(a')$	2304	2238	2214
$\omega_2(a')$	1962	1936	1919
$\omega_3(a')$	917	837	818
$\omega_4(a')$	641	597	588
$\omega_5(a')$	267	232	222
$\omega_6(a'')$	323	282	269

[a] All electrons correlated, within a cc-pCVQZ basis set. The internal coordinates are defined in the text. For a description of computing force constants at a non-stationary geometry, see W. D. Allen and A. G. Császár, J. Chem. Phys. **98,** 2983 (1993). F_{ij} units are consistent with energies in aJ, distances in Å, and angles in radians.

Table B2 Cubic force constants for NCCO[a]

ijk	RHF	CCSD	CCSD(T)	*ijk*	RHF	CCSD	CCSD(T)
111	–121.509	–119.099	–119.169	511	–0.4471	–0.5325	–0.5633
211	0.8586	0.5136	0.5489	521	0.85677	1.0232	1.0706
221	–2.8073	–2.7089	–2.9237	522	–1.889	–1.9829	–2.0165
222	–31.0505	–30.7563	–30.5399	531	0.3458	0.3786	0.3831
311	0.0306	0.0748	–0.0208	532	–1.1176	–1.1384	–1.1619
321	0.5634	0.5716	0.7103	533	–1.1002	–0.82083	–0.7494
322	0.8606	0.5964	0.2948	541	–0.07758	0.002	0.0126
331	–0.8252	–0.7993	–0.8752	542	0.06712	0.08512	0.09454
332	–3.5063	–3.5839	–3.5028	543	–0.34599	–0.35068	–0.35018
333	–106.22	–103.613	–103.502	544	0.03534	0.02979	0.03314
411	–0.07098	0.016	0.0163	551	–0.51654	–0.54586	–0.57699
421	–0.08046	–0.1805	–0.195	552	0.61071	0.60092	0.59496
422	–0.3643	–0.4169	–0.4533	553	–1.0222	–1.0229	–1.0399
431	–0.1495	–0.181	–0.1928	554	–0.13502	–0.1247	–0.12654
432	–0.2005	–0.1668	–0.1457	555	–1.32286	–1.1362	–1.1125
433	0.3879	0.5249	0.53287	661	–0.76766	–0.69174	–0.69799
441	–0.71401	–0.76227	–0.77451	662	–0.2459	–0.32358	–0.35339
442	–0.59429	–0.58928	–0.60613	663	0.1227	0.2205	0.2423
443	0.00928	0.08231	0.09888	664	–0.12843	–0.1355	–0.13751
444	–0.36241	–0.33898	–0.33483	665	–0.07074	–0.0765	–0.08057

[a] All electrons correlated, within a cc-pCVQZ basis set. The internal coordinates are defined in the text. Units are consistent with energies in aJ, distances in Å, and angles in radians

Table B3 Quartic force constants (cm^{-1}) for NCCO[a]

ijkl	RHF	CCSD	CCSD(T)	*ijkl*	RHF	CCSD	CCSD(T)
1111	632.46	642.32	642.95	5333	1.48	1.92	2.03
2111	6.21	0.65	1.19	5311	1.27	0.932	0.856
2211	–9.09	–3.32	–4.36	5411	0.383	0.43	0.374
2221	13.12	9.23	9.99	5421	–0.23	0.16	1.04
2222	135.39	135.29	135.84	5422	–0.661	–0.763	–0.888
3111	0.48	0.95	0.49	5431	–0.317	0.463	0.655
3211	–0.48	–0.27	–0.33	5432	–0.14	0.536	0.735
3221	–0.55	–1.58	–2.91	5433	1.13	0.951	0.839
3222	7.47	8.72	8.69	5441	0.073	–0.169	–0.194
3311	–1.21	–1.5	–1.76	5442	–0.229	–0.21	–0.218
3321	0.17	1.26	0.84	5443	–0.138	–0.195	–0.228
3322	–7.28	–6.47	–6.19	5444	–0.062	0.13	0.165
3331	2.58	3.44	3.33	5511	–2.35	–1.74	–1.73
3332	12.65	10.82	9.95	5521	3.016	2.69	2.28
3333	584.16	589.15	592.17	5522	–3.883	–2.72	–2.529
4111	–0.43	0.748	0.621	5531	1.26	1.32	1.32
4211	0.48	–0.19	–0.607	5532	–0.9	–0.869	–0.849
4221	–0.508	–0.572	–1.03	5533	0.8	0.738	0.672
4222	1.51	1.47	1.52	5541	0.336	0.14	0.067
4311	–0.38	–0.524	–0.5	5542	0.717	0.822	0.863
4321	0.36	1.3	2.63	5543	0.086	0.061	0.08
4322	0.875	0.749	0.766	5544	0.464	0.273	0.234
4331	0.692	0.39	0.29	5551	–0.964	–0.756	–0.7
4332	0.511	–0.05	–0.15	5552	3.124	2.62	2.495
4333	–2.94	–2.4	–2.17	5553	1.988	1.959	1.961
4411	0.619	–0.027	–0.031	5554	–0.299	–0.555	–0.583
4421	–0.21	0.328	0.089	5555	–1.068	–0.9994	–0.8904
4422	0.942	0.518	0.45	6611	–0.639	0.34	0.335
4431	0.073	–0.027	–0.009	6621	0.394	0.428	0.16
4432	0.716	0.381	0.24	6622	–0.11	0.12	0.271
4433	–0.869	–1.05	–1.03	6631	–0.091	0.11	0.078
4441	0.741	0.786	0.764	6632	0.595	0.418	0.342
4442	0.544	0.596	0.631	6633	–1.12	–1.33	–1.29
4443	0.11	0.154	0.183	6641	0.248	0.129	0.09
4444	2.12	1.928	1.869	6642	0.222	0.165	0.15
5111	–2.51	–1.38	–1.23	6643	0.11	0.039	–0.01
5211	2.89	2.69	2.39	6644	0.505	0.432	0.37
5221	–4.97	–4.32	–4.65	6651	–0.12	–0.153	–0.256
5222	3.83	2.01	1.58	6652	–0.055	–0.12	–0.171
5311	1.27	0.932	0.856	6653	0.144	0.19	0.187
5321	–1.83	–2.21	–1.26	6654	–0.149	–0.148	–0.182
5322	3.22	3.03	3.06	6655	–0.036	–0.013	0.012
5331	–1.41	–1.35	–1.25	6666	1.195	1.263	1.156
5332	2.68	2.96	2.98				

[a] All electrons correlated, within a cc-pCVQZ basis set. The internal coordinates are defined in the text. Units are consistent with energies in aJ, distances in Å, and angles in radians

APPENDIX C

SUPPLEMENTARY MATERIAL FOR CHAPTER 3

Table C1. Quadratic force constants F_{ij} for acetylene at the CCSD(T)/cc-pCVQZ level of theory. Units are consistent with energies in aJ, distances in Å, and angles in radians.

i,j	F_{ij}	*i,j*	F_{ij}	*i,j*	F_{ij}
1,1	6.389078	3,3	6.392357	6,6	0.149945
2,1	-0.151675	4,4	0.345403	7,7	0.149945
2,2	16.397263	5,5	0.345403		

Table C2. Cubic force constants F_{ijk} for acetylene at the CCSD(T)/cc-pCVQZ level of theory. Units are consistent with energies in aJ, distances in Å, and angles in radians.

i,j,k	F_{ijk}	*i,j,k*	F_{ijk}	*i,j,k*	F_{ijk}
1,1,1	-25.5761	4,4,1	-0.1267	6,6,1	-0.1303
2,1,1	0.3057	4,4,2	-0.5544	6,6,2	-1.0650
2,2,1	-0.1207	5,5,1	-0.1267	7,5,3	-0.0824
2,2,2	-95.9539	5,5,2	-0.5544	7,7,1	-0.1303
3,3,1	-25.5593	6,4,3	-0.0824	7,7,2	-1.0650
3,3,2	0.3437				

Table C3. Quartic force constants F_{ijkl} for acetylene at the CCSD(T)/cc-pCVQZ level of theory. Units are consistent with energies in aJ, distances in Å, and angles in radians.

i,j,k,l	F_{ijkl}	*i,j,k,l*	F_{ijkl}	*i,j,k,l*	F_{ijkl}
1,1,1,1	92.95	5,5,1,1	-0.04	6,6,5,5	0.07
2,1,1,1	-1.22	5,5,2,1	0.14	6,6,6,6	1.42
2,2,1,1	-1.29	5,5,2,2	0.30	7,5,3,1	0.00
2,2,2,1	-0.13	5,5,3,3	-0.08	7,5,3,2	0.15
2,2,2,2	472.54	5,5,4,4	-0.04	7,6,5,4	0.02
3,3,1,1	92.86	5,5,5,5	-0.13	7,7,1,1	0.02
3,3,2,1	-1.19	6,4,3,1	0.00	7,7,2,1	0.04
3,3,2,2	-1.33	6,4,3,2	0.15	7,7,2,2	0.09
3,3,3,3	92.97	6,6,1,1	0.02	7,7,3,3	0.10
4,4,1,1	-0.04	6,6,2,1	0.04	7,7,4,4	0.07
4,4,2,1	0.14	6,6,2,2	0.09	7,7,5,5	0.10
4,4,2,2	0.30	6,6,3,3	0.10	7,7,6,6	0.47
4,4,3,3	-0.08	6,6,4,4	0.10	7,7,7,7	1.42
4,4,4,4	-0.13				

Table C4. Quadratic force constants F_{ij} for diacetylene at the CCSD(T)/cc-pCVQZ level of theory. Units are consistent with energies in aJ, distances in Å, and angles in radians.

i,j	F_{ij}	*i,j*	F_{ij}	*i,j*	F_{ij}
1,1	6.399100	5,4	-0.103599	9,9	0.338624
2,1	-0.107820	5,5	16.104565	10,10	0.228315
2,2	15.524410	6,6	0.219276	11,11	0.228315
3,1	-0.005995	7,7	0.219276	12,10	0.113412
3,2	0.827502	8,6	0.087274	12,12	0.339623
3,3	7.257167	8,8	0.338624	13,11	0.113412
4,4	6.397115	9,7	0.087274	13,13	0.339623

Table C5. Cubic force constants F_{ijk} for diacetylene at the CCSD(T)/cc-pCVQZ level of theory. Units are consistent with energies in aJ, distances in Å, and angles in radians.

i,j,k	F_{ijk}	*i,j,k*	F_{ijk}	*i,j,k*	F_{ijk}
1,1,1	-25.6137	7,7,3	0.0737	11,11,1	-0.1110
2,1,1	0.2286	8,6,1	0.0064	11,11,2	-0.6134
2,2,1	-0.0618	8,6,2	0.1853	11,11,3	0.0968
2,2,2	-66.5411	8,6,3	0.0289	12,6,4	0.0020
3,1,1	0.0283	8,8,1	-0.0176	12,6,5	0.2523
3,2,1	-0.0414	8,8,2	-0.4039	12,8,4	-0.0323
3,2,2	1.2888	8,8,3	-0.4872	12,8,5	-0.6216
3,3,1	0.0009	9,7,1	0.0064	12,10,1	0.0008
3,3,2	-3.5349	9,7,2	0.1853	12,10,2	0.1828
3,3,3	-38.7514	9,7,3	0.0289	12,10,3	0.0117
4,4,1	-25.5974	9,9,1	-0.0176	12,12,1	-0.0262
4,4,2	0.2236	9,9,2	-0.4039	12,12,2	-0.7504
4,4,3	0.0314	9,9,3	-0.4872	12,12,3	-0.4575
5,4,1	0.2216	10,6,4	-0.1053	13,7,4	0.0020
5,4,2	-0.0545	10,6,5	-0.5726	13,7,5	0.2523
5,4,3	-0.0004	10,8,4	0.0009	13,9,4	-0.0323
5,5,1	-0.0443	10,8,5	0.1485	13,9,5	-0.6216
5,5,2	-65.4588	10,10,1	-0.1110	13,11,1	0.0008
5,5,3	-1.3564	10,10,2	-0.6134	13,11,2	0.1828
6,6,1	-0.1135	10,10,3	0.0968	13,11,3	0.0117
6,6,2	-0.6584	11,7,4	-0.1053	13,13,1	-0.0262
6,6,3	0.0737	11,7,5	-0.5726	13,13,2	-0.7504
7,7,1	-0.1135	11,9,4	0.0009	13,13,3	-0.4575
7,7,2	-0.6584	11,9,5	0.1485		

Table C6. Quartic force constants F_{ijkl} for diacetylene at the CCSD(T)/cc-pCVQZ level of theory. Units are consistent with energies in aJ, distances in Å, and angles in radians.

i,j,k,l	F_{ijkl}	*i,j,k,l*	F_{ijkl}	*i,j,k,l*	F_{ijkl}
1,1,1,1	92.12	7,7,2,1	0.13	9,9,2,2	0.19
2,1,1,1	-0.60	7,7,2,2	-0.20	9,9,3,1	0.59
2,2,1,1	0.22	7,7,3,1	0.66	9,9,3,2	0.11
2,2,2,1	-0.95	7,7,3,2	0.72	9,9,3,3	1.97
2,2,2,2	228.76	7,7,3,3	0.64	9,9,4,4	0.16
3,1,1,1	-2.69	7,7,4,4	-0.02	9,9,5,4	0.05
3,2,1,1	2.61	7,7,5,4	-0.01	9,9,5,5	0.09
3,2,2,1	2.47	7,7,5,5	0.00	9,9,6,6	0.04
3,2,2,2	-1.93	7,7,6,6	0.06	9,9,7,7	0.06
3,3,1,1	4.86	7,7,7,7	0.18	9,9,8,6	-0.03
3,3,2,1	2.42	8,6,1,1	0.11	9,9,8,8	0.12
3,3,2,2	-2.15	8,6,2,1	-0.55	9,9,9,7	-0.08
3,3,3,1	-4.80	8,6,2,2	0.13	9,9,9,9	0.37
3,3,3,2	6.83	8,6,3,1	-3.51	10,6,4,1	-14.06
3,3,3,3	193.06	8,6,3,2	-2.86	10,6,4,2	0.14
4,4,1,1	93.69	8,6,3,3	0.40	10,6,4,3	-3.31
4,4,2,1	-0.43	8,6,4,4	-0.02	10,6,5,1	0.72
4,4,2,2	-0.45	8,6,5,4	-0.24	10,6,5,2	1.20
4,4,3,1	2.62	8,6,5,5	-0.09	10,6,5,3	5.58
4,4,3,2	13.38	8,6,6,6	-0.16	10,8,4,1	-14.05
4,4,3,3	4.42	8,7,7,6	-0.05	10,8,4,2	-0.18
4,4,4,4	93.15	8,8,1,1	0.16	10,8,4,3	-3.30
5,4,1,1	-0.59	8,8,2,1	0.07	10,8,5,1	-1.71
5,4,2,1	-3.92	8,8,2,2	0.19	10,8,5,2	-1.28
5,4,2,2	-0.22	8,8,3,1	0.59	10,8,5,3	3.43
5,4,3,1	-18.15	8,8,3,2	0.11	10,10,1,1	0.17
5,4,3,2	-26.45	8,8,3,3	1.97	10,10,2,1	0.19
5,4,3,3	1.94	8,8,4,4	0.16	10,10,2,2	0.03
5,4,4,4	-0.79	8,8,5,4	0.05	10,10,3,1	-0.77
5,5,1,1	0.06	8,8,5,5	0.09	10,10,3,2	-0.07
5,5,2,1	1.13	8,8,6,6	0.06	10,10,3,3	-3.59
5,5,2,2	230.30	8,8,7,7	0.04	10,10,4,4	-0.21
5,5,3,1	3.15	8,8,8,6	-0.08	10,10,5,4	-0.33
5,5,3,2	-0.05	8,8,8,8	0.37	10,10,5,5	-0.48
5,5,3,3	7.08	9,7,1,1	0.11	10,10,6,6	0.12
5,5,4,4	-0.84	9,7,2,1	-0.55	10,10,7,7	0.08
5,5,5,4	0.42	9,7,2,2	0.13	10,10,8,6	-0.12
5,5,5,5	227.15	9,7,3,1	-3.51	10,10,8,8	0.03
6,6,1,1	0.16	9,7,3,2	-2.86	10,10,9,7	-0.06
6,6,2,1	0.13	9,7,3,3	0.40	10,10,9,9	0.02
6,6,2,2	-0.20	9,7,4,4	-0.02	10,10,10,10	0.24
6,6,3,1	0.66	9,7,5,4	-0.24	11,7,4,1	-14.06
6,6,3,2	0.72	9,7,5,5	-0.09	11,7,4,2	0.14
6,6,3,3	0.64	9,7,6,6	-0.05	11,7,4,3	-3.31
6,6,4,4	-0.02	9,7,7,7	-0.16	11,7,5,1	0.72
6,6,5,4	-0.01	9,8,7,6	0.01	11,7,5,2	1.20
6,6,5,5	0.00	9,8,8,7	-0.03	11,7,5,3	5.58
6,6,6,6	0.18	9,9,1,1	0.16	11,9,4,1	-14.05
7,7,1,1	0.16	9,9,2,1	0.07	11,9,4,2	-0.18

Table C6 (continued). Quartic force constants F_{ijkl} for diacetylene at the CCSD(T)/cc-pCVQZ level of theory. Units are consistent with energies in aJ, distances in Å, and angles in radians.

i,j,k,l	F_{ijkl}	*i,j,k,l*	F_{ijkl}	*i,j,k,l*	F_{ijkl}
11,9,4,3	-3.30	12,10,6,6	-0.13	13,10,9,8	-0.03
11,9,5,1	-1.71	12,10,7,7	-0.07	13,11,1,1	0.27
11,9,5,2	-1.28	12,10,8,6	-0.82	13,11,2,1	-0.92
11,9,5,3	3.43	12,10,8,8	-0.12	13,11,2,2	0.01
11,10,7,6	0.02	12,10,9,7	-0.27	13,11,3,1	3.01
11,10,8,7	-0.03	12,10,9,9	-0.06	13,11,3,2	2.89
11,10,9,6	-0.03	12,10,10,10	-0.19	13,11,3,3	-1.68
11,10,9,8	0.00	12,11,7,6	-0.03	13,11,4,4	-0.19
11,11,1,1	0.17	12,11,8,7	-0.27	13,11,5,4	1.41
11,11,2,1	0.19	12,11,9,6	-0.27	13,11,5,5	-0.03
11,11,2,2	0.03	12,11,9,8	-0.03	13,11,6,6	-0.07
11,11,3,1	-0.77	12,11,11,10	-0.06	13,11,7,7	-0.13
11,11,3,2	-0.07	12,12,1,1	0.17	13,11,8,6	-0.27
11,11,3,3	-3.59	12,12,2,1	0.10	13,11,8,8	-0.06
11,11,4,4	-0.21	12,12,2,2	0.56	13,11,9,7	-0.82
11,11,5,4	-0.33	12,12,3,1	0.63	13,11,9,9	-0.12
11,11,5,5	-0.48	12,12,3,2	0.33	13,11,10,10	-0.06
11,11,6,6	0.08	12,12,3,3	1.80	13,11,11,11	-0.19
11,11,7,7	0.12	12,12,4,4	-0.03	13,12,7,6	0.00
11,11,8,6	-0.06	12,12,5,4	-0.09	13,12,8,7	-0.04
11,11,8,8	0.02	12,12,5,5	-0.16	13,12,9,6	-0.04
11,11,9,7	-0.12	12,12,6,6	0.03	13,12,9,8	0.02
11,11,9,9	0.03	12,12,7,7	0.02	13,12,11,10	0.01
11,11,10,10	0.08	12,12,8,6	-0.14	13,12,12,11	-0.06
11,11,11,11	0.24	12,12,8,8	0.09	13,13,1,1	0.17
12,6,4,1	-3.91	12,12,9,7	-0.07	13,13,2,1	0.10
12,6,4,2	-0.12	12,12,9,9	0.06	13,13,2,2	0.56
12,6,4,3	-2.99	12,12,10,10	0.08	13,13,3,1	0.63
12,6,5,1	-3.56	12,12,11,11	0.05	13,13,3,2	0.33
12,6,5,2	-0.03	12,12,12,10	-0.19	13,13,3,3	1.80
12,6,5,3	-2.45	12,12,12,12	0.55	13,13,4,4	-0.03
12,8,4,1	-1.18	13,7,4,1	-3.91	13,13,5,4	-0.09
12,8,4,2	-0.80	13,7,4,2	-0.12	13,13,5,5	-0.16
12,8,4,3	-3.63	13,7,4,3	-2.99	13,13,6,6	0.02
12,8,5,1	-1.58	13,7,5,1	-3.56	13,13,7,7	0.03
12,8,5,2	-0.36	13,7,5,2	-0.03	13,13,8,6	-0.07
12,8,5,3	-2.98	13,7,5,3	-2.45	13,13,8,8	0.06
12,10,1,1	0.27	13,9,4,1	-1.18	13,13,9,7	-0.14
12,10,2,1	-0.92	13,9,4,2	-0.80	13,13,9,9	0.09
12,10,2,2	0.01	13,9,4,3	-3.63	13,13,10,10	0.05
12,10,3,1	3.01	13,9,5,1	-1.58	13,13,11,11	0.08
12,10,3,2	2.89	13,9,5,2	-0.36	13,13,12,10	-0.06
12,10,3,3	-1.68	13,9,5,3	-2.98	13,13,12,12	0.18
12,10,4,4	-0.19	13,10,7,6	-0.03	13,13,13,11	-0.19
12,10,5,4	1.41	13,10,8,7	-0.27	13,13,13,13	0.55
12,10,5,5	-0.03	13,10,9,6	-0.27		

Table C7. Changes in the fundamental frequencies (cm^{-1}), relative to the parent species, upon isotopic substitution for various isotopologs of diacetylene computed at the all electron CCSD(T) cc-pCVQZ level of theory using vibrational perturbation theory.[a]

	H–C≡C–C≡C–D	H–C≡^{13}C–C≡C–H	H–^{13}C≡C–C≡C–H
ν_1 (σ_g)	-25.8	-1.1	-15.2
ν_2 (σ_g)	-39.8	-26.3	-8.5
ν_3 (σ_g)	-15.1	-8.1	-8.2
ν_4 (σ_u)	-714.5	0.1	-0.4
ν_5 (σ_u)	-81.3	-23.6	-16.1
ν_6 (π_g)	-122.1	0.1	-1.3
ν_7 (π_g)	-11.1	-8.6	-0.7
ν_8 (π_u)	-10.3	-0.2	1.7
ν_9 (π_u)	-8.2	-2.1	-1.4

[a] The symmetry labels correspond to the unsubstituted molecule, with the ordering for other species determined by overlap of normal mode eigenvectors.

APPENDIX D

SUPPLEMENTARY MATERIAL FOR APPENDIX A

Table D1. Optimum geometric structures (Å) of acetylene and diacetylene at various levels of theory[a]

	Diacetylene			Acetylene	
	r_1	r_2	r_3	r_1	r_2
HF / cc-pVDZ	1.0637	1.1936	1.3920	1.0639	1.1918
HF / cc-pVTZ	1.0538	1.1822	1.3850	1.0540	1.1801
MP2 / cc-pVDZ	1.0762	1.2372	1.3842	1.0755	1.2297
MP2 / cc-pVTZ	1.0620	1.2194	1.3687	1.0615	1.2114
CCSD / cc-pVDZ	1.0777	1.2258	1.3984	1.0776	1.2228
CCSD / cc-pVTZ	1.0620	1.2067	1.3821	1.0620	1.2033
CCSD(T) / cc-pVDZ	1.0793	1.2336	1.3953	1.0790	1.2287
CCSD(T) / cc-pVTZ	1.0639	1.2150	1.3789	1.0637	1.2097
c~CCSD(T)-AE / cc-pCVQZ	1.0620	1.2093	1.3741	1.0620	1.2038
CCSD(T)-AE / cc-pCVQZ	1.0621	1.2091	1.3742	1.0621	1.2037

[a] See text figures for coordinate labels.

Table D2. CCSD(T)/cc-pVDZ vibrational frequencies along the retro-Diels-Alder fragmentation path of *o*-benzyne

mode	*o*-benzyne	transition state	products
$\omega_1(a_1)$	3220	3412	3500 (σ_g C_2H_2)
$\omega_2(a_1)$	3195	3369	3454 (σ_g C_4H_2)
$\omega_3(a_1)$	1881	1995	2215 (σ_g C_4H_2)
$\omega_4(a_1)$	1474	1742	1986 (σ_g C_2H_2)
$\omega_5(a_1)$	1324	1106	885 (σ_g C_4H_2)
$\omega_6(a_1)$	1147	832	734 (π_u C_2H_2)
$\omega_7(a_1)$	1054	686	584 (π_u C_4H_2)
$\omega_8(a_1)$	995	391	220 (π_u C_4H_2)
$\omega_9(a_1)$	599	615*i*	0
$\omega_{10}(a_2)$	925	595	598 (π_g C_4H_2)
$\omega_{11}(a_2)$	848	553	527 (π_g C_2H_2)
$\omega_{12}(a_2)$	551	447	453 (π_g C_4H_2)
$\omega_{13}(a_2)$	413	245	0
$\omega_{14}(b_1)$	896	650	734 (π_u C_2H_2)
$\omega_{15}(b_1)$	734	597	584 (π_u C_4H_2)
$\omega_{16}(b_1)$	379	218	220 (π_u C_4H_2)
$\omega_{17}(b_2)$	3217	3370	3455 (σ_u C_4H_2)
$\omega_{18}(b_2)$	3178	3353	3410 (σ_u C_2H_2)
$\omega_{19}(b_2)$	1494	1833	2034 (σ_u C_4H_2)
$\omega_{20}(b_2)$	1411	813	598 (π_g C_4H_2)
$\omega_{21}(b_2)$	1249	710	527 (π_g C_2H_2)
$\omega_{22}(b_2)$	1101	466	0
$\omega_{23}(b_2)$	840	414	453 (π_g C_4H_2)
$\omega_{24}(b_2)$	455	93*i*	0

Table D3. Optimum geometric structures (Å or deg) of *o*-benzyne at various levels o theory[a]

	r_1	r_2	r_3	r_4	r_5	r_6	θ_1	θ_2	θ_3	θ_4	θ_5
HF / cc-pVDZ	1.4119	1.3942	1.3866	1.2272	1.0833	1.0798	122.60	109.93	127.47	118.45	127.19
HF / cc-pVTZ	1.4075	1.3877	1.3807	1.2160	1.0744	1.0704	122.54	109.88	127.58	118.45	127.18
MP2 / cc-pVDZ	1.4197	1.4165	1.4008	1.2801	1.0965	1.0940	122.73	110.64	126.63	118.72	126.94
MP2 / cc-pVTZ	1.4071	1.4055	1.3866	1.2622	1.0828	1.0798	122.68	110.48	126.84	118.75	127.04
CCSD / cc-pVDZ	1.4221	1.4150	1.4019	1.2670	1.0968	1.0939	122.53	110.73	126.74	118.63	126.69
CCSD / cc-pVTZ	1.4092	1.4019	1.3871	1.2472	1.0819	1.0786	122.51	110.52	126.98	118.63	126.83
CCSD(T) / cc-pVDZ	1.4235	1.4218	1.4055	1.2800	1.0987	1.0959	122.48	111.06	126.46	118.75	126.48
CCSD(T) / cc-pVTZ	1.4106	1.4093	1.3906	1.2603	1.0840	1.0808	122.47	110.80	126.73	118.75	126.66
c~CCSD(T)-AE / cc-pCVQZ	1.4048	1.4035	1.3846	1.2539	1.0819	1.0788	122.46	110.78	126.76	118.77	126.72

[a] See figures in Appendix A for coordinate labels.

Table D4. Optimum geometric structures (Å or deg) of the (C_{2v}) retro-Diels Alder transition state for *o*-benzyne fragmentation at various levels of theory[a]

	r_1	r_2	r_3	r_4	r_5	r_6	θ_1	θ_2	θ_3	θ_4	θ_5
HF / cc-pVDZ	1.2342	2.1487	1.2346	1.3324	1.0679	1.0684	117.98	101.06	140.96	149.28	152.89
HF / cc-pVTZ	1.2246	2.1325	1.2241	1.3220	1.0583	1.0582	118.03	100.82	141.15	148.67	153.22
MP2 / cc-pVDZ	1.2640	2.2209	1.2718	1.3507	1.0797	1.0830	117.81	100.88	141.32	152.62	151.68
MP2 / cc-pVTZ	1.2475	2.2046	1.2538	1.3334	1.0655	1.0680	117.90	100.06	142.04	152.70	153.00
CCSD / cc-pVDZ	1.2589	2.1972	1.2630	1.3556	1.0814	1.0832	117.86	101.36	140.78	150.78	151.69
CCSD / cc-pVTZ	1.2411	2.1712	1.2437	1.3370	1.0658	1.0669	117.95	100.83	141.23	150.63	152.76
CCSD(T) / cc-pVDZ	1.2643	2.2327	1.2712	1.3594	1.0831	1.0854	117.69	101.17	141.14	151.64	151.22
CCSD(T) / cc-pVTZ	1.2466	2.2068	1.2518	1.3410	1.0676	1.0692	117.81	100.51	141.69	151.67	152.59
c~CCSD(T)-AE / cc-pCVQZ	1.2409	2.1975	1.2457	1.3350	1.0659	1.0673	117.84	100.35	141.81	151.50	152.98

[a] See figures in Appendix A for coordinate labels.